NASA SP-8125

NASA
SPACE VEHICLE
DESIGN CRITERIA
(CHEMICAL PROPULSION)

LIQUID ROCKET ENGINE AXIAL-FLOW TURBOPUMPS

APRIL 1978

NATIONAL AERONAUTICS AND SPACE ADMINISTRATION

FOREWORD

NASA experience has indicated a need for uniform criteria for the design of space vehicles. Accordingly, criteria are being developed in the following areas of technology:

Environment
Structures
Guidance and Control
Chemical Propulsion

Individual components of this work will be issued as separate monographs as soon as they are completed. This document, part of the series on Chemical Propulsion, is one such monograph. A list of all monographs issued prior to this one can be found on the final pages of this document.

These monographs are to be regarded as guides to design and not as NASA requirements, except as may be specified in formal project specifications. It is expected, however, that these documents, revised as experience may indicate to be desirable, eventually will provide uniform design practices for NASA space vehicles.

This monograph, "Liquid Rocket Engine Axial-Flow Turbopumps", was prepared under the direction of Howard W. Douglass, Chief, Design Criteria Office, Lewis Research Center; project management was by Harold W. Schmidt. The monograph was written by D. D. Scheer of the Lewis Research Center; M. C. Huppert* of Rocketdyne Division, Rockwell International Corporation; and F. Viteri and J. Farquhar** of Aerojet Liquid Rocket Company. The monograph was edited by Russell B. Keller, Jr. of Lewis. To assure technical accuracy of this document, scientists and engineers throughout the technical community participated in interviews, consultations, and critical review of the text. In particular, Austin King of Rocketdyne Division, Rockwell International Corporation; D. M. Sandercock of the Lewis Research Center; and W. W. Wilcox of NASA Headquarters individually and collectively reviewed the monograph in detail.

Comments concerning the technical content of this monograph will be welcomed by the National Aeronautics and Space Administration, Lewis Research Center (Design Criteria Office), Cleveland, Ohio 44135.

April 1978

---

*Currently with Aerojet Liquid Rocket Co.

**Currently with Westinghouse Electric Corp.

GUIDE TO THE USE OF THIS MONOGRAPH

The purpose of this monograph is to organize and present, for effective use in design, the significant experience and knowledge accumulated in development and operational programs to date. It reviews and assesses current design practices, and from them establishes firm guidance for achieving greater consistency in design, increased reliability in the end product, and greater efficiency in the design effort. The monograph is organized into two major sections that are preceded by a brief introduction and complemented by a set of references.

The State of the Art, section 2, reviews and discusses the total design problem, and identifies which design elements are involved in successful design. It describes succinctly the current technology pertaining to these elements. When detailed information is required, the best available references are cited. This section serves as a survey of the subject that provides background material and prepares a proper technological base for the *Design Criteria* and Recommended Practices.

The *Design Criteria,* shown in italics in section 3, state clearly and briefly what rule, guide, limitation, or standard must be imposed on each essential design element to assure successful design. The *Design Criteria* can serve effectively as a checklist of rules for the project manager to use in guiding a design or in assessing its adequacy.

The Recommended Practices, also in section 3, state how to satisfy each of the criteria. Whenever possible, the best procedure is described; when this cannot be done concisely, appropriate references are provided. The Recommended Practices, in conjunction with the *Design Criteria,* provide positive guidance to the practicing designer on how to achieve successful design.

Both sections have been organized into decimally numbered subsections so that the subjects within similarly numbered subsections correspond from section to section. The format for the Contents displays this continuity of subject in such a way that a particular aspect of design can be followed through both sections as a discrete subject.

The design criteria monograph is not intended to be a design handbook, a set of specifications, or a design manual. It is a summary and a systematic ordering of the large and loosely organized body of existing successful design techniques and practices. Its value and its merit should be judged on how effectively it makes that material available to and useful to the designer.

CONTENTS

LIST OF FIGURES

LIST OF TABLES

LIQUID ROCKET ENGINE AXIAL-FLOW TURBOPUMPS

1. INTRODUCTION

An axial-flow pump consists of a set of disks or a cylinder, carrying airfoil-shaped blades on the periphery, that rotates at high speed within a casing or housing that contains sets of fixed blades (stator vanes) positioned between the rotor blades; small clearances at the blade tips and between rotor blades and stator vanes are maintained under all operating conditions. The pumped fluid flows nearly parallel with the pump shaft, and headrise is produced by summation of increases of pressure produced as the fluid traverses each set (stage) of rotor blades and stator vanes. A centrifugal-flow pump consists of a bladed rotor (impeller) shaped so that the rotation of the impeller sweeps the pumped fluid roughly 90° outward from the impeller shaft. This action imparts a high-speed spiral velocity to the fluid; much of this velocity is converted to pressure increase (headrise) by the diffuser that surrounds the impeller and collects the fluid.

Both axial- and centrifugal-flow pumps have been utilized in rocket-engine propellant-feed systems. By far, greater use has been made of the centrifugal type, which is well suited for dense propellants and the pressure/flow requirements of current rocket engines. The use of liquid hydrogen as a propellant, however, logically led to consideration of the axial-flow type with its potential higher efficiency, lower weight, and relative ease of staging. In five instances, axial-flow pumps were designed and carried through various levels of development and production; one pump (the Mark 15-F) saw extensive operational service on the J-2 engine used on the S-II and S-IVB stages of the Apollo Saturn V vehicle. This monograph is based on the experience with these five pumps and as such reflects pump technology based on a relatively small number of configurations, all of which involved liquid hydrogen as the pumped fluid. In the development of this technology, particularly in the area of hydrodynamic design and the mechanical design of the blading, extensive use was made of applicable experience that had been acquired in the design of axial-flow compressors. It is important to note, however, that no attempt has been made to incorporate in this document any axial-flow-compressor technology that evolved subsequent to the design of the pumps discussed herein, even though some of that technology may be useful in the design of axial-flow pumps. Some of the areas treated in this monograph are applicable to both axial and centrifugal pumps. In most instances, areas generally applicable to both types of pumps (primarily volutes) are discussed briefly herein, because the subject matter is covered fully in the design criteria monograph on centrifugal pumps (ref. 1).

The axial-pump design process is directed toward achieving a hydrodynamic and mechanical design configuration that will meet the requirements of the engine system within the constraints imposed by other components in the turbopump assembly. Thus, the axial-pump design cannot be divorced from the design of components such as the turbine, inducer, bearings, and seals. In instances where components or systems influence the axial-pump design, appropriate reference is made to other monographs in the Chemical Propulsion series.

The hydrodynamic design of an axial pump involves basically (1) the selection of appropriate fluid-velocity diagrams and (2) the design of blading that will achieve fluid turning per the diagrams with the predicted loss. Major problems in hydrodynamic design include (1) failure to achieve pump headrise because of improper fluid turning or low efficiency, and (2) failure to maintain adequate stall margin during transient or steady-state pump operation. Structural adequacy of the axial pump is achieved by keeping operating stresses within material limits and by maintaining adequate clearances between rotating and stationary components. Major problems in structural (mechanical) design include blade and vane fatigue failures, excessive housing and rotor deflections, and failure of the thrust-balance system to keep rotor axial loads within manageable magnitudes.

The monograph begins with a section that provides a brief background on the axial-pump applications and views the pump in terms of the total turbopump assembly. The remaining sections treat the pump design in the order in which a pump designer would proceed. These sections deal with stage hydrodynamic design, pump rotor assembly, pump stator assembly, pump materials for liquid-hydrogen applications, and safety factors as utilized in state-of-the-art pumps. In each of these areas, the monograph establishes the basis for successful axial-flow pump design.

2. STATE OF THE ART

2.1 OVERALL TURBOPUMP DESIGN

The use of axial-flow pumps in rocket engines has been limited to liquid-hydrogen applications in which high volumetric flowrate and headrise were required. Additionally, the relatively narrow operating-range capability of axial pumps has restricted their use to applications that did not require significant throttling or operation over a wide fixed-speed flow range. As noted, the state of the art is reflected in five configurations that were designed and carried through various levels of development and production. Chief design features of these pumps and their use are tabulated in table I*. Head-vs-flow characteristics are shown in figure 1; readily apparent are the steep slope of the characteristic curves and the abrupt drop in head at the stall** points. The choice of an axial pump for the applications noted in table I was not incisive; a centrifugal pump could have been designed to deliver the flow at the required discharge pressure. Considerations favoring the axial pump included potential advantages in efficiency, weight, and packaging (size). Additionally, in those applications where engine thrust uprating was a design requirement (e.g., on the M-1), the axial configuration was favored because of relative simplicity in adding stages to achieve the necessary uprated condition.

Required operating duration and service life for state-of-the-art axial-flow pumps have been relatively short. Design duration for the M-1 pump, for example, was 500 sec, with a service life (between overhauls) of 10 000 sec. This short life requirement has been a significant factor in the development of components for the axial-flow pumps discussed in this monograph.

Cross-sectional and cutaway views of the Mark 15-F and M-1 liquid-hydrogen turbopumps are presented in figures 2 and 3, respectively. In general, configurations of the other axial-flow turbopumps are similar to the two shown; i.e., an inducer stage with the inducer stator integral with the front bearing housing, an axial-flow pump assembly that includes a thrust-balance system, a rear-bearing-housing assembly, and a direct-drive turbine. The turbines on the Mark 15-F, M-1, and Mark 26 turbopumps were overhung from the rear bearing, whereas the drives for the Mark 9 and Mark 25 were mounted on separate bearings.

The Mark 9 was the first of the rocket engine axial-flow pumps to be developed. With the exception of an additional stage, the blading on the Mark 15-F was identical to that utilized on the Mark 9. The Mark 26, in turn, was an uprated version of the basic Mark 15-F in which more highly loaded blading was utilized to achieve increased headrise per stage.

The inducers on axial pumps have been designed to operate at low values of net positive suction head (NPSH) and to develop sufficient pressure to prevent cavitation in the

*Factors for converting U.S. customary units to the International System of Units (SI Units) are given in Appendix A.

**Terms, symbols, materials, and abbreviations are defined or identified in Appendix B.

Table I. – Chief Design Features of Axial-Flow Liquid-Hydrogen Pumps

Pump	Delivered flow, gpm	Headrise,* ft	Speed, rpm	Number of stages	Application
Mark 9	10 230	51 500	32 800	Inducer plus six main stages	Phoebus (Development)
Mark 15-F	9 062	40 300	28 266	Inducer plus seven main stages	J-2 engine (Operational)
Mark 25	18 500	62 000	34 000	Tandem inducer plus four main stages	Phoebus (Development)
Mark 26	9 000	40 000	24 000	Inducer plus seven main stages	J-2 engine (Experimental)
M-1	62 300	56 500	13 225	Inducer plus transition plus eight main stages	M-1 engine (Development)

*Overall headrise – inducer inlet to volute discharge.

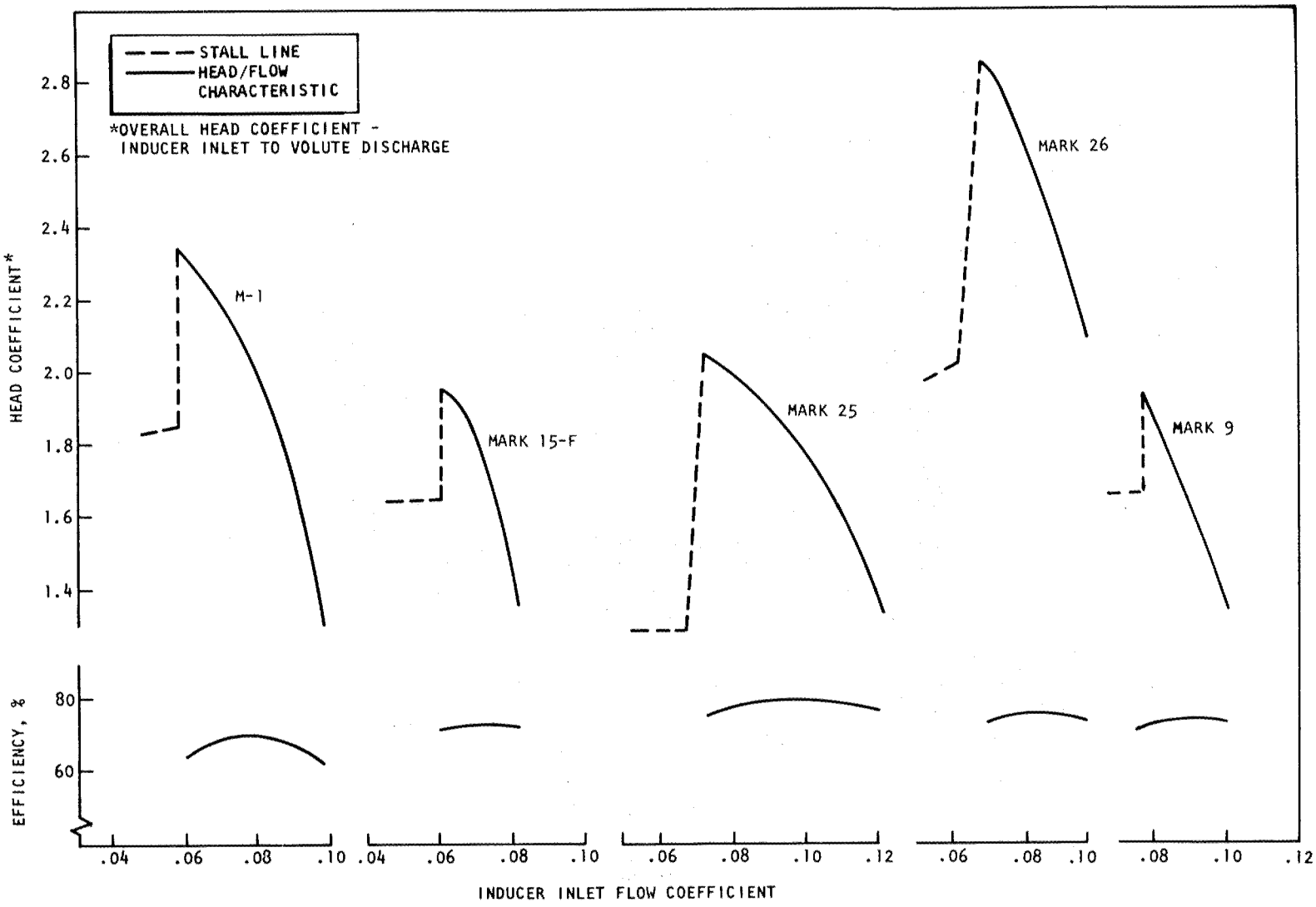

Figure 1. — Head coefficient and efficiency vs flow coefficient for axial-flow pumps.

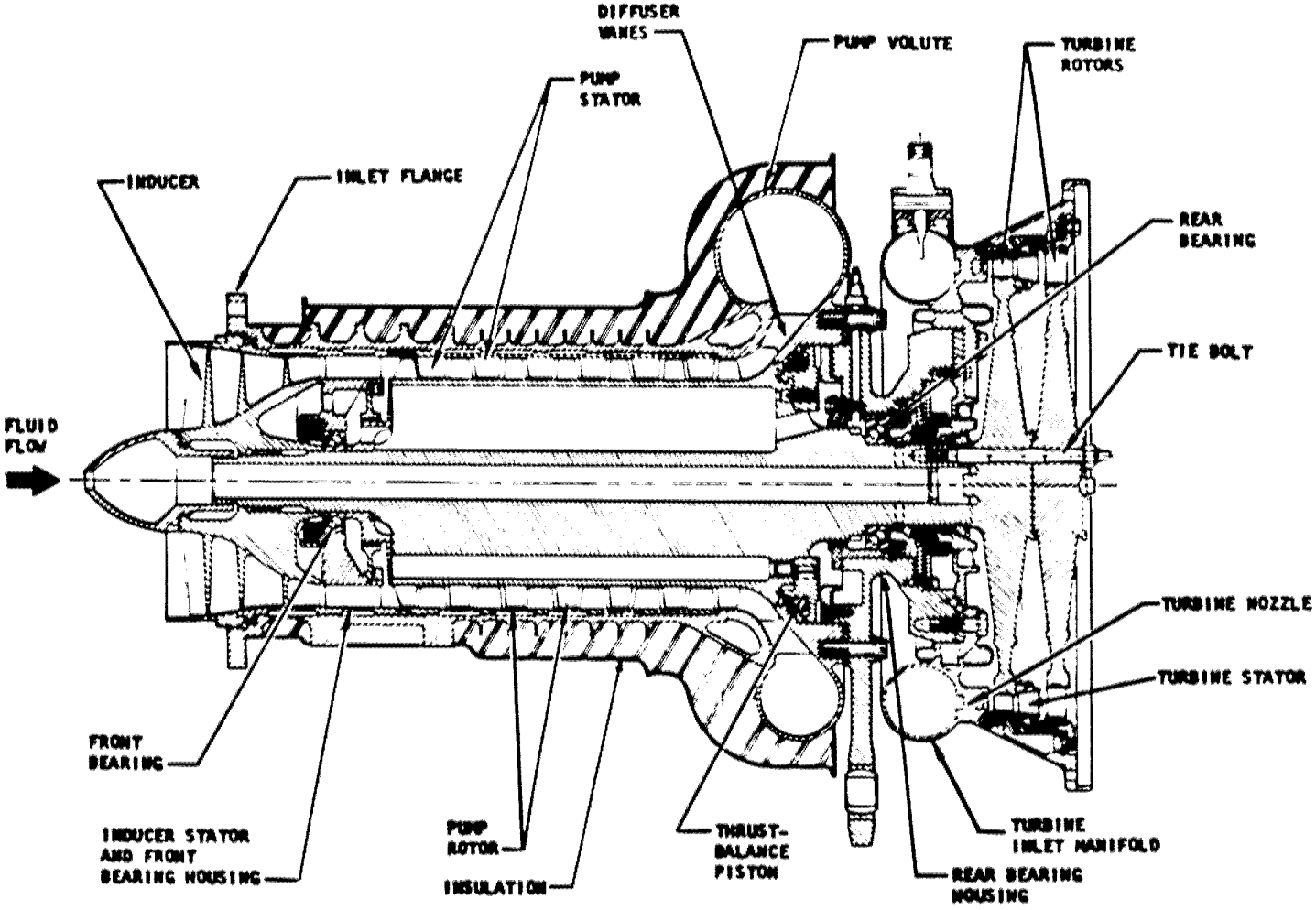

Figure 2. – Cross-sectional view of Mark 15-F turbopump.

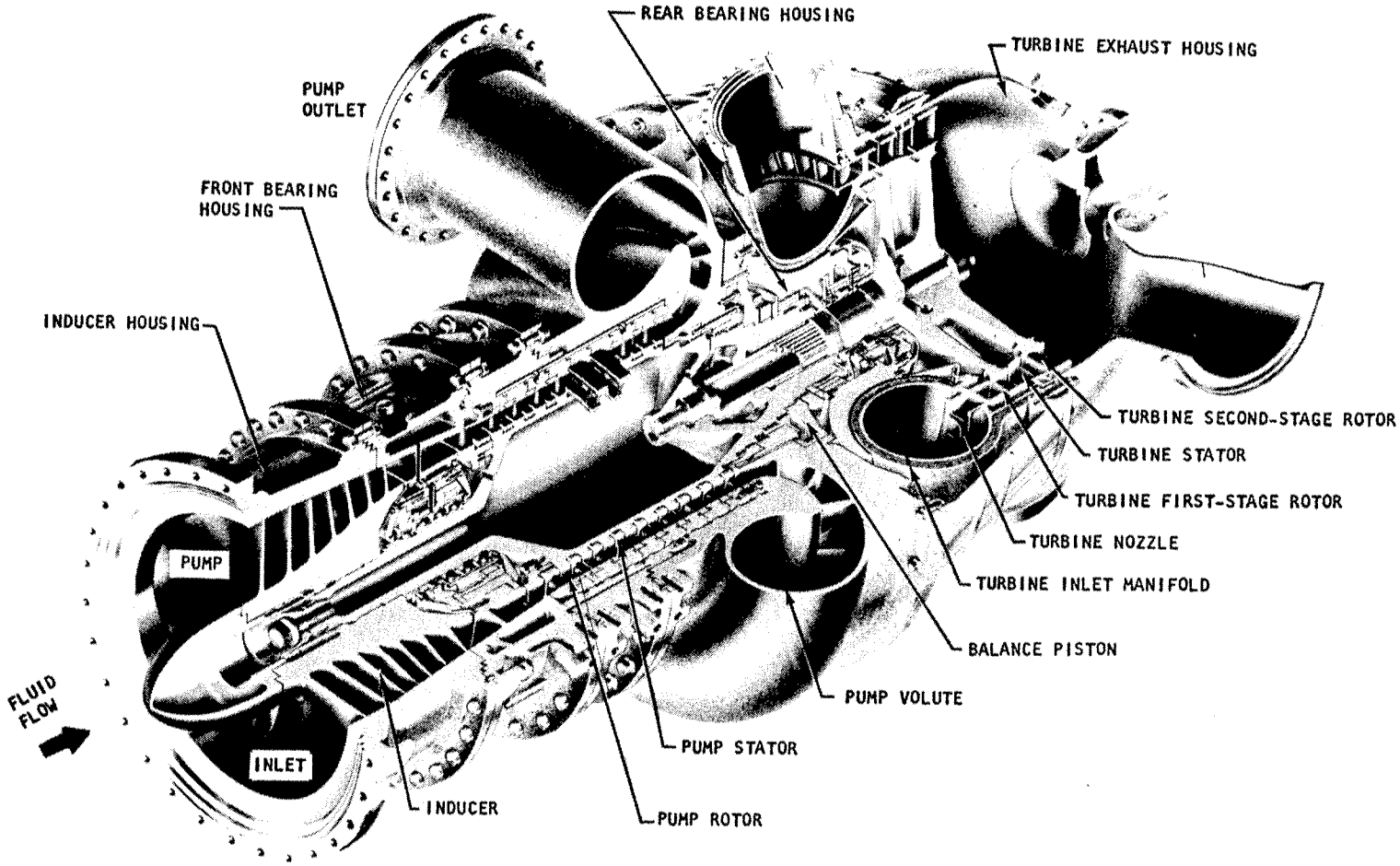

Figure 3. — Cutaway view of M-1 fuel turbopump.

following blade rows (ref. 2). Both roller and ball bearings have been utilized and have been cooled by the liquid hydrogen; bearing DN values of 2×10^6 are considered state-of-the-art limits for relatively short-life pumps (ref. 3). Labyrinth and shaft-riding seals have been employed to control internal flow. Face-riding and lift-off seals have been utilized at the turbine end of pump to prevent propellant leakage into the turbine area during static conditions and to control the leakage during operation; the face-riding seals have been operated successfully at surface speeds up to 400 ft/sec (ref. 4).

2.1.1 Turbopump Speed

In normal rocket-engine applications, the turbopump is operated at high speed in order to minimize turbopump weight and to achieve increased pump and turbine efficiencies. During the initial design phase of a new turbopump, the usual practice is to set the design speed as high as possible consistent with the hydrodynamic and mechanical constraints associated with the total turbopump assembly. These constraints include inducer cavitation (ref. 2), bearing DN (ref. 3), seal rubbing speed (ref. 4), turbine stress (ref. 5), and pump critical speeds (ref. 6). Details of speed restrictions and the effects of speed on the turbopump and vehicle are given in reference 7.

Important design parameters in establishing turbopump speed are pump rotational speed N, specific speed N_s, and suction specific speed S_s. These parameters are related by the expressions

$$N_s = \frac{NQ^{1/2}}{H^{3/4}} \tag{1}$$

$$S_s = \frac{NQ^{1/2}}{(NPSH)^{3/4}} \tag{2}$$

where

N_s = specific speed, rpm - $(gpm)^{1/2}/ft^{3/4}$

N = rotational speed, rpm

Q = volume flowrate, gpm

H = headrise, ft

S_s = suction specific speed, $\frac{\text{rpm} \cdot (\text{gpm})^{1/2}}{\text{ft}^{3/4}}$

NPSH = net positive suction head, ft

The design speed constraint on the M-1 turbopump was inducer cavitation based on a design suction specific speed S_s of 43 000. The Mark 15-F and Mark 26 pumps were limited in operating speed in order to avoid resonance of the pump blades with speed-dependent forcing functions. Note that these were operating-speed limits and were not established by design constraints in the strict sense, since redesign of the blading could have resulted in a change in blade natural frequency and the proximity to resonance. It was noted previously that the designs of the Mark 15-F and Mark 26 were sequential, and both were akin to the Mark 9. This sequential relation in effect precluded the type of speed-selection study usually conducted for a new turbopump design.

2.1.2 Turbopump Rotor Dynamics

The dynamic behavior of turbopump rotors has received considerable attention in rocket engine design and development programs. An extensive bibliography and discussion of the stability aspects of turbopump rotor systems applicable to both centrifugal and axial machines are presented in reference 6. It is appropriate here, however, to discuss briefly the overall design concepts and problems associated with rotor dynamics in the state-of-the-art axial-flow configurations. Two approaches have been used in the design of the rotor/bearing systems for axial-flow turbopumps. In the M-1 turbopump, the shaft-and-bearing system was designed so that the turbopump maximum operating speed was below the first critical speed of the shaft and its supports. In the Mark 9, 15-F, 25, and 26 turbopumps, the systems were designed so that the operating speeds were above system criticals but below the rotor first-flexural mode. The advantages and disadvantages of each of these design approaches are discussed in reference 6.

In the M-1 approach (operation below the system first critical speed), high rotor/bearing system stiffness is desired in order to achieve a high first critical speed. Thus, roller bearings, which have high radial load and stiffness characteristics, were used to support the shaft. Axial loads were reacted by a triple set of ball bearings encased in a radially flexible housing, this being done to ensure that radial shaft support would be at the intended roller-bearing locations. Extensive analysis along with experimental effort to determine bearing spring rates and rear (turbine) bearing housing flexibility was performed (ref. 8). The predicted system critical speed for the so-called M-1 Mod 1 (initial test configuration) turbopump was 16 000 rpm. Limited testing was performed with this turbopump, because the M-1 engine

program was terminated. However, during one of the tests an inadvertent overspeed to 15 500 rpm occurred. At this speed level, the bearing and support-strut accelerometer traces indicated that the critical speed was being approached, thus lending credibility to the analytical model, which is described in reference 8.

The axial turbopumps that have been designed to operate above the rotor/bearing system critical speeds have had ball bearings at the support locations, a configuration that achieves a relatively low radial spring rate and low system critical speed. A rotor operating above the first critical speed may develop nonsynchronous whirl (ref. 6); this phenomenon occurred in varying degrees of severity on the Mark 9, 15-F, 25, and 26 turbopumps (refs. 9, 10, and 11). Nonsynchronous whirl and axial oscillations that occurred with the Mark 9 were examined extensively both analytically and experimentally (ref. 10). In the Mark 15-F, nonsynchronous whirl was identified as a major source of alternating stress in the turbine disks and disk-to-pump shaft coupling (the turbine disks resist plane-of-rotation changes associated with the whirl); in addition, rotor radial displacement as high as 0.030 in. peak-to-peak was measured. These problems were solved by increasing the axial preload on the ball bearings, which increased the threshold of shaft stability and suppressed shaft deflections to tolerable magnitudes. Severe nonsynchronous whirl also was observed during development testing of the Mark 25 pump (ref. 11). In this pump, single ball bearings were used at the rotor support locations; a design change to duplex ball bearings eliminated the severe whirl problem in the pump operating-speed range.

In general, the rotor dynamics problems that have occurred in axial-flow pumps have been difficult to diagnose and solve. Suitable analytical models for the prediction of nonsynchronous whirl were not available at the time the pumps treated herein were designed. In the design process, an attempt was made to avoid whirl by considering those factors then known to be related to whirl problems and by designing so that the operating speed was not near a critical speed. However, as indicated in the preceding paragraph, these measures were not always adequate. Effort to solve nonsynchronous-whirl problems in centrifugal turbopumps was exerted subsequent to the design of the axial-flow pumps discussed in this monograph. This effort has provided improved analytical methods that permit a more thorough treatment of rotor instability during the design phase (refs. 12 and 13).

2.2 STAGE DESIGN

2.2.1 Realm of Operation

The considerations involved in the selection of the type of pump for a given application are discussed in reference 7. The discussion herein is limited essentially to an identification of the specific speed range in which axial stages have been used.

Figure 4 (adptd. from ref. 14) shows design-point performance for various types of pumps in terms of specific speed N_s and specific diameter D_s ($D_s = DH^{1/4}/Q^{1/2}$, where D = rotor diameter, ft).

This kind of figure is useful in the pump selection process, in that it identifies specific areas where different types of pumps are suitable and gives an estimate of pump efficiency and diameter. As shown on the figure, axial-flow-pump stages have specific speeds ranging from approximately 3200 to 11 000. It should be noted that these are stage characteristics; considerable difference occurs when the entire pump is examined. For example, the figure indicates that for the M-1 mainstage specific speed of 4470 an axial flow configuration is suitable; however, the specific speed of the entire M-1 pump is approximately 900, and examination of this region on the N_s-D_s diagram indicates that a centrifugal pump could have been selected, some decrease in efficiency being anticipated.

2.2.2 Stage Hydrodynamic Design

The procedures used in the hydrodynamic design of axial pumps generally have followed design practices for axial-flow compressors (ref. 18). The three-dimensional flow conditions that exist in the pump are approximated by a two-dimensional flow model in which it is assumed that the average flow in the circumferential (blade-to-blade) plane at discrete radial stations can be used to describe the flow in the meridional (hub-to-tip) plane. A typical flow model for a pump stage is illustrated in figure 5; nomenclature for the blading is shown in figure 6. In the flow model illustration (fig. 5), the velocity diagrams represent the average flow condition at a given streamline. Radial (i.e., streamline-to-streamline) variations in the flow are determined from continuity, energy addition, and radial-equilibrium considerations. Losses at each streamline location are accounted for by applying experimental loss data or estimated efficiences to the flow model.

Specifications given to the designer of the axial-flow stages include propellant weight flowrate and pressure rise, turbopump speed, and fluid conditions at the inlet of the first stage (i.e., fluid pressure, temperature, velocities, and angles at the inducer stage exit). Weight flowrate and pressure rise are dictated by engine thrust and pressure requirements, and speed usually is prescribed by constraints associated with the total turbopump assembly, as noted previously. Additionally, the required engine operating range and desired start characteristic provide the designer with off-design flow requirements of the pump. In the pump analysis, weight flowrate and pressure rise are converted to volume flowrate and headrise. For incompressible propellants, the conversion is straightforward, propellant density being used as the conversion factor. When propellant heating and density changes are significant (e.g., in high-pressure-hydrogen pumps), the headrise requirement of the pump (or stage) for a given pressure rise is determined from the thermodynamic state points of the propellant at the beginning and end of the pumping process or an increment of the pumping process. In reference 7, a method is described in which the required headrise is

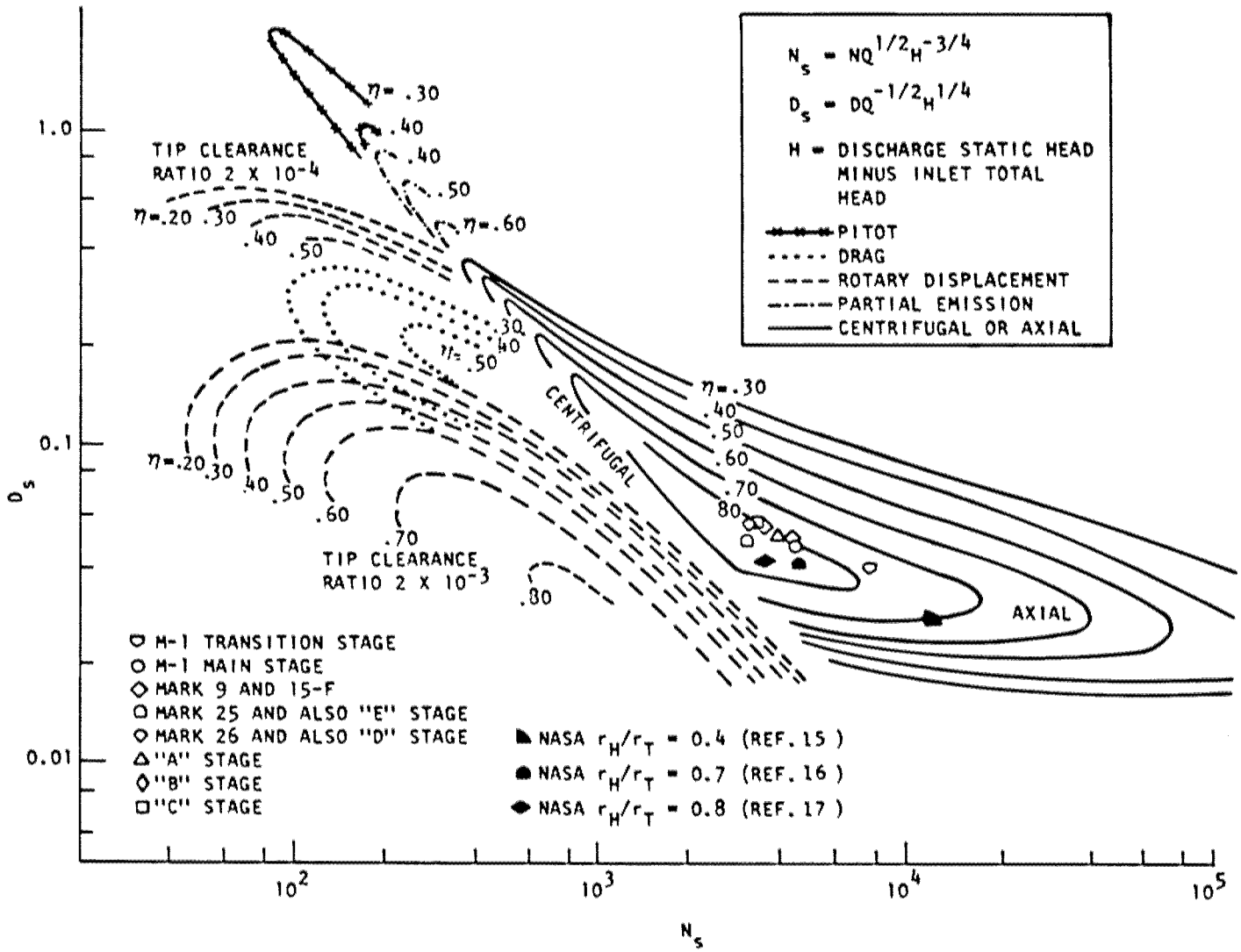

Figure 4. — Approximate $N_s - D_s$ diagram for single-disk pumps and low-pressure-ratio compressors (adptd. from ref. 14).

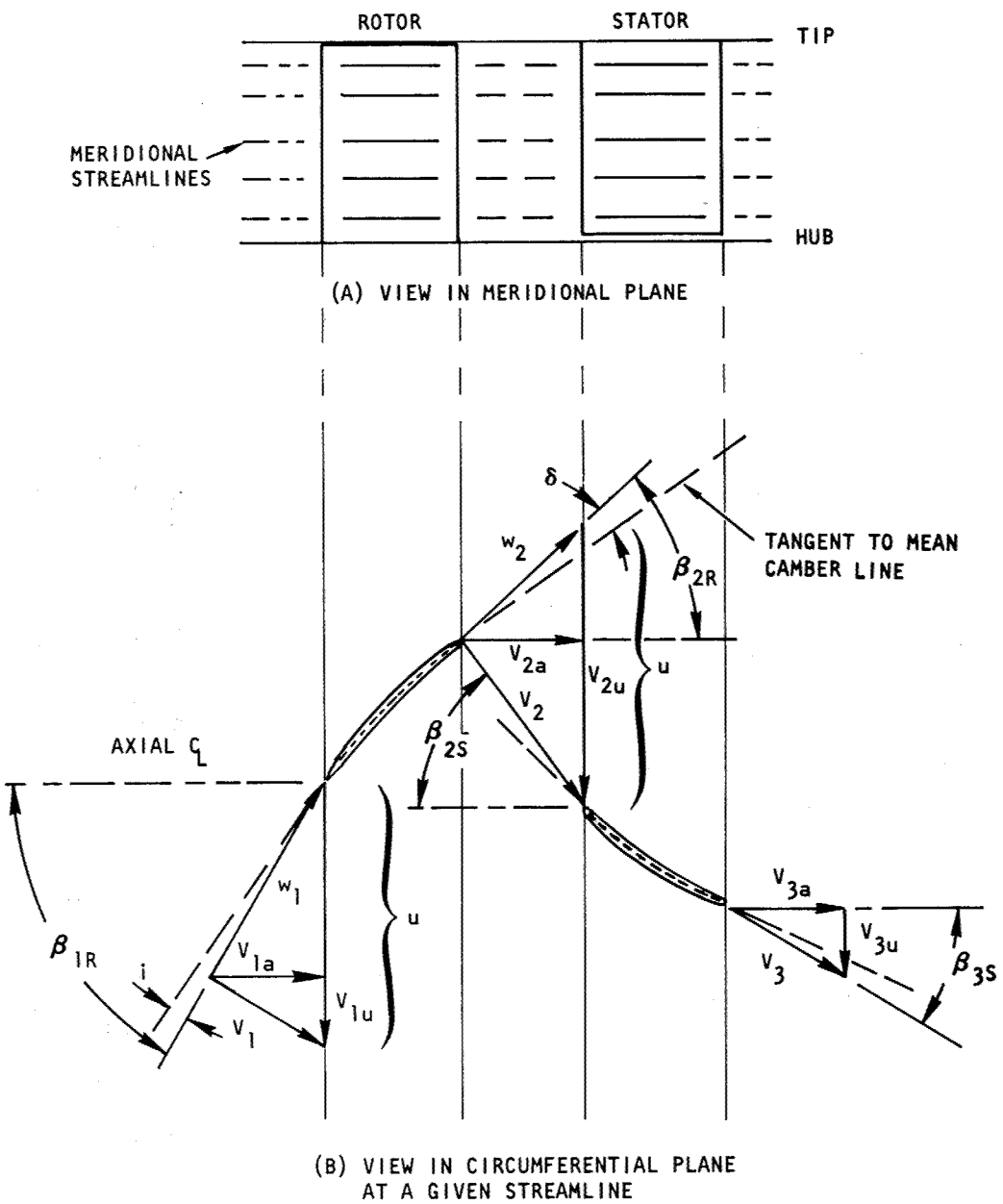

Figure 5. — Typical flow model for an axial pump stage.

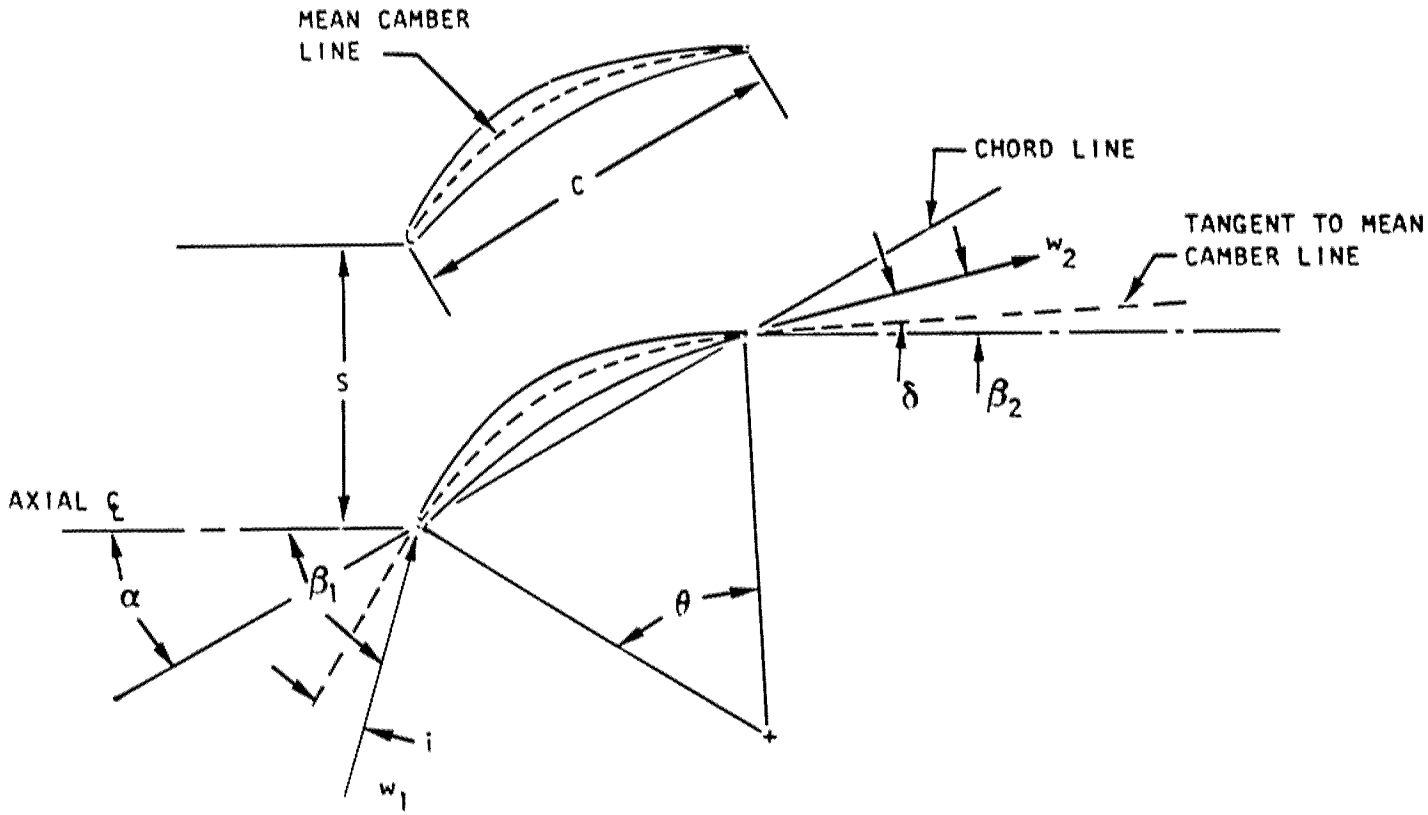

Figure 6. – Nomenclature for axial pump blading.

determined from the summation of incremental increases in isentropic enthalpy. The state point at the end of each pumping increment is determined by dividing the isentropic-enthalpy increase by the efficiency. Propellant densities at the state points can then be determined and used in sizing local flow-passage areas in the pump.

With inputs of volume flowrate, headrise, turbopump speed, and off-design requirements, a parametric study usually is conducted, conditions at the 50% streamline being used to evolve an overall pump configuration that will satisfy both hydrodynamic and mechanical requirements (ref. 19). The studies normally are conducted using the dimensionless forms for flowrate and headrise:

$$\phi = \frac{V_a}{U} \tag{3}$$

$$\psi = \frac{g_c H}{U^2} = \frac{\eta_H (V_{2u} - V_{1u})}{U} \tag{4}$$

where

ϕ = flow coefficient

V_a = fluid absolute velocity (axial), ft/sec

U = blade tangential velocity, ft/sec

ψ = head coefficient

g_c = gravitational conversion factor, $32.17 \frac{\text{lbm-ft}^*}{\text{lbf-sec}^2}$

H = headrise, $\frac{\text{ft-lbf}^*}{\text{lbm}}$

η_H = stage hydraulic efficiency (sec. 2.2.2.1.2)

V_{2u} = tangential component of absolute velocity at rotor exit, ft/sec

V_{1u} = tangential component of absolute velocity at rotor inlet, ft/sec

*The use of g_c in units of $32.17 \frac{\text{lbm-ft}}{\text{lbf-sec}^2}$ instead of g in units of ft/sec^2 and the use of H in units of $\frac{\text{ft-lbf}}{\text{lbm}}$ instead of ft make equation (4) and similar equations dimensionally correct under all environments.

Typically the procedure involves a preliminary selection of blade and vane profile type (sections 2.3.1.1 and 2.4.1.1), velocity diagram type (section 2.2.2.2), hydrodynamic loading (section 2.2.2.1.1), and solidity (section 2.2.2.4), all of which are interrelated with flow coeffcient, head coefficient, and efficiency. Blade tip speed (which is related to rotor diameter) and flow coefficient (which is related to blade tip speed and hub/tip ratio) are then studied over a range of values to determine stage head coefficients and the number of stages necessary to produce the required headrise. This procedure allows a number of pump configurations with different diameters and lengths to be examined in terms of stress, weight, and turbopump critical speed.

Changes in the preliminary selections of profile type, velocity diagram type, etc., may be necessary in the process of arriving at a suitable configuration. When the configuration has been established, velocity diagrams, hydrodynamic loading, and efficiency at each streamline in the meridional plane are determined, and the blade and vane angles (section 2.2.2.3) are selected to produce the desired diagrams. Off-design performance is then estimated, iterations again being made if necessary to compromise properly the design-point and operating-range requirements.

Basic design data for the state-of-the-art stages are given in tables II and III. In the multistage pump configurations, the stages have been essentially identical within the given configuration. The M-1 pump had a lightly loaded "transition" stage behind the inducer to provide a uniform head distribution to the first mainstage and to provide better cavitation characteristics than were possible with the more heavily loaded mainstage. Additionally, the M-1 pump had a linearly decreasing outside diameter between the third-stage stator discharge and the fifth-stage rotor discharge to account for hydrogen compressibility. Stages for the Mark 9, 15-F, 25, and 26 pumps were identical within each configuration with the exception that none of the last stages in these pumps utilized a stator. The flow path on the Mark 25 was adjusted linearly from the first rotor inlet to the last rotor discharge to account for hydrogen compressibility. Adjustments for hydrogen compressibility were not incorporated in the design of the Mark 9, 15-F, and 26 pumps.

2.2.2.1 BLADE LOADING, STALL MARGIN, AND EFFICIENCY

2.2.2.1.1 Blade Loading and Stall Margin

Blade loading. – The energy added to the fluid by the pump rotor blade is a function of the increase in the tangential velocity of the fluid between the rotor inlet and the rotor exit. High blade loading, i.e., large changes in tangential velocity ($V_{2u} - V_{1u}$ in fig. 5), are desirable in order to obtain high stage headrise and therefore a small number of stages. It can be observed in figure 5 that an increase in blade loading could be achieved by a blade shape that would increase fluid turning in the direction of rotation. However, this configuration would decrease the fluid relative velocity at the rotor exit (w_2), thereby increasing flow

Table II. – Stage Design Data for Axial-Flow Pumps

Stage	r_H	r_T	ν	ϕ_T	ψ_T	N_s	D_s	η	Diffusion Factor			
									Rotor		Stator	
									Hub	Tip	Hub	Tip
M-1 transition stage	6.80	8.00	0.850	0.396	0.126	7640	0.0400	0.916	0.352	0.037	0.392	0.333
M-1 main stage	6.80	8.00	0.850	0.420	0.258	4470	0.0478	0.894	.448	.598	.477	.477
Mark 9	2.99	3.61	0.829	0.294	0.226	4450	0.0511	-------	.52	.41	.57	.54
Mark 15-F	Same as Mark 9											
Mark 25	Same as "E"											
Mark 26	Same as "D"											
"A" stage	3.13	3.63	0.861	0.390	0.279	4000	0.0511	0.87	.58	.48	.58	.56
"B" stage	3.13	3.63	0.861	0.390	0.316	3650	0.0533	0.87	.64	.54	.64	.62
"C" stage	3.13	3.63	0.861	0.390	0.338	3460	0.0538	0.86	.68	.57	.68	.66
"D" stage	3.13	3.63	0.861	0.390	0.35	3380	0.0542	0.84	.72	.61	.72	.70
"E" stage	3.13	3.63	0.861	0.465	0.35	3220	0.0500	0.85	.53	.47	.55	.50
NASA ν = 0.4	1.78	4.53	0.393	0.284	0.135	10650	0.0272	0.800	.593	.223	.577	.373
NASA ν = 0.7 (rotor only)	3.15	4.50	0.700	0.294	0.282	4760	0.0429	0.937	.693	.426	NA	NA
NASA ν = 0.8 (rotor only)	3.60	4.50	0.800	0.466	0.391	3850	0.0436	0.955	.631	.664	NA	NA

NA = not applicable

Table III. – Design Parameters for Blade and Vane Profiles in Axial-Flow Pumps

Pump	Profile	Profile type	Chord, in.			Maximum thickness-to-chord ratio			Solidity			Camber, deg			Stagger, deg		
			Hub	Mean	Tip	Hub	Mean	Tip	Hub	Mean	Tip	Hub	Mean	Tip	Hub	Mean	Tip
M-1 transition stage	Blade	C-4	1.430	1.315	1.200	0.120	0.095	0.070	1.037	0.872	0.745	19.30	13.85	3.40	47.30	53.10	59.20
	Vane	C-4	0.991	0.991	0.991	0.08	0.08	0.08	1.19	1.08	0.99	14.60	17.50	43.60	33.50	32.72	39.90
M-1 mainstage	Blade	C-4	1.302	1.176	1.070	0.120	0.097	0.075	1.43	1.13	0.915	27.86	21.86	18.50	36.39	45.02	51.17
	Vane	C-4	1.057	0.968	0.882	0.15	0.15	0.15	1.42	1.18	1.00	26.04	29.57	37.56	36.83	35.27	34.12
Mark 9	Blade	Nonstandard	1.37	———	1.36	0.09	———	0.05	1.21	———	1.05	18.5	———	12.0	61.9	———	67.9
	Vane	Nonstandard	0.87	———	0.98	0.117	———	0.065	1.9	———	1.8	40.0	———	40.0	38.0	———	35.3
Mark 15-F	Blade																
	Vane						Same as Mark 9										
Mark 25	Blade																
	Vane						Same as "E"										
Mark 26	Blade																
	Vane						Same as "D"										
"A" stage	Blade		0.923	———	0.892	0.140	———	0.051	1.37	———	1.14	38.7	———	21.36	40.35	———	54.39
	Vane	Modified double-circular-arc	1.00	———	0.924	0.120	———	0.050	1.4	———	1.31	36.9	———	34.8	37.38	———	40.35
"B" stage	Blade		0.912	———	0.872	0.138	———	0.052	1.34	———	1.11	43.1	———	24.9	39.05	———	53.75
	Vane		0.99	———	0.860	0.121	———	0.054	1.31	———	1.3	39.4	———	39.4	35.12	———	38.99
"C" stage	Blade		0.899	———	0.852	0.14	———	0.054	1.33	———	1.09	46.0	———	27.1	38.0	———	53.15
	Vane		0.980	———	0.850	0.122	———	0.054	1.30	———	1.29	43.0	———	43.1	34.1	———	37.85
"D" stage	Blade	Modified	0.909	———	0.836	0.132	———	0.062	1.33	———	1.06	50.0	———	28.9	36.5	———	52.22
	Vane	double-circular-arc	0.975	———	0.874	0.123	———	0.058	1.33	———	1.29	47.8	———	46.1	34.1	———	36.85
"E" stage	Blade	Nonstandard	1.667	———	1.268	0.104	———	0.081	1.9	———	1.28	45.9	———	29.1	30.0	———	41.0
	Vane	Nonstandard	1.538	———	1.394	0.085	———	0.089	1.7	———	1.61	35.1	———	36	41.1	———	38.9
NASA ν = 0.4	Blade	Double-circular-arc	1.50	1.50	1.50	0.10	0.085	0.07	2.5	1.44	1.0	61.35	13.84	5.43	19.97	———	70.19
	Vane		1.50	1.50	1.50	0.08	0.08	0.08	2.37	1.36	0.95	62.20	51.40	44.15	20.34	———	9.61
NASA ν = 0.7	Blade (no stator)		1.52	1.52	1.52	0.085	0.0775	0.070	1.44	1.19	1.01	27.6	19.8	0	52.2	60.5	67.1
NASA ν = 0.8	Blade (no stator)		1.49	1.49	1.49	0.09	0.08	0.07	1.25	1.11	1.00	43.4	42.7	27.0	39.8	46.2	55.0

diffusion in the blade row. Large velocity gradients on the blade surfaces associated with large amounts of diffusion tend to produce thick boundary layers and relatively high losses in total headrise. In reference 20, a blade-loading parameter based on diffusion in the blade row was developed for axial-flow compressors. The parameter, the diffusion factor DF, is an index of local diffusion on the blade suction surface in terms of fluid inlet and outlet velocities or angles and blade-row solidity. In axial-compressor work, the diffusion factor was used for correlating experimental total-pressure-loss data and for indicating limiting loading, i.e., the loading at which the boundary layer separates from the suction surface. In axial-flow pump work, the diffusion factor has been used similarly in estimating loss in total head and loading limits.

In the notation of figure 5, diffusion factors for the rotor and stator, with constant radius over the stage length, are given by the expressions

$$(DF)_R = 1 - \frac{w_2}{w_1} + \frac{\Delta w_u}{2\sigma w_1} \tag{5}$$

where

$(DF)_R$ = diffusion factor for rotor

w_1 = fluid inlet relative velocity, ft/sec

w_2 = fluid exit relative velocity, ft/sec

Δw_u = change in tangential component of relative velocity = $w_1 \sin\beta_{1R} - w_2 \sin\beta_{2R}$, ft/sec

σ = solidity = C/S (fig. 6), dimensionless

and

$$(DF)_S = 1 - \frac{V_3}{V_2} + \frac{\Delta V_u}{2\sigma V_2} \tag{6}$$

where

$(DF)_S$ = diffusion factor for stator

V_2 = fluid inlet absolute velocity, ft/sec

V_3 = fluid exit absolute velocity, ft/sec

ΔV_u = change in tangential component of absolute velocity = $V_{2u} - V_{3u}$, ft/sec

σ = solidity as above

Diffusion-factor values for hub and tip for the state-of-the-art axial-flow-pump blading are given in table II. Values generally fall within the range appropriate to axial-flow compressors.

Stall margin. – Stall is the loss of pumping capability that occurs in an axial-flow-pump stage when flow separation in the rotor or stator passage progresses to the point where the headrise drops abruptly. Three different conditions have been used to define the stall point in the state-of-the-art axial pumps. Experience with the Mark 9 and "A" through "E" blading (table II) indicated that stall occurred when the rotor-hub or stator-tip diffusion factor reached a value of 0.75 or the retardation factor (RF) dropped to a value of 0.5. As with the diffusion factor, the retardation factor is an index of blade-passage diffusion. It is defined as the ratio of fluid outlet-to-inlet relative velocity:

$$(RF)_R = \frac{w_2}{w_1} \quad \text{(rotor)} \tag{7}$$

$$(RF)_S = \frac{V_3}{V_2} \quad \text{(stator)} \tag{8}$$

In the M-1 design, stall prediction was based on the method reported in reference 21, in which the equivalent diffusion ratio or factor DF_{eq} is used an an indicator of stall. The equivalent diffusion factor is approximately equal to the ratio of the fluid maximum relative velocity on the blade suction surface to the fluid outlet relative velocity. For a blade with thickness-to-chord ratio of 0.10, the equivalent diffusion factors, at minimum loss, for rotor and stator with constant radius are

$$(DF_{eq})_R = \frac{\cos\beta_{2R}}{\cos\beta_{1R}} \left(1.12 + \frac{0.61}{\sigma} \left[\frac{V_{1a}}{w_1} \right]^2 \left[\frac{w_1 \sin\beta_{1R}}{V_{1a}} - \frac{w_2 \sin\beta_{2R}}{V_{2a}} \right] \right) \tag{9}$$

$$(DF_{eq})_S = \frac{\cos\beta_{3S}}{\cos\beta_{2S}} \left(1.12 + \frac{0.61}{\sigma} \left[\frac{V_{2a}}{V_2} \right]^2 \left[\frac{V_{2u}}{V_{2a}} - \frac{V_{3u}}{V_{3a}} \right] \right) \tag{10}$$

In the M-1, stall was considered to occur when either DF_{eq} had a value of 2 (ref. 19).

Figure 7 shows the relation of ideal head coefficient, diffusion factor, efficiency, and flow coefficient for an axial pump stage with a reaction of 0.5 (sec. 2.2.2.2) and a solidity of 1.5. The curves are based on analysis at the 50% streamline (pitchline) and, as noted on the figure, the efficiencies do not include tip clearance loss or other secondary flow losses. Examination of the figure indicates that a design point could be selected to obtain maximum stage efficiency. However, in the state-of-the-art pumps, the design point selection has been made consistent with maintaining a stall margin. The trend has been to design for higher flow coefficients to take advantage of the increased ideal head coefficient at a given diffusion factor. However, for a given flow, pump diameter, and speed, a limit is reached, since as the flow coefficient is increased the blade heights become small and the tip leakage losses become increasingly significant. Note also from the figure that increased stall margin (decreased diffusion factor) for a given flow coefficient, reaction, and solidity can be achieved only at the expense of ideal head coefficient.

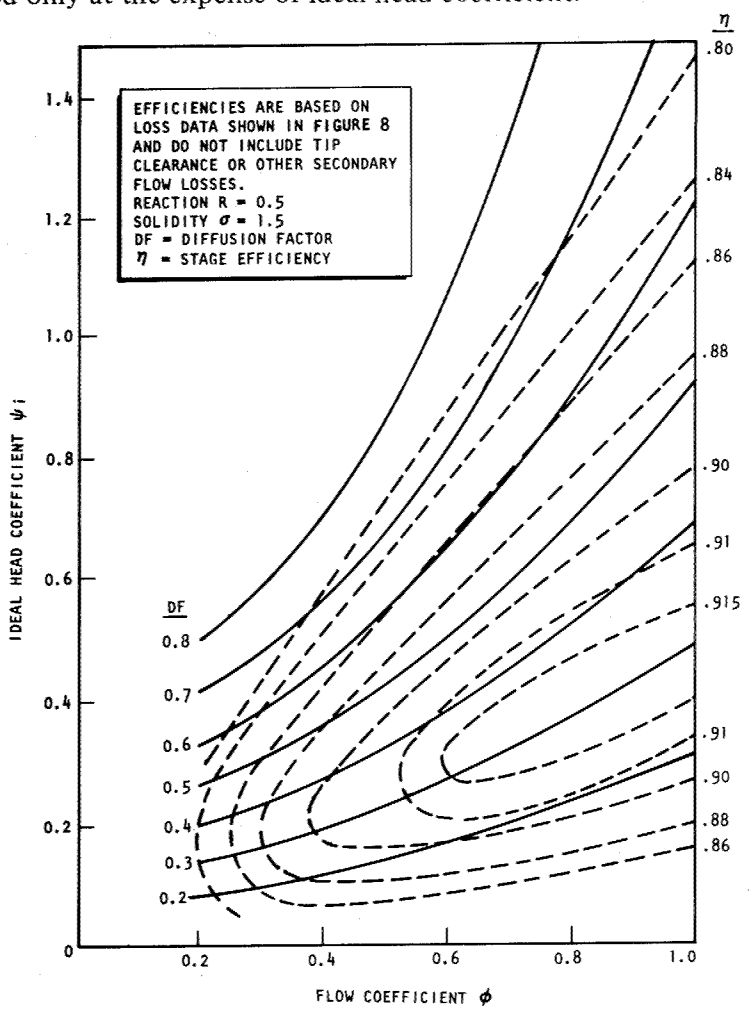

Figure 7. — Relationship of stage ideal head coefficient, efficiency, diffusion factor, and flow coefficient.

2.2.2.1.2 Efficiency

Stage hydraulic efficiency is defined as the ratio of actual headrise H to the ideal headrise H_i:

$$\eta_H = \frac{H}{H_i} = \frac{H_i - H_{loss}}{H_i} \tag{11}$$

where H_{loss} is the sum of the head losses in the stage.

Stage head loss can be broken down into blade profile losses, end-wall friction (annulus) losses, and secondary flow losses produced by the boundary layers and tip clearance. Design-point efficiencies for the axial-flow pump stages are given in table II.

Two methods have been used to predict losses and hydraulic efficiency in the state-of-the-art pumps. In the Mark 9, 15-F, 25, and 26 pumps, an average efficiency was estimated, and the radial loss distribution from hub-to-tip was assumed to be constant. In the M-1 pump, losses were based on the diffusion-factor/total-pressure-loss correlation at reference (minimum loss) incidence developed for axial-flow compressors. The correlation is reproduced here as figure 8 (adptd. from ref. 18). The total-pressure-loss parameter is given by

$$\frac{\bar{\omega}\cos\beta_{exit}}{2\sigma} \tag{12a}$$

where, using the conventions of figures 5 and 6,

$\bar{\omega}$ = total-pressure (head) - loss coefficient

$$= \frac{H_{loss}}{w_1^2/2g_c} \quad \text{(rotor)} \tag{12b}$$

$$= \frac{H_{loss}}{V_2^2/2g_c} \quad \text{(stator)} \tag{12c}$$

β_{exit} = fluid angle at the rotor or stator exit (β_{2R} or β_{3S} in figure 5), deg

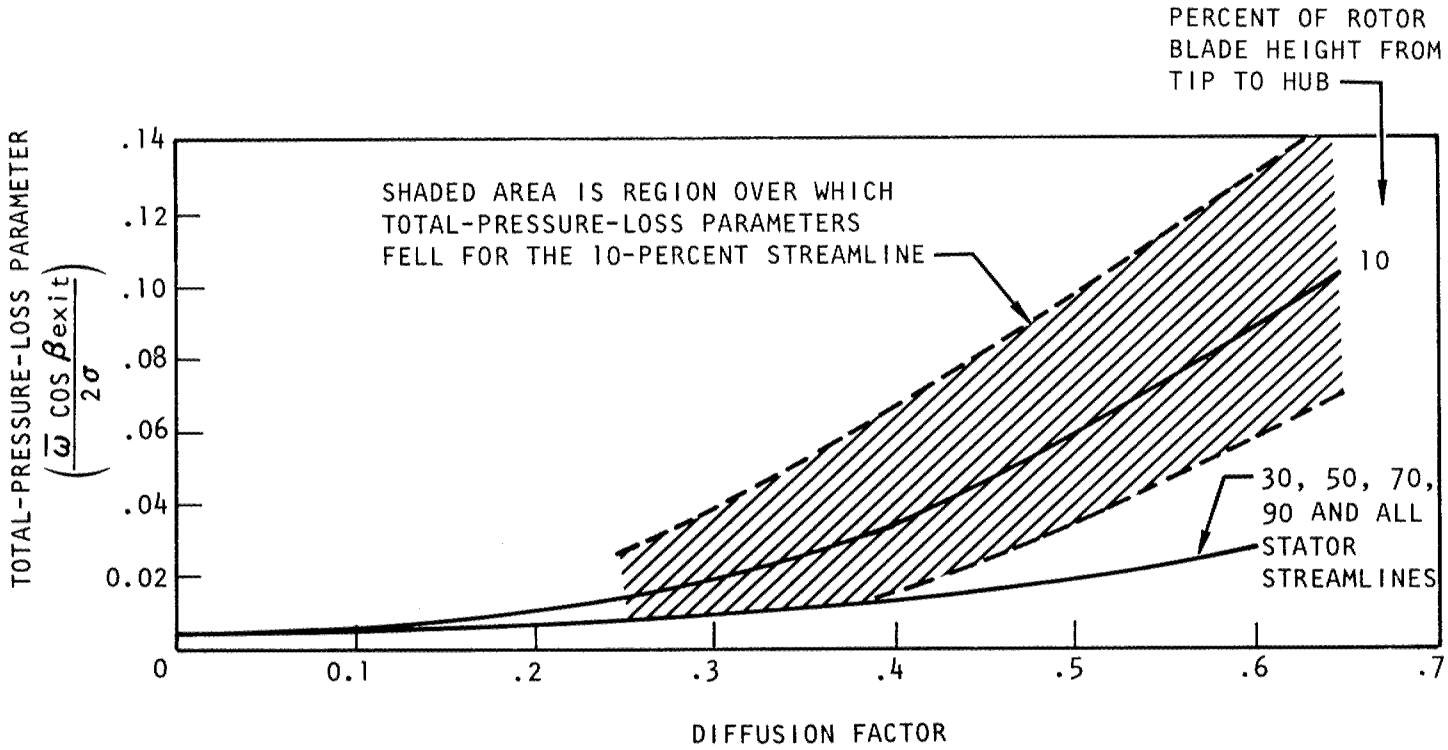

Figure 8. — Variation of total-pressure-loss parameter with diffusion factor at reference incidence for NACA-65-series and double-circular-arc blades (adptd. from ref. 18).

In the design of the M-1 blading, minimum-loss incidence angles were determined by the methods given in reference 18. The lower portion of the shaded area in figure 8 was used to determine the loss parameters for the streamlines at and near the rotor tip. This practice was based on results given in reference 16 that indicated that the magnitudes of the total-pressure-loss correlating parameter for axial-flow pump rotors generally were lower, especially near the tip, than those determined for axial-flow compressor rotors. Reference 16 indicated that a specific explanation for the lower magnitudes was not readily apparent, and in view of limited number of rotors that were tested, no generalization of the results was attempted.

It is important to note that the correlation given in figure 8 cannot be used indiscriminately in the design of axial-flow pumps. This restriction is emphasized in reference 22, which, in summarizing the test results of three axial-pump rotors (including the rotors of ref. 16), cautions that care should be exercised when applying the total-pressure-loss parameter correlation of reference 18 to highly staggered blading in which the flow outlet angles are likely to be outside the range used in the correlation. Effort to extend the range of experimental data was conducted subsequent to the design of the axial-flow pumps discussed in this monograph. Results of this effort are reported in references 23 through 26.

2.2.2.2 VELOCITY DIAGRAMS

For any stage in an axial-flow pump, the type of velocity diagram is in effect established by the selection of a design value for stage reaction R (reaction is defined as the ratio of the static headrise in the rotor to the static headrise in the stage). This selection then sets the degree of velocity diffusion to be accomplished in the rotor and stator and to a great extent influences the efficiency and stall margin magnitudes attainable in the stage. In the state-of-the-art pumps, the dominant factor in the selection of reaction has been stall margin. A symmetrical velocity diagram (i.e., R = 0.5) is therefore desirable, since equal diffusion in the rotor and stator implies that a maximum stage stall margin can be obtained. It has also been shown that maximum profile efficiency for the stage occurs with a symmetrical diagram when the axial velocity of the fluid is equal to one-half the velocity of the rotor blade element (ref. 27).

A free-vortex radial flow pattern has been used in all state-of-the-art axial pumps. In the free-vortex flow the fluid axial velocity is constant from hub to tip while the fluid tangential velocity varies inversely with radius; a symmetrical diagram therefore can be achieved at one radial location only. A selected pump design with a hub-tip ratio of 0.8 was studied parametrically to determine if a forced-vortex flow pattern that imposed a symmetrical diagram at all radii would offer lower loading, better efficiency, or higher head coefficient (ref. 28). It was concluded that for hub/tip ratios of 0.8 and higher, there was no appreciable benefit in using the selected forced-vortex flow pattern. Additionally, it was

concluded that with the free-vortex flow pattern, the radial location of the symmetrical diagram was not critical as long as it was near the mean radius.

Blockage factors are included in the determination of velocity diagrams to account for the reduced flow areas resulting from end wall and blade surface (profile) boundary layers. The magnitudes selected for these factors are dependent on the particular design as well as the design method being used. A design method employing appropriate experimental loss data (used on M-1) automatically accounts for profile boundary-layer blockage and it is necessary only to account additionally for end-wall boundary-layer blockage. In the M-1 pump, this blockage was estimated as 4% of the annulus area. A design method in which average stage efficiencies are estimated must utilize blockage factors that take into account the area reduction due to both end-wall and blade-surface boundary layers. In the Mark 9, 15-F, 25, and 26 pumps, these factors were estimated at approximately 10% of the annulus area on the basis of compressor blade-surface and end-wall boundary-layer information obtained from reference 18.

Analytical and experimental investigations of stages with impulse blading have been conducted (refs. 29 and 30), but to date this type of blading has not been utilized in rocket engine pumps.

2.2.2.3 BLADE ANGLES

With the velocity diagrams established in the meridional plane, the blade angles and blade shape are selected to turn the flow in accordance with the desired diagrams. This selection involves determination of the incidence angle, camber angle, and deviation angle at each of the hub-to-tip streamlines (figs. 5 and 6). The incidence angle is selected by the designer and, for the pumps discussed herein, was based on either minimum-loss or cavitation considerations. Note on figure 6 that, with the incidence angle selected, the amount of fluid turning $(\beta_1 - \beta_2)$ is dependent on the camber angle θ and deviation angle δ. Accurate prediction of the deviation angle is extremely important in achieving the desired diagrams. For example, in reference 27, analysis of a 50%-reaction stage with blade and vane camber angles of 30° and a solidity of 1.0 indicated that an error of 1° in prediction of deviation angle for the rotor and stator row would reduce the stage work by about 8%.

References 18, 27, and 31 give procedures for selection of incidence angles and prediction of deviation angles. In the M-1, incidence angles (at minimum loss) and deviation angles were determined by use of the methods established for compressors in reference 18 on the basis of experimental data obtained from low-Mach-number testing in air. In the Mark 9 and Mark 15-F pumps, a design incidence angle of +3° was selected on the basis of achieving good cavitation performance. In the Mark 25 and 26 pumps, a design incidence angle of 0° was selected on the basis of achieving low loss. In all of these pumps (Mark 9, 15-F, 25, and 26), the design deviation angle was determined from the relationship (ref. 31)

$$\delta = \left[0.23 \left(\frac{2a}{c} \right)^2 + 0.1 \frac{\beta_{exit}}{50} \right] \frac{\theta}{\sqrt{\sigma}} \qquad (13)$$

where

a = distance to the point of maximum camber from leading edge, in.

β_{exit} = fluid exit angle, deg

$\frac{\beta_{exit}}{50}$ = dimensionless ratio

Subsequent to the design of the pumps discussed herein, cascade tests using water as the test fluid were conducted in order to provide an extended range of experimental data applicable to design methods such as those given in reference 18. The data obtained included fluid-turning characteristics and performance for double-circular-arc, multiple-circular-arc, and slotted double-circular-arc profiles over a relatively wide range of fluid inlet angle, camber angle, and solidity (refs. 23 through 26).

2.2.2.4 SOLIDITY

The solidities (σ) of state-of-the-art axial-pump stages are given in table III. These values have, in general, been selected within the limits of available test data. Both hydrodynamic and mechanical design considerations enter into the selection. From a hydrodynamic standpoint it is usually desirable to use as many blades (high solidity) as possible, because for fixed values of reaction, diffusion factor, and flow coefficient the ideal head coefficient increases as the solidity is increased (fig. 9). However, limits are soon reached, since losses increase with increasing solidity (increased skin friction area). Additionally, for a given chord length, high-solidity stages require thin blades, a requirement that may conflict with the thickness desired from a structural standpoint. In such a case, an attempt can be made to achieve the desired solidity by reducing the number of blades and increasing the chord length. Here, the designer is confronted with increased blade row length, increased rotor weight, and potential critical-speed problems with the turbopump rotor.

2.2.2.5 CAVITATION

Rocket engine turbopumps as a rule incorporate inducers as the initial pumping element to provide the capability for operation at low inlet pressures. Inducers are designed to achieve high suction performance and increase the pressure of the pumped fluid to a magnitude that is sufficient to preclude cavitation in the following stage (ref. 2). In order to achieve high

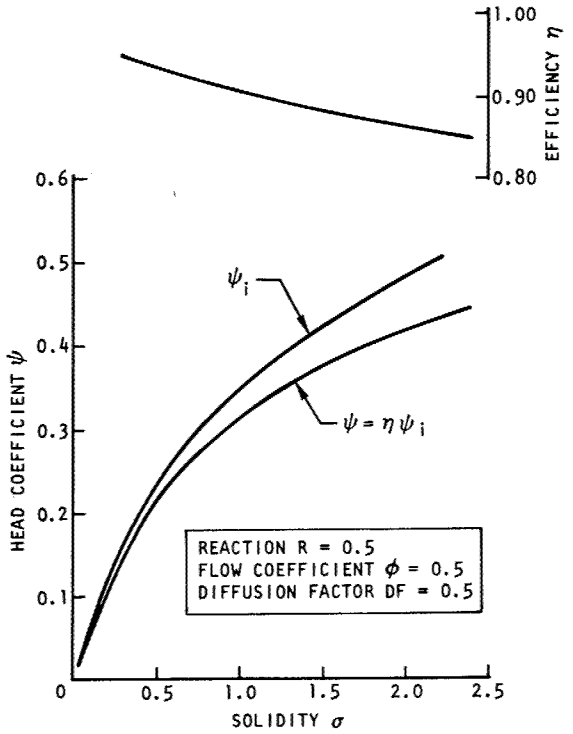

Figure 9. – Effect of solidity on head coefficient and efficiency.

suction performance, low flow coefficients at the inlet are necessary. The inducer stage therefore must provide a transition in flow area from the pump inlet to the inlet of the pumping elements of the higher-flow-coefficient mainstage. Additionally, the exit flow conditions (i.e., fluid velocities and angles from hub-to-tip) must be compatible with the inlet flow requirements of the initial mainstage.

All the state-of-the-art axial-flow turbopumps have utilized inducers as the initial pumping element. In the Mark 9, 15-F, 25, and 26 pumps, the headrise, flow area transition, and mainstage inlet flow requirements were accomplished totally in the inducer stage. In the M-1 pump, a "transition" stage between the inducer stage exit and the mainstage inlet was utilized. The transition stage was a lightly loaded axial stage that provided acceptable flow conditions for the mainstage inlet and achieved better cavitation performance than that possible with the more heavily loaded mainstage blading. A discussion of inducer cavitation along with design criteria and recommended practices for inducers is presented in reference 2. Discusssion here will be limited to transition and mainstage types of axial-flow stages.

Analyses are conducted on the initial axial-flow stages following the inducer to ensure that sufficient pressure is available to prevent headrise degradation caused by cavitation. This can be accomplished by comparison with cavitating test results of similar designs or by analysis of fluid velocities on the blade surface. The cavitation parameter τ_t

$$\tau_R = \frac{NPSH}{u^2/2g_c} \tag{14}$$

and cavitation number K

$$K = \frac{P_f - P_v}{\rho_f w_1^2/2g_c} \tag{15}$$

where

NPSH = net positive suction head, ft-lbf/lbm

P_f = fluid static pressure, lbf/ft^2

P_v = fluid vapor pressure, lbf/ft^2

ρ_f = fluid density, lbm/ft^3

which are commonly used in inducer design, have also been used to evaluate the cavitation characteristics of the axial-flow blading.

Cavitation performance data on axial-flow blading are relatively limited. Several axial pump rotors with double-circular-arc blade profiles have been tested and the results are reported in references 15 through 17 and 32 through 34. Cavitation head loss data for these rotors are given in figure 10 in terms of the cavitation parameter τ_t and a cavitation breakdown correlation parameter Z developed for inducers (ref. 35). The solid line in the figure represents the cavitation parameter magnitudes at which head breakdown will occur for flat-plate inducers according to the modified two-dimensional theory of reference 35. The figure shows that the high-head-loss (i.e., head breakdown) data for the NASA $\nu = 0.4$ and $\nu = 0.7$ axial rotors compare favorably with the inducer theory of reference 35. These rotors were lightly loaded with little or no camber at the tip (DF = 0.223, $\theta = 5.43°$, and DF = 0.426, $\theta = 0°$, respectively). As might be expected, data from the more heavily loaded and highly cambered NASA $\nu = 0.8$ axial rotor (DF = 0.664, $\theta = 27°$) did not correlate well with the flat-plate inducer theory.

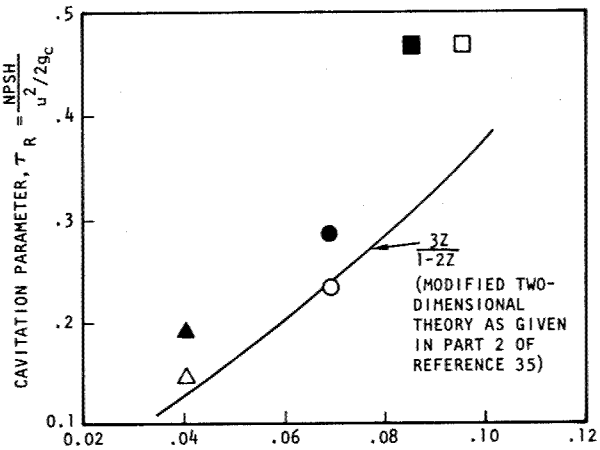

HEAD LOSS	β_T	r_H/r_T	REF.
▲ 3% △ 40%	17.1°	0.4	15
● 0% ○ 34%	22.9°	0.7	16
■ 5% □ 46%	21.5°	0.8	17

NOTE: β_T AS USED HERE IS THE BLADE TIP ANGLE MEASURED FROM A PLANE NORMAL TO THE AXIS OF ROTATION.

Figure 10. — Comparison of theoretical and experimental cavitation breakdown parameter for double-circular-arc profiles.

In view of the lack of cavitation performance data on similar designs, analysis of fluid velocities on the blade surface has been used to evaluate the cavitation characteristics of the state-of-the-art blading. In the Mark 9, 15-F, 25, and 26 pumps, fluid velocities on the blade surface were determined by use of a stream-filament method (ref. 18). The minimum local static pressure on the blade surface was then determined and compared with the fluid vapor pressure to ensure that the pumps would be free from cavitation. An approximate method for predicting incipient cavitation of airfoil-type blading was used in the M-1. The method utilizes the equivalent diffusion factor DF_{eq} (sec. 2.2.2.1) along with the cavitation parameter τ_R and the cavitation number K. An approximate value for the ratio of maximum fluid velocity on the blade surface to fluid velocity at the blade inlet was derived by using the equivalent diffusion factor. This ratio was then related to the NPSH requirement for the blade by use of the cavitation number K and the cavitation parameter τ_R. The results of this method for blade profiles with a thickness-to-chord ratio of 0.10, reaction = 0.5, and solidity = 1.5 are shown in figure 11. For a blade row with a given design flow coefficient

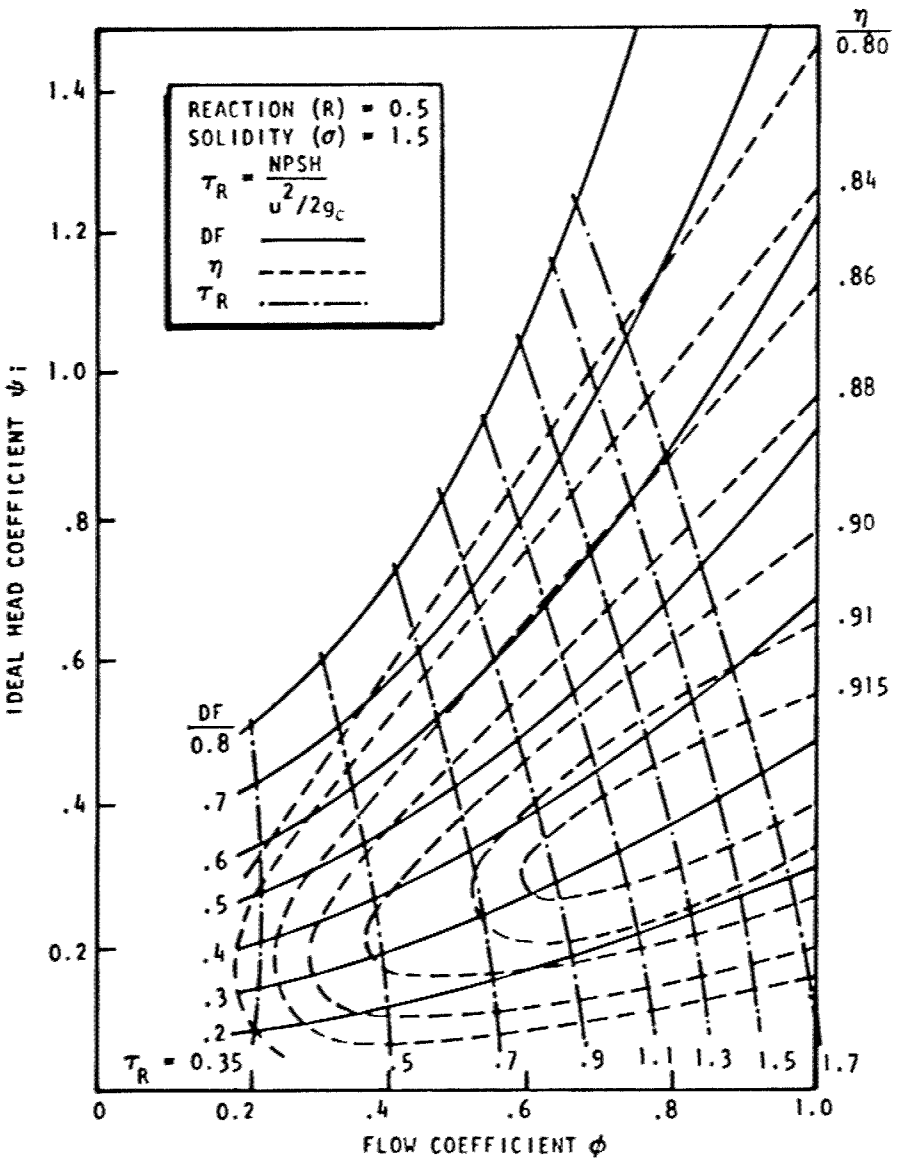

NOTES: VALUES FOR CAVITATION PARAMETER (τ_R) ARE BASED ON BLADE WITH THICKNESS-TO-CHORD RATIO OF 0.10.

STAGE EFFICIENCIES ARE BASED ON THE CORRELATION OF TOTAL-PRESSURE-LOSS PARAMETER VERSUS DIFFUSION FACTOR AT THE 50% STREAMLINE AS SHOWN ON FIGURE 8 AND DO NOT INCLUDE TIP-CLEARANCE OR END-WALL LOSSES.

Figure 11. – Correlation of pump cavitation parameter with ideal head coefficient, flow coefficient, stage efficiency, and diffusion factor.

and ideal head coefficient, the required NPSH can be determined from the cavitation parameter τ_R. With the required NPSH known, the headrise requirement of the previous (inducer) stage then can be determined.

2.2.2.6 OFF-DESIGN PERFORMANCE

Analysis of off-design performance must be made so that pump performance can be predicted for engine transients, mixture-ratio excursions, and chamber-pressure excursions. In general, the prediction methods involve assumptions as to how the deviation angle and blade-element losses vary with incidence angle.

Reference 19 gives off-design predictions for the M-1 based on (1) the two-dimensional blade-element method of reference 36 and (2) a one-dimensional mean-line analysis* in which deviation angle was assumed to be constant at the design point value and blade channel losses were assumed to vary according to results of low-Mach-number air tests at the 50% streamline but at a higher level to account for tip leakage and end-wall boundary-layer losses. Comparision of predictions with M-1 test results indicated that the one-dimensional mean-line analysis was the more reliable prediction method. Off-design performances of the Mark 15-F and Mark 25 were predicted with a one-dimensional mean-line analysis in which deviation angle and blade channel losses were assumed to be constant at their design point values. Off-design loss was assumed to be equal to the velocity head of the normal velocity component that resulted from the variation in incidence angles on the rotors and stators at the off-design flow conditions (see sketch below). This method correlated favorably with test results. Curves of predicted and measured headrise versus flowrate for the Mark 25 pump are given in reference 9.

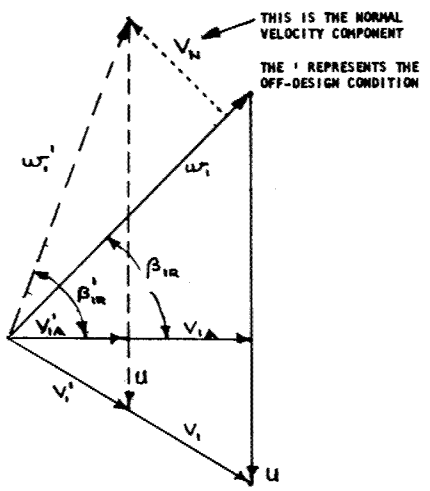

In general, the off-design performance required of the state-of-the-art pumps in regard to engine mixture-ratio or chamber-pressure excursion (at design point thrust) has not caused any problems. However, there was a tendency for the Mark 15-F pump to stall at three distinct operating levels during the engine transients in the J-2 engine start.

*Analysis based on values at the 50% streamline (fig. 5).

Start problems are not unique to engines with axial-flow pumps but are related to the interaction of the pump (whether axial or centrifugal) and the thrust chamber. For example, the RL10 engine, which employed centrifugal pumps for both oxidizer and fuel, had start problems similar to those on the J-2. Both the J-2 and the RL10 are regeneratively cooled engines in which the hydrogen flow from pump discharge is routed through tubes around the thrust-chamber walls and serves as a coolant before it is injected into the combustion chamber. Start anomalies have been associated with reduced fuel flow coincident with rapid increases in thrust-chamber coolant-circuit pressure or in chamber pressure. The consequence of the reduced fuel flow (which in the axial pump may be a stalled condition) is somewhat dependent on the engine system cycle, but in severe cases the typical result is damage to the thrust chamber as a result of inadequate cooling.

Figure 12 illustrates the three potential stall points of the Mark 15-F pump during the J-2 engine start transient; these potential stall points were termed spin-down stall, LOX-dome-prime stall, and high-speed stall.

Spin-down stall. – Spin-down stall occurred during initial fuel-pump acceleration (start-tank discharge) and prior to main propellant ignition. The fuel flowrate was rapidly accelerated by the pump and was discharged relatively unrestricted into the thrust-chamber cooling tubes. During this interval, the fuel was warmed by the thrust chamber, and a portion was vaporized. The warm fuel then encountered the high resistance of the upper combustion zone and injector, and injector pressure drop increased quickly. The head demand on the fuel pump quickly increased, and flowrate dropped. Thus the process of priming the chamber with fuel was characterized by an initial flowrate overshoot followed by an undershoot. Spin-down stall was avoided on the J-2 by thermal preconditioning of the chamber.

Several methods of chamber preconditioning were utilized: a long fuel lead (up to 8 sec.), pre-start purge with cold nitrogen, and pre-start purge with cold helium. With some development, each of these methods produced satisfactory starts. However, each produced a different temperature gradient on the chamber, so that an index of the degree of chill from a single temperature measurement was uncertain. Thrust-chamber preconditioning is undesirable from an operational point of view, and several alternatives have been employed. The RL10 engine system incorporates an overboard fuel dump to avoid the high resistance of the injector during start. On the J-2S and J-2X engines, a bypass line around the thrust-chamber cooling tubes has been employed successfully. The cooling-tube-bypass technique was attractive from the standpoint of utilizing the hydrogen as a film coolant in the combustion chamber during the start and during low-level operation.

LOX-dome-prime stall. – The second stall point, indicated as LOX-dome-prime stall on figure 12, occurred when the oxidizer flow primed the dome manifold of the injector, and chamber pressure quickly increased to over 150 psi. This increase in chamber pressure caused an immediate demand for increased fuel-pump head. Since the speed change could not occur

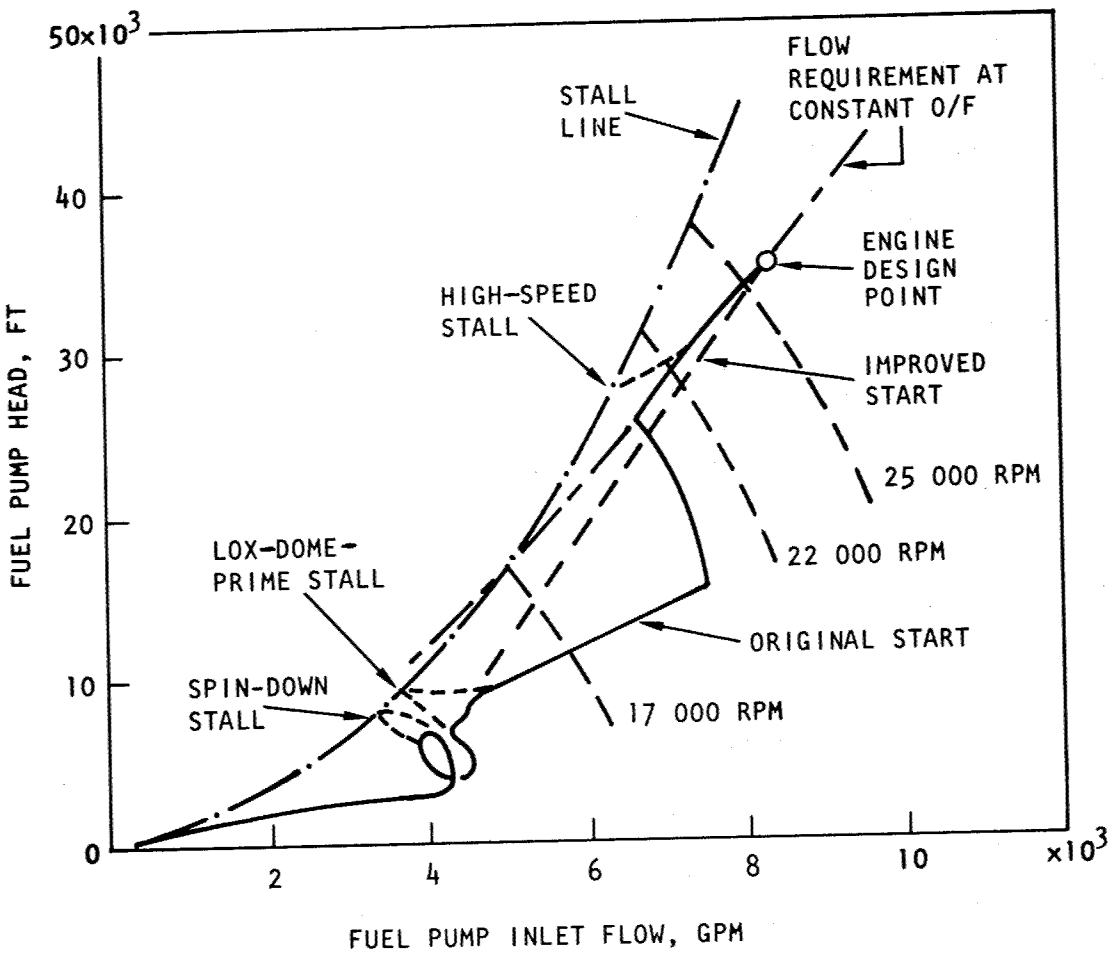

Figure 12. — Potential stall points of Mark 15-F pump during start of the J-2 engine.

instantaneously, pump head was achieved at the expense of reduced fuel flow. Thus, as shown in figure 12, the fuel pump underwent a transient along a constant speed line from high flow and low pressure to low flow and high pressure.

Control of fuel-pump flow coefficient (and therefore contol of nearness to stall) was achieved by regulating the magnitude of the chamber pressure following dome prime. The most effective technique utilized a throttleable main oxidizer valve. In both the J-2 and RL10 engines, this method was used to restrict oxidizer flow during the early portion of engine start. Initial Mark 15-F pump stall problems at LOX dome prime were relieved on the J-2 by two system changes: (1) the initial opening of the main oxidizer valve was reduced; and (2) the pump speed during this portion of the start was increased by utilizing a higher pressure in the hydrogen-gas spin bottle.

High-speed stall. — The third stall point, high-speed stall, was similar in nature to the LOX-dome-prime stall. The J-2 engine is orificed for an oxidizer/fuel mixture ratio (O/F) of 5.0 at the design-point thrust level (fig. 12). During thrust buildup, the engine seeks this O/F value; as noted in the previous paragraph, O/F control was necessary and was achieved by restricting oxidizer flow with the main oxidizer valve. The so-called high-speed stall became a problem if the main oxidizer valve reached full open before engine thrust had built up to a sufficiently high level.

2.2.2.7 CLEARANCES

As the hub/tip ratio of an axial pump increases, the tip clearance area becomes an increasingly high percentage of the total annular flow area, and the tip clearance losses become an increasingly high percentage of the stage work. In state-of-the-art stages hub/tip ratios are relatively high, and considerable attention has been given to maintaining small tip clearances in order to keep these losses low. The rotor-blade radial tip clearance on the Mark 15-F pump was set so that the running clearance was approximately 0.005 in.; the stator-vane tip clearance was 0.015 in. The M-1 pump was designed to operate at a blade running clearance of 0.020 in. with a vane running clearance of 0.049 in. (this was a shrouded configuration — see fig. 3).

The Mark 9 pump was tested in air to determine the effect of variations in rotor and stator tip clearances. The results showed that the pump was rather insensitive to changes in stator tip clearance within the range tested (0.95% to 3.25% of vane height) (ref. 37). However, an appreciable amount of head was lost, particularly near the stall point, as the rotor tip clearance was increased from 1.58% to 3.57% of the blade height. The more pronounced effect of changing rotor clearance was not unexpected, since the velocity diagram for the Mark 9 pump is not symmetrical and the static pressure rise in the rotor is substantially higher than that in the stator. The air tests also showed that the stall margin of the pump decreased as the rotor tip clearance was increased. (This clearance effect on stall also was

observed in tests with liquid hydrogen but was not systematically investigated.) Attempts at determining the effects of tip clearance on efficiency during the tests were unsuccessful because of the relatively small rise in air temperature.

Axial clearances between blades and vanes in general have been selected to minimize overall pump length while maintaining adequate protection against blade and vane axial interference or vibration during pump operation. In the Mark 25 and 26 pumps, the mechanical design of the blades and vanes from a vibration standpoint was based in part on maintaining a specified axial clearance between rotor and stator rows. The analysis for establishing acceptable axial clearances considers the forced vibration amplitude of a blade or vane to be a function of the wake velocity fluctuation of the upstream row. The velocity fluctuation in turn is a function of the relation of axial spacing to upstream cord length and the proximity to resonance of the blade natural frequency with the wakes from the upstream row. The analysis is based on information presented in references 38 through 42.

2.3 PUMP ROTOR ASSEMBLY

The pump rotor assembly as discussed here consists of the blades, the pump rotor structure, and the thrust balance system. Three concepts have been utilized in the design of the state-of-the-art rotor assemblies (fig. 13): a one-piece rotor structure with integral blading (Mark 15-F and Mark 26), a builtup rotor assembly consisting of disks (with integral blading) clamped together by through-bolts (Mark 9 and Mark 25), and a builtup rotor assembly consisting of a welded rotor structure and dovetail blades (M-1).

2.3.1 Blades

2.3.1.1 PROFILE TYPES

As indicated in section 2.2.2, the hydrodynamic design procedure involves the selection and setting of blade profiles that will turn the fluid so that the desired velocity diagrams are achieved (i.e., the fluid will be turned through the desired angle with the predicted loss). Research and development of blading for axial-flow compressors yielded considerable data on so-called standard profiles These profiles included the NACA-65 series, the British-C series, and the double circular arc with maximum thickness at midchord. In the M-1, a standard profile (British C-4) was used. The remaining state-of-the-art pumps utilized "non-standard" profiles that were either modified double-circular-arc profiles or special profiles designed to achieve a prescribed blade surface velocity distribution to avoid excessive surface diffusion. Values for the significant profile design parameters employed in axial pumps are listed in table III; typical profile nomenclature is illustrated in figure 14.

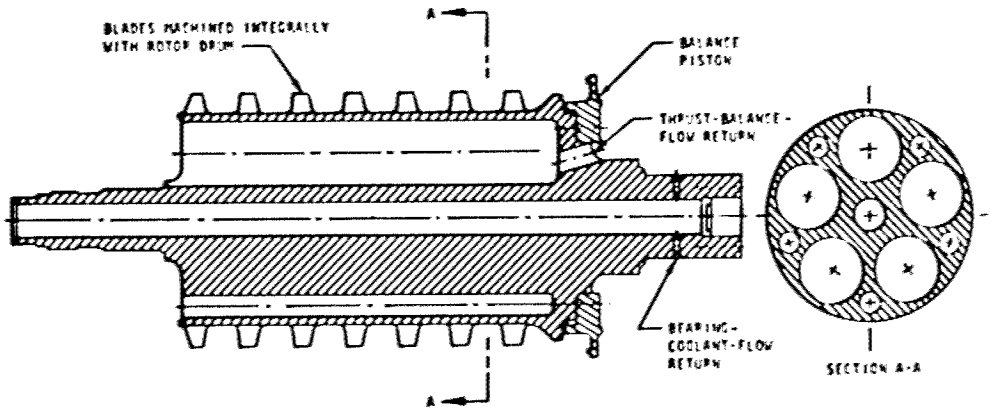

(A) MARK 15-F

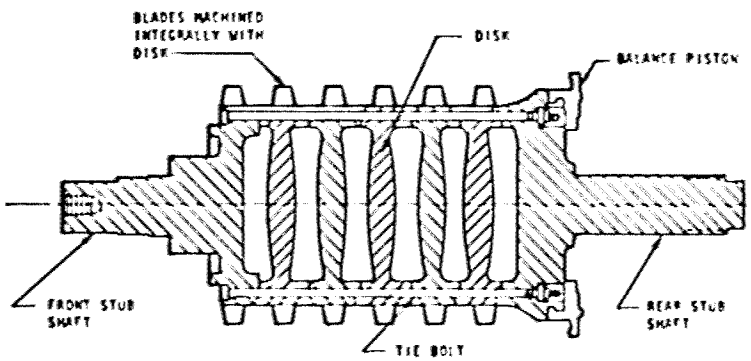

(B) MARK 9

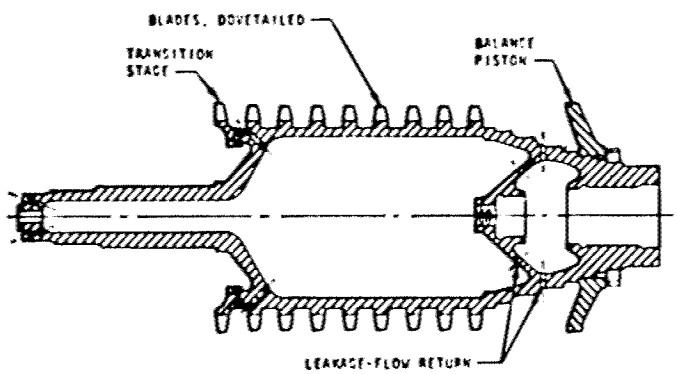

(C) M-1

Figure 13. – Three types of rotor assemblies.

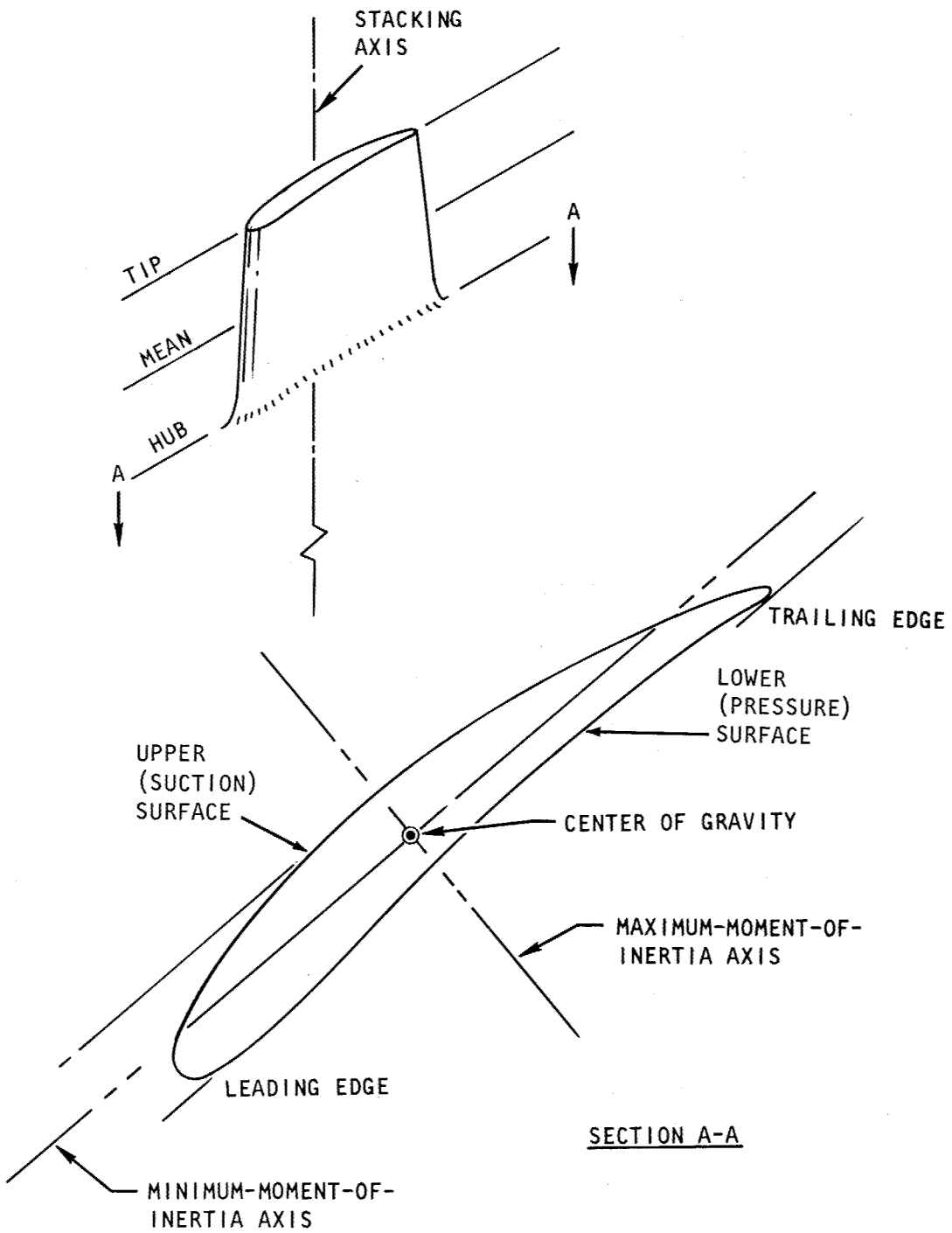

Figure 14. — Typical profile nomenclature.

Standard profile shapes are defined by a specified thickness distribution about a mean camber line (fig. 6). Basic thickness distributions for some of the profiles used in compressors are compared in figure 15 (adptd. from ref. 18). On the non-standard profiles, the thickness distribution is that which is required to satisfy the desired distribution of surface velocity on the blade profile.

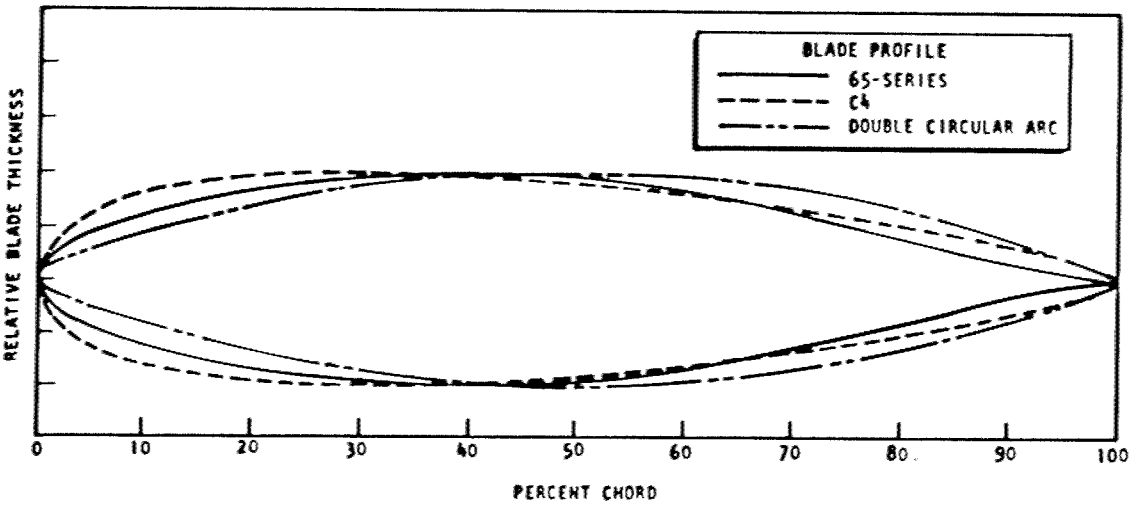

Figure 15. – Comparison of basic thickness distributions for three profiles (adptd. from ref. 18).

The selection of a blade profile is based on both hydrodynamic and mechanical design considerations. According to reference 43, within maximum thickness requirements imposed by stress considerations, profiles for axial-flow pumps would have a flat velocity distribution in order to reduce cavitation to a minimum. Further, the ideal velocity distribution would be one in which the (limited) maximum local surface velocity is maintained over as much of the upper (suction) surface as is possible, commensurate with good diffusion on the rear portion. In achieving a flat velocity distribution, maximum thickness and maximum camber are positioned well back. The non-standard profiles used on the Mark 9, 15-F, and 25 pumps were designed (with the stream-filament method of ref. 18) to control the velocity distribution such that the maximum suction-surface velocity did not exceed 1.2 times the inlet velocity. The resulting profiles had a thin leading edge with maximum thickness at about 0.6 of the chord. The Mark 26 pump utilized a modified double-circular-arc profile with leading-edge radius larger than trailing-edge radius (primarily to obtain a stiffer blade for stress reasons). As previously noted, the British C-4 profile was used for the M-1 axial-flow stages. Research has also been conducted on standard

double-circular-arc profiles (refs. 15 through 17, 23, and 32 through 34), on multiple-circular-art and slotted double-circular-arc profiles (refs. 24 and 25) and on variations of profiles similar to those used on the Mark 26 (ref. 44).

From a mechanical-design standpoint, the structural merit of the profile is reflected in the camber angle, the chord length, the thickness distribution, and the maximum thickness-to-chord ratio. The camber angle is established by the hydrodynamic design. For a given chord and thickness distribution, increased blade strength is achieved by increasing maximum thickness-to-chord ratio. From the hydrodynamic standpoint, however, it is desirable to maintain low blade thickness. Thus, a mechanically desired maximum thickness-to-chord ratio may not be achievable (note in table III that a maximum value of 0.15 was used in the state-of-the-art blading). Increased blade strength also may be achieved by increasing the chord, maximum thickness-to-chord ratio being held constant. However, with a given solidity (sec. 2.2.2.4), this procedure requires a decrease in the number of blades so that, again, a limit may be reached from the hydrodynamic standpoint.

2.3.1.2 MECHANICAL DESIGN

The predominant requirement in the mechanical design of axial pump rotor blades is that the blade withstand the combined steady-state and vibratory stresses for the required life of the pump. Basically, the design procedure is an iterative one in which steady-state stress is kept within specified material property limits based on either yield or ultimate strength, and vibratory stress is kept below the material fatigue limit corresponding to the steady-state stress condition. These structural considerations must be met without unacceptable compromises in the hydrodynamic design. The steady-state stresses due to centrifugal and hydrodynamic loads are predictable (ref. 45); the unsteady hydrodynamic loads and the response of the blading to these loads can, at best, only be estimated. As a result, analysis of blade vibratory stress is one of the more intractable areas in axial-flow pump design.

The type of stresses to which the blade is subject is highly dependent on the blade geometry. In the state-of-the-art blading, it usually has been necessary to consider only the normal stresses due to the centrifugal, steady-state hydrodynamic (fluid force), and vibratory loads. The normal and shear stresses due to gyroscopic forces and untwist forces due to centrifugal load and hydrodynamic moment about the stacking line have been of negligible magnitudes. Blade tilt (to provide a recovery moment to counteract hydrodynamic moment) has not been utilized in the blading discussed in this monograph.

In appraising structural adequacy, the combined steady-state and vibratory stresses predicted to occur during pump operation are compared with blading material properties by the use of modified Goodman diagrams (fig. 16). As indicated above, vibratory stress magnitudes in general are not accurately predictable. This uncertainty has been handled by assuming that the vibratory stress was proportional to the hydrodynamic stress

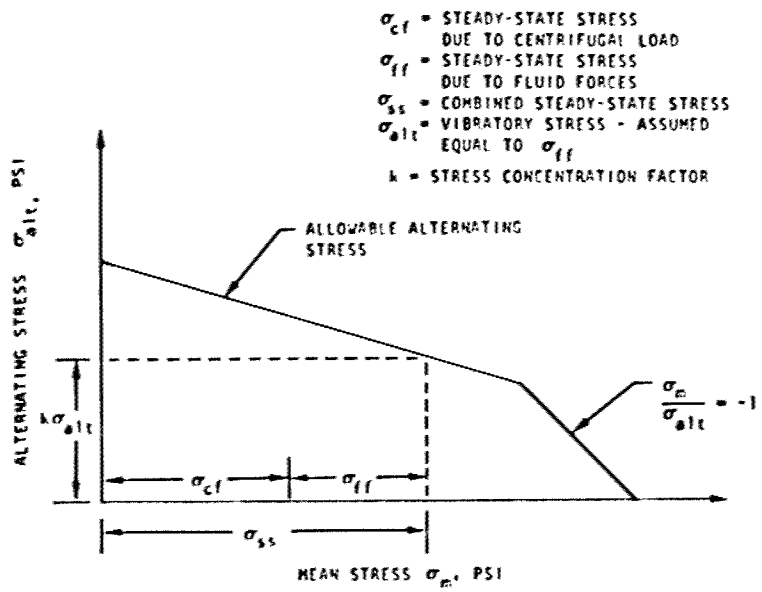

Figure 16. – Typical modified Goodman diagram for blade stress.

(proportionality factors have ranged from 0.3 to 1). A stress-concentration factor for the blade root fillet is estimated and applied to the vibratory stress; this stress magnitude is then plotted on the Goodman diagram along with the calculated maximum steady-state stress. The design is deemed acceptable if the point falls within the material failure envelope and a blade resonant condition is known not to exist at the design speed.

To identify resonant conditions, Campbell diagrams (plots of pump speed vs blade frequency, with forcing function as a variable) have been used. A typical Campbell diagram for rotor blade resonant conditions is shown in figure 17. Typically, blades have been designed so that at least a 15-percent margin on operating speed was maintained between blade natural frequencies and known sources of excitation. Wakes from preceding blade rows or other obstacles in the flow stream are the predominant sources of excitation in axial-flow pumps. Rotating stall has been observed but has not been identified as an excitation source for any of the axial-pump blade failures that have occurred.

There have been no known instances of self-excited blade vibration (flutter) in the axial-flow pumps discussed in this monograph. In general, the aspect ratio (blade length divided by the chord length at the root) of the blading has been low and has resulted in relatively stiff blades with little likelihood of flutter. Adequacy of the blading in regard to flutter has been checked by the empirical rules given in reference 39.

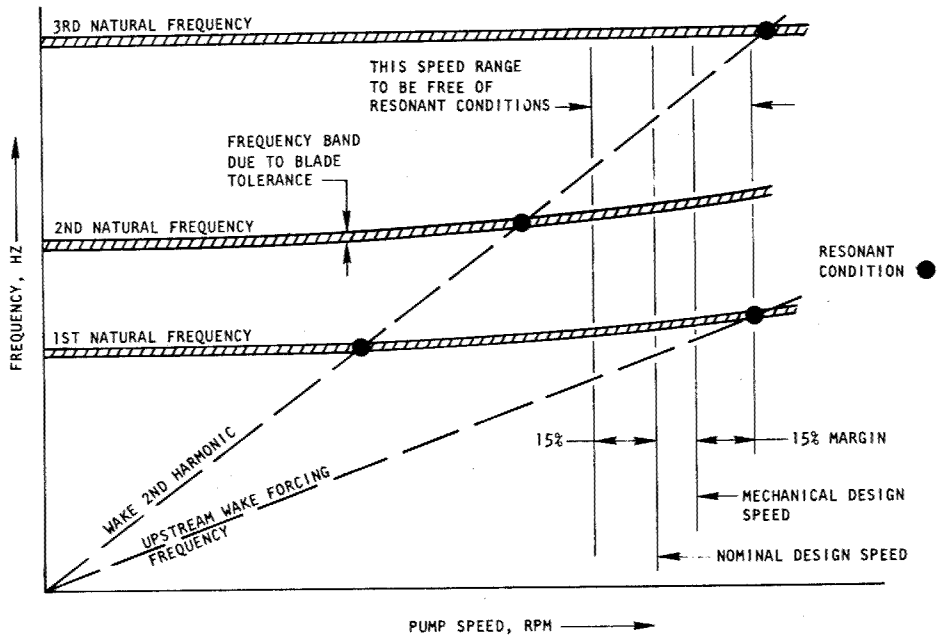

Figure 17. – Typical Campbell diagram for identifying blade resonant conditions.

Considerable effort has been devoted to the difficult problem of analytically determining the blade natural frequencies for Campbell-diagram and flutter analyses. In the M-1, the aspect ratio of the blading was approximately 1, and computer solutions of lumped parameter models of cantilevered beams (ref. 46) predicted natural frequencies that compared reasonably well with experimental results (ref. 47). Other pumps have had blading with lower aspect ratios, and the cantilevered-beam approach has not been sufficiently accurate to predict all the natural frequencies. Blade fatigue failures that have occurred have been attributed largely to this inadequacy, in that unpredicted natural frequencies were in resonance with upstream sources of excitation.

In most cases, the expedient solution to failure problems has been to modify the existing blade rather than to redesign it. For example, instances of first-stage rotor-blade fatigue failures on the Mark 15-F were eliminated by cutting back the chord at the tip by ¼ in. and tapering the leading edge to the hub as shown in figure 18. This change increased the natural frequency of the blade to a magnitude that was above the forcing frequency, so that the resonant condition during pump operation was eliminated, as shown by the Campbell diagram in figure 19. A course of action involving modification of existing parts rather than

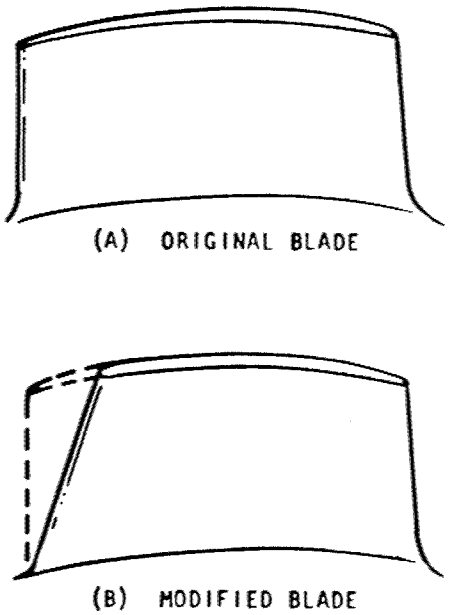

Figure 18. – Modification of Mark 15-F first-stage blade to eliminate resonance

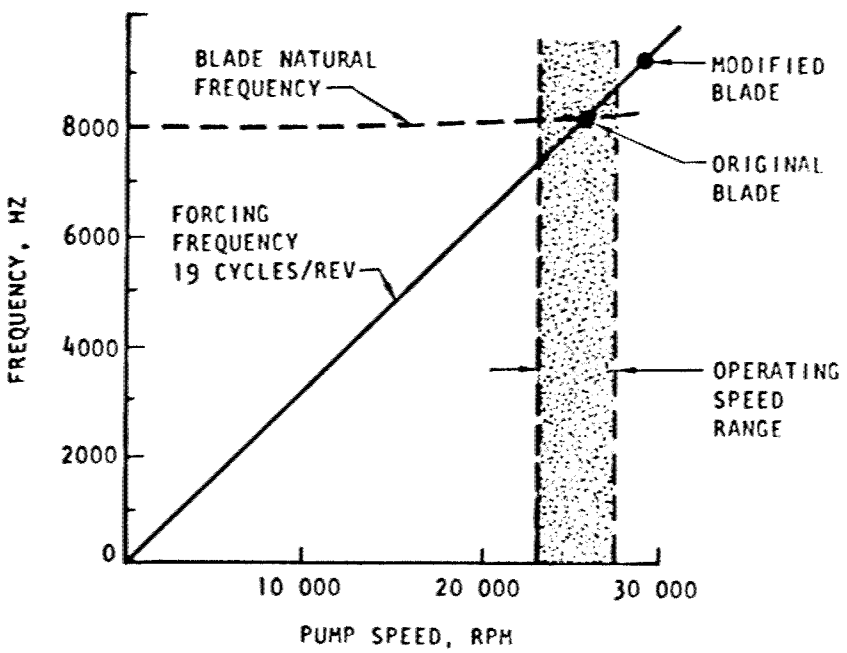

Figure 19. – Campbell diagram for Mark 15 F first-stage blade

redesign can be taken only when the performance penalty associated with the modification is at a tolerable magnitude from the engine system standpoint. The Mark 15-F first-stage rotor blades were not tested to determine the degradation in stage performance caused by the modification described. However, the modification did not noticeably affect overall pump performance.

2.3.1.3 PROFILE TOLERANCES, SURFACE FINISH, AND FILLET RADII

It is necessary to manufacture blade profiles within fairly strict tolerance limits in order to achieve the desired hydrodynamic performance. Typically, the tolerance on the basic blade profile has been specified as ± 0.002 in. with the requirement of a smooth and continuous fairing in both the transverse and longitudinal directions. In order to achieve the desired fluid angles (fig. 6), the blade angles typically have been held to within ± ¼°. The surface finish of the profile can affect both the performance and the fatigue strength of the blade. A maximum surface roughness of 63 microinches (μin.) rms has been specified as a requirement for the state-of-the-art blading. In practice, the methods necessary to manufacture the blade within dimensional tolerances usually have produced a surface finish better than 63 μin. For example, the M-1 blades as manufactured typically had surface finishes of 32 μin. rms.

Fillet radii at the juncture of the blade profile and its support (root section) have been kept as small as possible consistent with maintaining a reasonably small stress-concentration factor. Fillet radii have ranged from approximately 30% to 60% of the profile maximum thickness. Stress-concentration factors, applied to the vibratory stress (sec. 2.3.1.2), have been estimated on the basis of information such as that given in reference 48.

2.3.2 Blade Attachment

2.3.2.1 METHODS

Axial-pump blading has been machined integrally with disks or a rotor drum on all state-of-the-art pumps with the exception of the M-1 mainstage blades, which had dovetail attachments (fig. 20). The selection of a blade attachment method for an axial pump is based principally on weight, manufacturing, and assembly considerations. In general, a pump rotor in which the blades are mechanically attached will be heavier than one with integrally machined blades. This difference is due to the heavier rotor structure required to carry the centrifugal load of the attachment. However, if large manufacturing lots of blades are required, it may be possible to produce a lower-cost rotor assembly by using individual blades, and this cost benefit may override the weight benefit of integrally machined configurations. The M-1 pump rotor, for example, had 376 mainstage blades in comparison

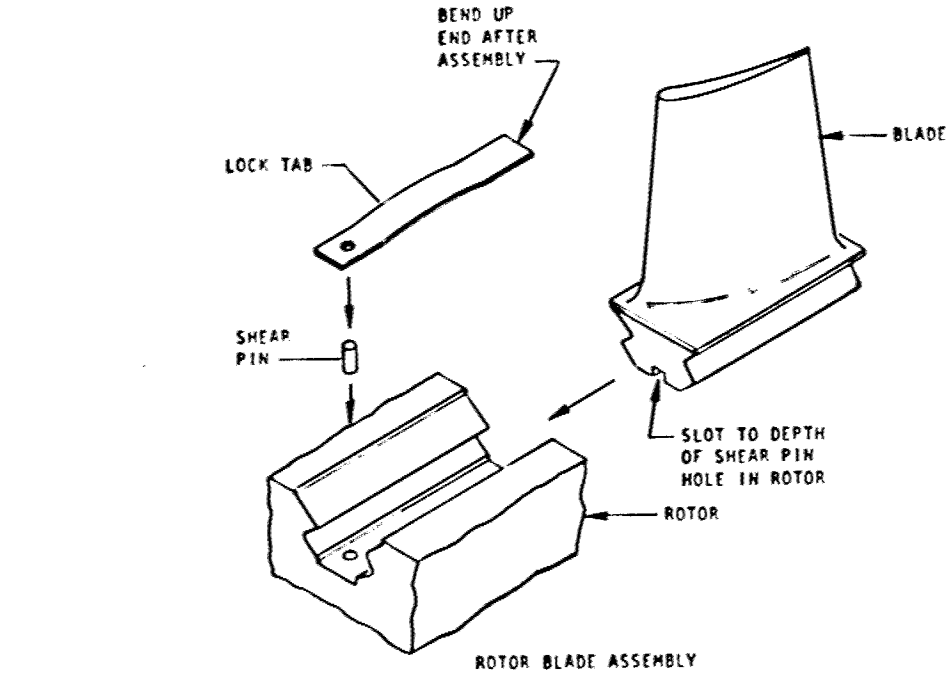

ROTOR BLADE ASSEMBLY

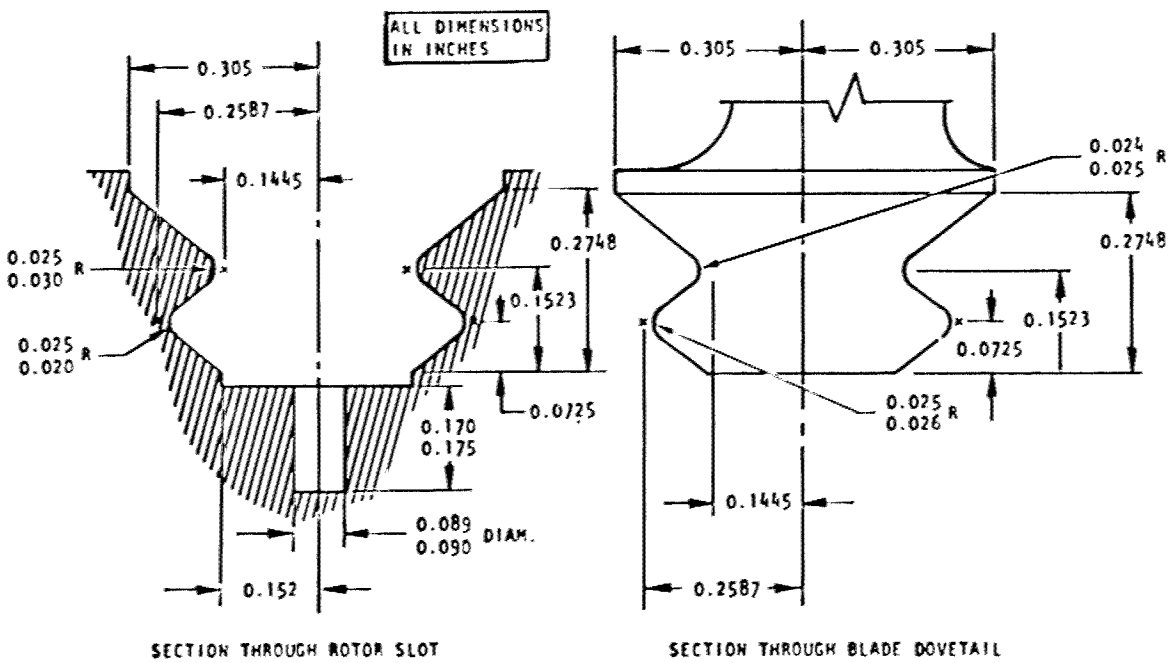

SECTION THROUGH ROTOR SLOT

SECTION THROUGH BLADE DOVETAIL

Figure 20 – Design details for M-1 dovetail attachment.

with 102 for the Mark 9; the cost of machining such a large number of blades made an integral-blade design very expensive. The requirement for individual blade replacement because of potential damage by foreign objects has not been a consideration in selecting the attachment method, because this type of damage is rare in rocket engine pumps.

2.3.2.2 MECHANICAL DESIGN

The blade attachment must be designed to carry the centrifugal load of the blade and to transmit the airfoil steady-state and vibratory bending loads to the rotor structure. The M-1 utilized a single tang dovetail as the blade attachment method (fig. 20). Stress analysis at the critical section of the dovetail (the neck section) was based on the centrifugal load of the blade and design steady-state and vibratory airfoil loads (transposed to the neck section). Structural adequacy was achieved in the same manner as that used for the airfoil; that is, the maximum steady-state stress was kept within specified material property limits based on tensile strength and the vibratory stress was maintained below the material fatigue limit corresponding to the steady-state stress condition.

The attachment configuration must also include provisions for axial positioning and retention of the blade. In the M-1, it was additionally desired to position the blade radially outward so that the rotor assembly could be tip ground with the blades in the same dovetail contact situation that would exist during operation. These requirements were met with shear pins and the lock tabs (designed as leaf springs to exert a force on the bottom of the dovetail) as illustrated in figure 20. Note that incorrect assembly was not possible with this attachment method.

Stresses in the attachment were calculated by assuming that the pin acted as a cantilever beam with the blade force in the direction parallel to the dovetail slot acting at the tip of the pin. No allowance was made for frictional resistance to sliding that could occur at the blade dovetail and rotor slot interface. Note in figure 20 that reverse load (i.e., load in a direction toward pump discharge) would be counteracted by the bentup tab. The source and probability of such a load, however, were not definable.

2.3.3 Rotor

2.3.3.1 CONFIGURATION

Three rotor-structure concepts have been utilized in the state-of-the-art pumps. A one-piece rotor structure, machined from a single forging, was used on the Mark 15-F and Mark 26 pumps (fig. 13). A number of axial holes were machined in the forging to provide a return flow path for thrust balance system and bearing coolant flows and to lighten the structure. The M-1 rotor structure was a one-piece (hollow) configuration fabricated from four forged and machined ring components TIG welded together as shown in figure 21. The Mark 9 and

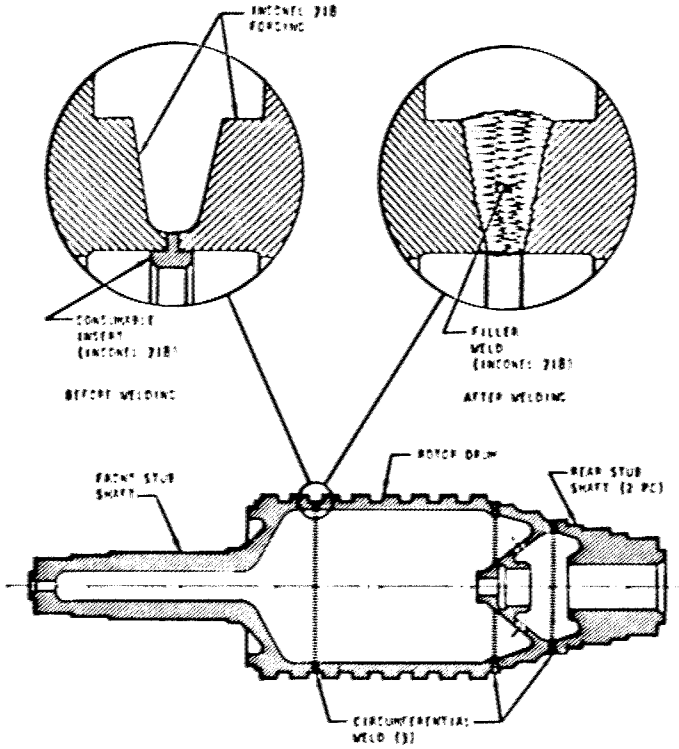

Figure 21. — Fabrication of M-1 fuel-pump rotor.

Mark 25 pump rotors used the builtup concept with the disks and stub shafts clamped together with through bolts (fig. 13). Rabbets were used to attain relative radial positioning, the torque loads being transmitted by shear in the tie bolts.

The choice between a one-piece or builtup pump rotor is made during the turbopump conceptual or preliminary design phase. Considerations such as size, manufacturing methods, assembly methods, and critical speed influence the selection. In the initial design of the Mark 15-F, a comparison of rotor types indicated that a one-piece design with integral blades would result in lowest cost and weight (ref. 49). In the M-1 pump, a lightweight one-piece design was desirable from the critical-speed standpoint (a one-piece rotor is stiffer than a builtup rotor), and a rotor machined from a single forging was considered. However, concern over achievable forging quality and difficulty in reducing the weight of a single forging of the size required for the M-1 was sufficient to eliminate this configuration, and the welded construction noted previously was selected (ref. 50). The two

pumps that have used the builtup concept (Mark 9 and Mark 25) were designed for ground application. In both cases, the relative ease of staging and the capability to test single stages during development were the primary considerations in selection.

2.3.3.2 MECHANICAL DESIGN

Reference 6 presents a complete discussion of loads, stresses, and critical speeds for the various types of rocket engine turbopump rotors. The discussion herein therefore is limited to the special features of axial-pump designs.

Pump rotors are subjected to simultaneous torque, centrifugal, bending, and differential-pressure loads along with possible thermal and inertial loads. The torque limit of the state-of-the-art rotors has, in effect, been established by permissible bearing DN, since all of the designs have had a bearing support between the pump and turbine. The maximum torque used in the design process has been the steady-state magnitude as determined from the pump hydrodynamic analysis (transient torque during startup and shutdown has been less than the steady-state value). An alternating torque, resulting from nonuniform power input from the turbine and power dissipation in the pump, has been estimated and superimposed on the steady-state torque (magnitudes of 5 percent of the steady-state torque are typical). Centrifugal load and bending moments due to unbalanced shaft and hydrodynamic forces have been determined and used along with the torque in defining the load condition at the torque-limited section. Loads have been calculated at a mechanical design speed that generally has been 10 percent above the nominal design speed of the turbopump. Average stresses in one-piece type rotors typically have been determined with finite-element or thin-shell theory and finite-difference methods. In the case of the Mark 15-F, the rotor was optimized by means of photoelastic evaluations and model tests (ref. 51). Finite-difference methods typically have been used in the disk stress analysis of the builtup-type rotors.

Splines have been used on all state-of-the-art rotors for attachment of the inducer. Curvic* couplings were used in the Mark 15-F and Mark 26 and splines were used in the M-1 to attach the drive turbine to the pump. In the Mark 9 and Mark 25, a ball spline coupling was employed, since the drive for these pumps was mounted on separate bearings. A complete discussion of rotor couplings is presented in reference 6.

2.3.4 Axial Thrust Balance System

2.3.4.1 TYPES OF SYSTEMS

Turbopump rotors are subjected to high axial thrust loads originating from pressure-times-area forces and fluid momentum changes in the pump and turbine. These

*Copyright, Gleason Works, Rochester, New York.

loads must be known accurately, and provisions must be made to counteract them by thrust bearings, back vanes (on centrifugal impellers), balance drums, compensating balance pistons, or some combination of these methods. In axial-flow turbopumps, thrust bearings and some form of compensating balance piston have been used.

The Mark 9, Mark 15-F, Mark 25, and Mark 26 pumps incorporated the so-called series-flow concept shown in figure 22. High-pressure fluid from pump discharge is introduced into the balance system and flows through two variable orifices in series to a low-pressure area. Shaft axial movement (resulting from changes in pump or turbine thrust) causes a change in orifice gap on both sides of the piston. Resultant changes in pressure differential across the piston provide a force change to counteract the unbalanced load. Typical performance characteristics are shown in figure 23. All these thrust-balance systems were designed such that at the nominal pump operating point the only axial load on the bearings would be the preload designed into the bearing package. Axial stops were incorporated into the bearing package to minimize or prevent rubbing of the balance-piston orifices.

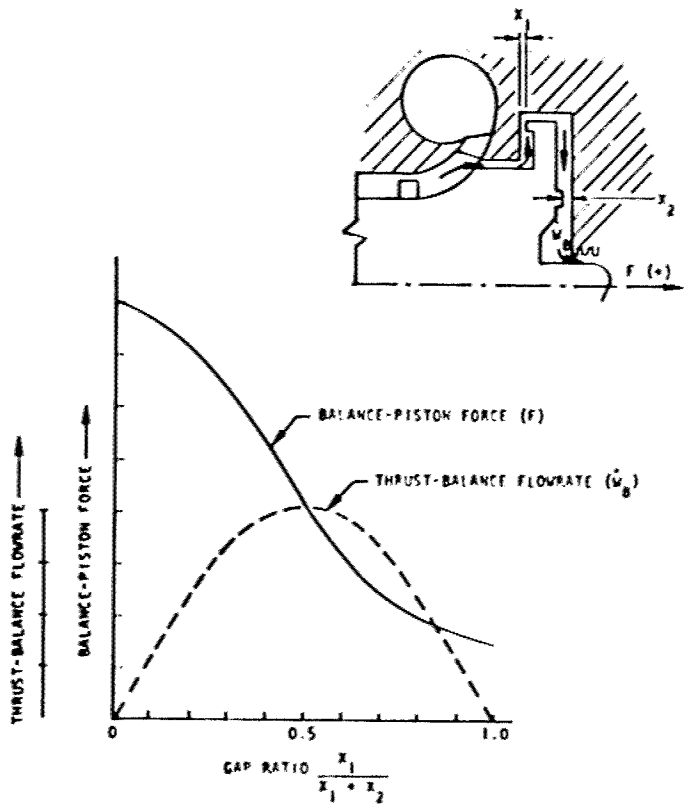

Figure 23. – Typical performance of a series-flow thrust-balance system.

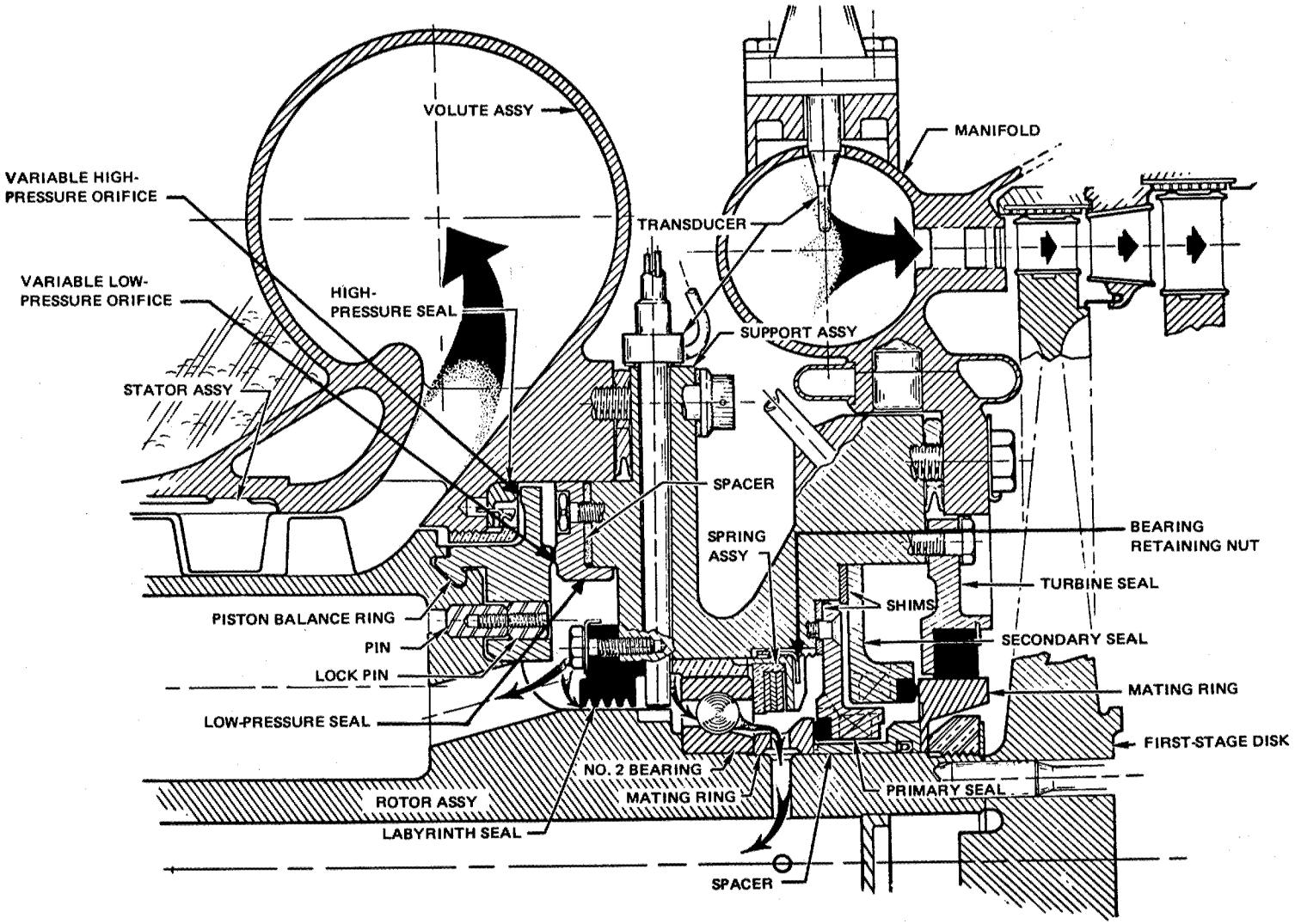

Figure 22. — Series-flow thrust-balance system used on Mark 15-F pump.

Balance-piston orifice gaps must be held to strict limits in order to achieve proper operation of the thrust-balance system. The balance piston on the Mark 15-F pump, for example, was designed such that the axial travel (sum of low-pressure and high-pressure orifice gaps) was 0.015 ± .001 in. The 0.015 in. setting was achieved during assembly by custom machining a spacer to fit between the low-pressure seal and the support assembly (fig. 22). Preload on the turbine end bearing (no. 2 bearing in fig. 22) was achieved by applying a specified axial load on the rotor assembly toward the turbine end and torquing the bearing retaining nut until the low-pressure orifice gap was zero (care had to be exercised to prevent load transmittal from the rotor assembly to the low-pressure seal). Preload on the pump end bearing was achieved in a similar manner with the axial load applied in the opposite direction. These assembly procedures (gap setting and bearing preloading) were accomplished with the pump rotor at liquid-nitrogen temperature.

The design for the thrust-balance system used in the M-1 hydrogen pump is shown in figure 24. High-pressure fluid was introduced from pump discharge and flowed through a single variable orifice. The system was designed to provide a bias load toward the turbine at the pump nominal operating point. This load was transmitted to the front bearing support through a set of ball bearings and springs shown in figure 25. As in the case of the previously discussed concept, shaft axial movement caused a change in pressure differential across the piston to counteract the unbalanced load. Thrust reversal (i.e., axial load toward pump suction) could be accommodated only up to the load capability of one bearing in the tandem set, because the bearing package necessarily was designed for load sharing in one direction.

The discharge flow of the thrust-balance system has been routed to a lower pressure area of the pump both internally (Mark 15-F and Mark 26) and externally (M-1). The flow also has been routed externally to the pump suction line (Mark 9 and Mark 25).

Additional information on bearing/balance-piston arrangements, including a parallel-flow system, is presented in references 1 and 3.

2.3.4.2 MECHANICAL DESIGN

It is difficult to predict accurately the axial thrust of a turbopump rotor. The analysis usually involves extremely high pressure-times-area forces, and the variation in predicted thrust magnitude thus can be significant even though inaccuracies, from a percentage standpoint, are small. Thrust loads obtained from pump hydrodynamic and turbine aerodynamic analyses are in themselves subject to inaccuracies. Additionally, assumptions in areas such as the magnitude of orifice coefficients in the thrust balance system, pressure drops in flow passages, and fluid rotation effects on pressure distribution (both in the balance system and in the pump and turbine proper) are involved. In order to cope with these

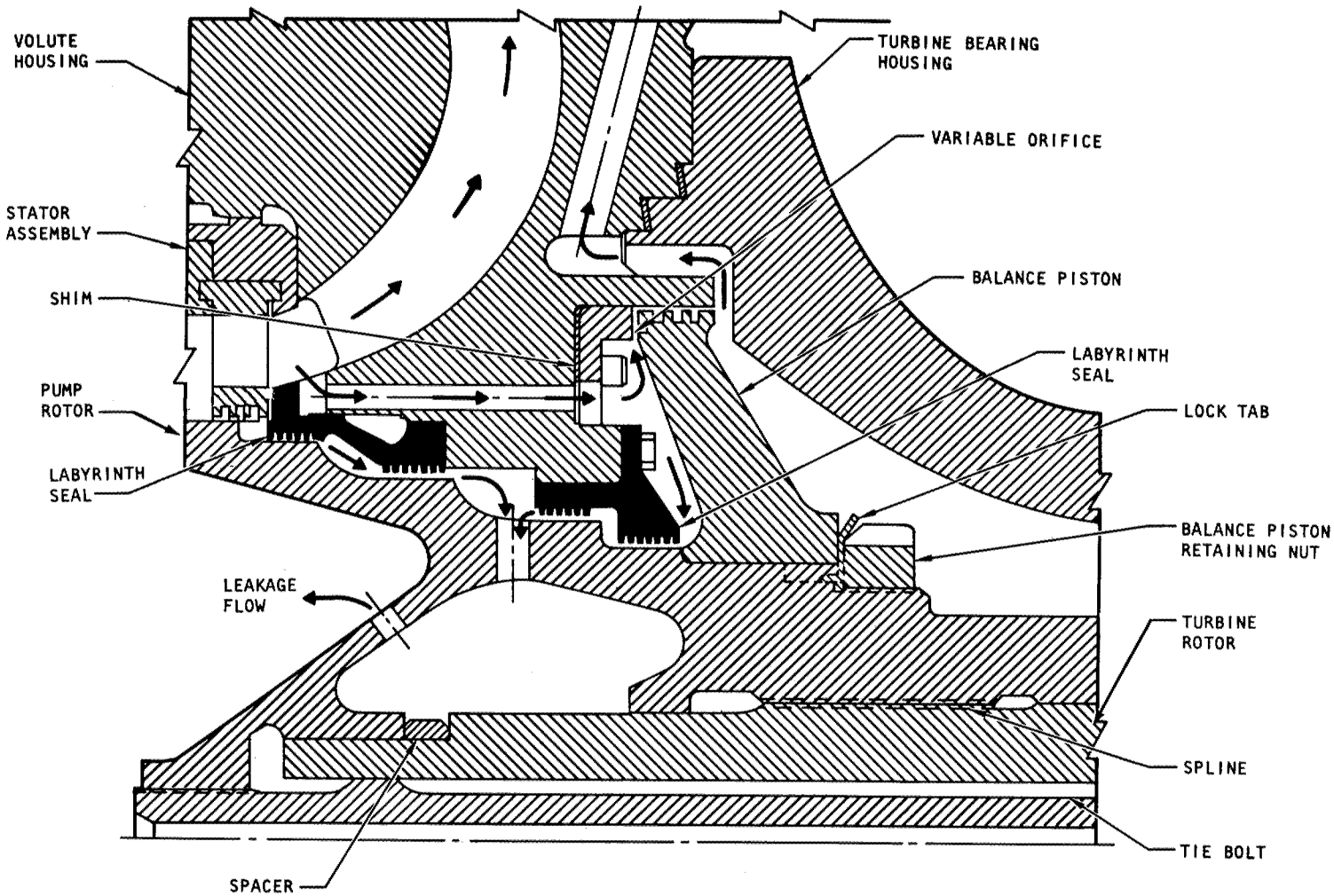

Figure 24. — Thrust-balance system for the M-1 fuel pump.

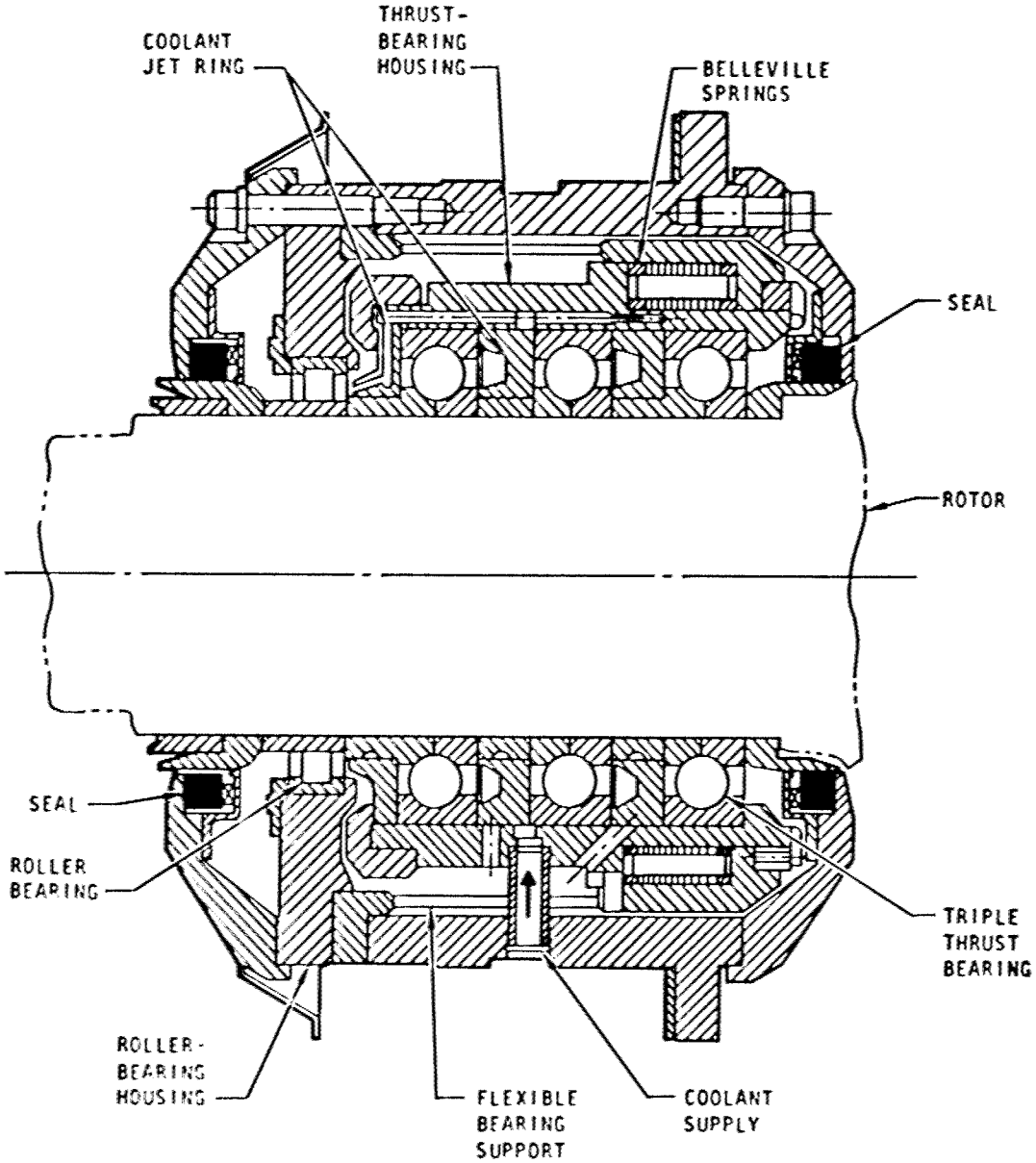

Figure 25 Thrust-bearing assembly on M 1 fuel pump

problems, design margins in the thrust-balance systems have been provided to permit correction capability during the development phase of the turbopump. For example, the balance pistons on the Mark 9, 15-F, 25, and 26 pumps were sized to handle twice the calculated axial thrust; i.e., if the high-pressure orifice were closed, the pressure-times-area force of the balance piston would be equal to twice the calculated pump thrust at design operating conditions. Analytical and experimental investigations of thrust-balance system and pressure distribution are reported in references 52 and 53.

There have been no structural problems with balance pistons *per se*. Stresses have been calculated by either disk analyses or finite-element techniques, the maximum calculated pressure differential across the piston and the mechanical design rotor speed being used for the analysis. Stresses due to differential thermal or centrifugal growths also have been included where necessary.

2.3.4.3 SYSTEM STABILITY

In the state-of-the-art pumps, considerable attention has been given to the stability of self-compensating thrust-balance systems. The axial oscillations of the rotor, which occur if the system is unstable, can cause damage to the thrust bearings and to rotating and stationary surfaces that make contact during the oscillations. Dynamic characteristics of the thrust-balance systems have been examined analytically either by analog simulation of the nonlinear equations describing balance-piston motion (refs. 52 and 54) or by simplified linear equations programmed for digital-computer solution (refs. 52 and 55).

The original balance-piston configuration designed for the Mark 9 pump functioned properly without change. Essentially the same design was adopted for the Mark 15-F, 25, and 26 pumps. Aside from scuffing on balance-piston surfaces, the Mark 9, 25, and 26 had no operational problems. During the development of the Mark 15-F, there were numerous occasions of instability in the form of abrupt changes in balance-piston cavity pressure. Hardware damage due to the oscillations normally was not of a catastrophic nature and primarily involved heavily worn or broken carbon inserts that (originally) formed the balance-piston orifices. This condition resulted in contamination of the bearing coolant and overheated or heavily loaded bearings, and in several instances, in bearing failure. Although the cause of the erratic balance-piston behavior was not explained completely, trouble-free operation was achieved through a series of changes involving clearances, flow restrictions, orifice insert material, and the method of orifice retention.

2.4 PUMP STATOR ASSEMBLY

The pump stator assembly as discussed herein consists of the vanes, the front and rear bearing housings, the volute, and the cylindrical housing that encases the vanes.

2.4.1 Vanes

2.4.1.1 PROFILE TYPES

The types of profiles used for the vanes in the state-of-the-art pumps and the factors considered in their selection are the same as those for the blades and are discussed in section 2.3.1.1. The significant profile design parameters are listed in table III.

2.4.1.2 VANE MECHANICAL DESIGN

With the exception of centrifugal force considerations, the analysis of load, stress, and vibration of stator vanes in axial flow pumps is identical to the rotor blade analysis (sec. 2.3.1.2).

Vane development problems have been similar to those that occurred with the blades. During the early development of the Mark 15-F, there were instances of vane cracking caused by fatigue. The cracking was diagnosed as the result of a vane natural frequency resonance with the forcing wakes off the rotor; the problem was corrected by increasing the profile thickness-to-chord ratio at the root section of the vane. This change decreased the steady-state stress and increased the vane natural frequencies to magnitudes above those excitable by known forcing frequencies.

During the design of the M-1 pump, it became necessary to compromise the hydrodynamic design of the vanes in order to alleviate a potential steady-state stress problem. Note on figure 3 that the M-1 vane was a shrouded configuration. As initially designed, the vane was structurally adequate to withstand the hydrodynamic loading on the profile portion of the vane. However, the additive stress due to the differential pressure across the shroud raised the calculated steady-state stress to a magnitude that necessitated a profile redesign. Since it was desirable to use the tooling that had already been fabricated, the pressure and suction surfaces of the profile were moved apart to obtain a thickness-to-chord ratio of 0.15 instead of the original 0.10. This action required larger radii on leading and trailing edges and resulted in an estimated 2 to 3% performance loss for the pump.

2.4.1.3 PROFILE TOLERANCES, SURFACE FINISH, AND FILLET RADII

Design considerations associated with tolerances, surface finish, and fillet radii for axial pump vanes are the same as those discussed for blades in section 2.3.1.3.

2.4.2 Vane Attachment

2.4.2.1 METHODS

In the Mark 15-F and Mark 26 pumps, the vanes were machined integrally on three 120° cylindrical segments that were assembled around the rotor and encased in a one-piece

volute/stator housing (fig. 26). In the Mark 9 and Mark 25 pumps, the assembly concept was similar. The vanes, however, were integral with segmented rings (three 120° segments comprising one stator row) with cylindrical spacers used between stator rows (fig. 27). The M-1 mainstages incorporated individual vanes with mounting lugs that, when assembled, were captive in cylindrical retaining rings (fig. 28). The rings and vanes were then encased in cylindrical housings.

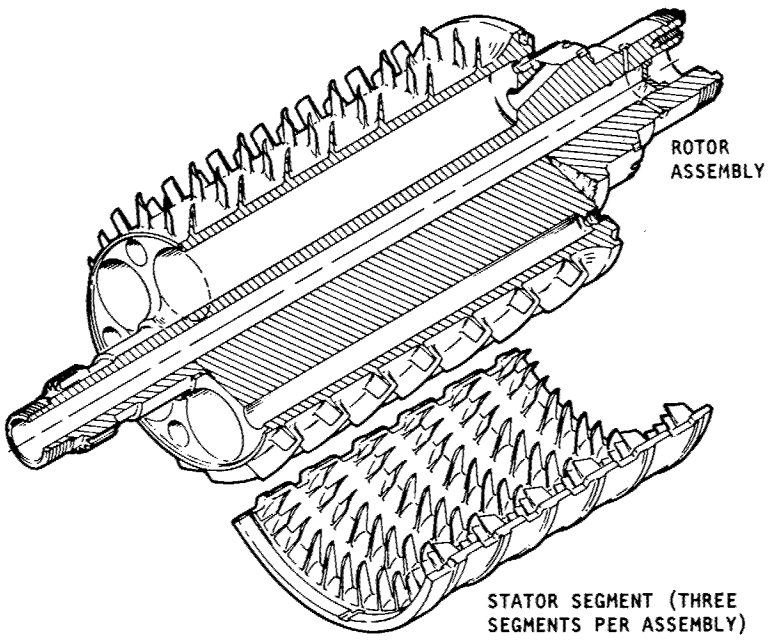

Figure 26. – Rotor-stator assembly for Mark 15-F pump.

As in the case of rotor blades, the selection of an attachment method for vanes is based on weight, manufacturing, and assembly considerations. Note that, in the state-of-the-art pumps, the methods selected have permitted the use of continuous cylinders for stator housings. These cylinders preclude the potential propellant leak paths and thermal distortion associated with an axially split housing.

2.4.2.2 MECHANICAL DESIGN

The vane attachment must be designed to transmit the steady-state and vibratory airfoil loads to the support structure and additionally, to position and retain the vane both axially

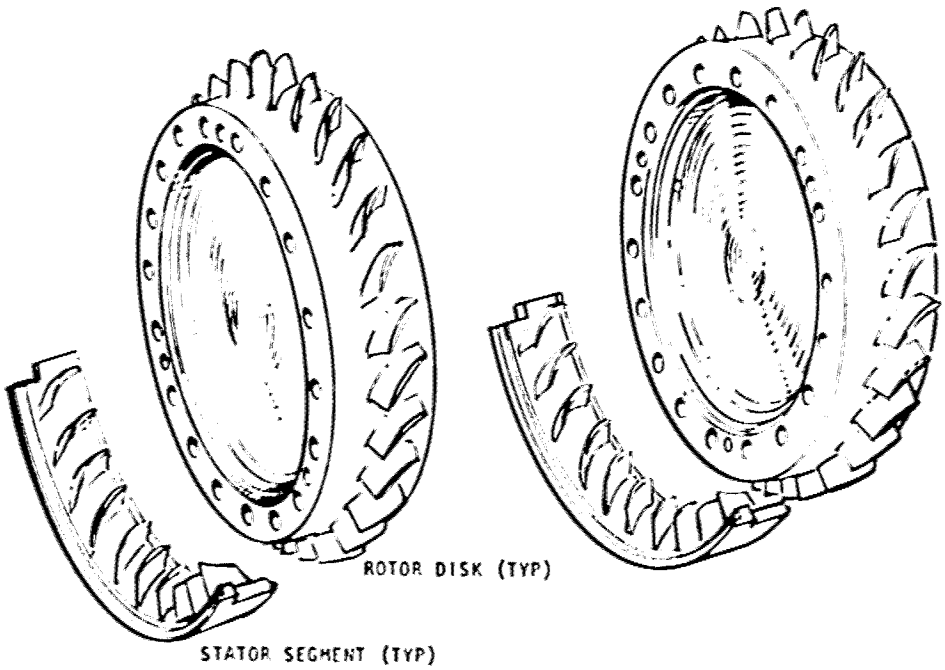

Figure 27 – Stator segments and rotor disks for Mark 9 pump

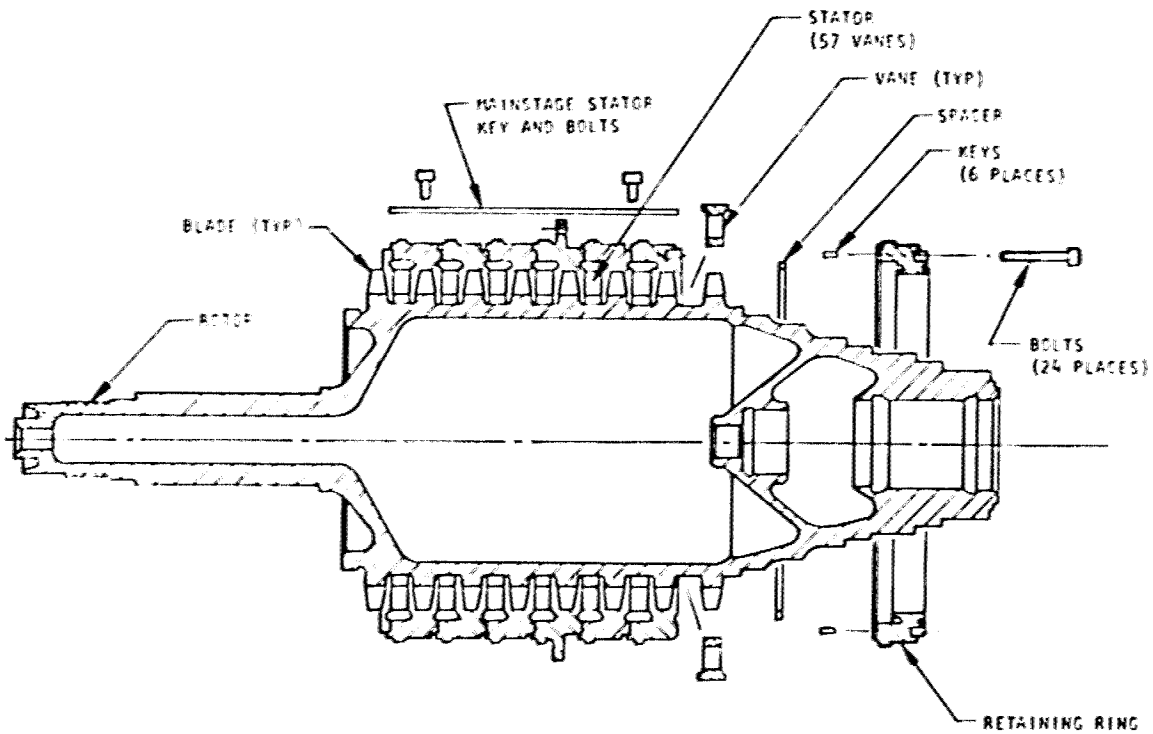

Figure 28 – Rotor-stator assembly for M-1 pump

and circumferentially. There have been no structural problems with the attachment methods used in the state-of-the-art pumps. The circumferential (torque) load on the stator assembly has been transmitted to the adjacent housing by keys acting in shear (fig. 28).

Individual attachment of vanes (e.g., that in the M-1 pump) usually does not present a critical stress problem, since only hydrodynamic loading must be transmitted through the attachment. Additionally, the necessity of forming a continuous flow path on the outside diameter gives the designer an appreciable arc length in which to design a suitable configuration. Thus, the airfoil steady-state and vibratory bending moments when transposed to the lug section of the attachment can be distributed over an appreciable length, and the resulting loads therefore are relatively low.

2.4.3 Stator and Volute Housings

Reference 1 presents a complete discussion of flow diffusion and collectors in rocket engine turbopumps. The material in the reference generally is applicable to both centrifugal or axial flow pumps; therefore the discussion herein is limited essentially to the particular features associated with the axial-flow designs.

2.4.3.1 HOUSING TYPES

The stator and volute housing is the pressure-containing structure that encases the vanes of the axial flow stages and collects and delivers the propellant flow to the discharge line. It is one of the major structural members of the turbopump housing assembly. It may consist of two housings (i.e., stator and volute) bolted together, as in the M-1, Mark 9, and Mark 25 pumps, or it may be a single housing, as in the Mark 15-F and Mark 26 pumps.

The selection of a stator/volute housing configuration in the design phase involves hydrodynamic, stress and deflection, weight, and fabrication considerations. Single housing units are preferred (especially in production pumps), since a potential propellant leak path is eliminated. All of the stator/volute housings for the state-of-the-art pumps have had vanes in the volute proper to turn and diffuse the flow as well as to minimize hydrodynamic radial load and to structurally tie the volute walls together. With the exception of the Mark 9, the volute sections have had some degree of "foldover" as illustrated in figure 29. Folding the volute permits a smaller overall housing envelope, which results in lower weight. Additionally, as noted in reference 1, a folded volute can be utilized to obtain a single-vortex rather than double-vortex motion in the volute; this kind of motion is particularly effective in maximizing the efficiency of a volute-exit conical diffuser and in stabilizing performance.

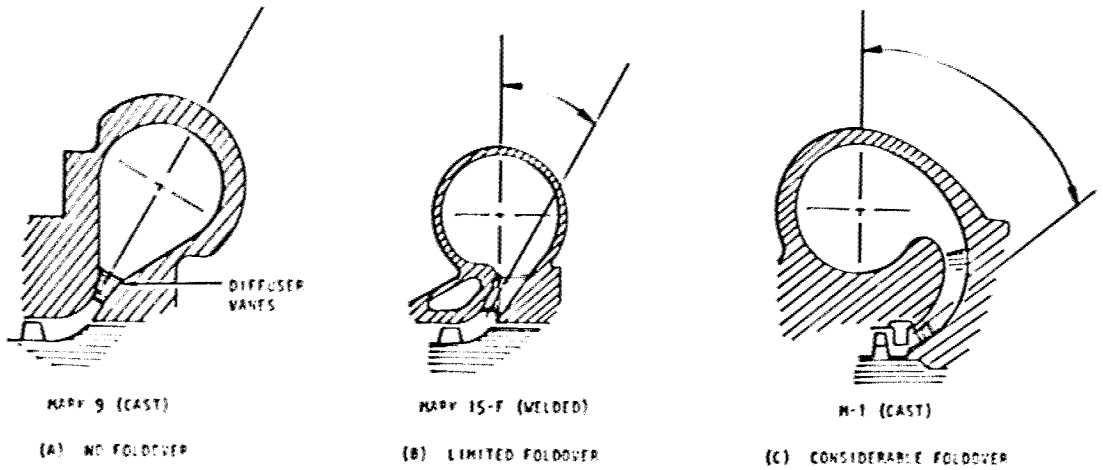

Figure 29. – Volute types showing various degrees of foldover.

Two standard techniques have been employed in fabricating the state-of-the-art axial pump stator/volute housings: casting and welding. Ideally, the fabrication lead time and cost for a cast housing is less than that for a welded structure. However, in practice these advantages, which can be obtained only at the expense of additional weight, are not always achieved. For example, steel castings were selected for the initial M-1 stator and volute housing because a flightweight design was not an immediate requirement (flightweight welded Inconel 718 structures were planned for the later configurations). Considerable difficulty in casting was encountered in the volute housing in the area of the diffuser vanes because of core breakdown from heat, erosion, and fluid pressures of the liquid metal. Problems of complete core breakdown were resolved. However, core erosion problems were not completely resolved, and considerable grinding of the diffuser vanes was necessary to achieve acceptable hydrodynamic passages. The volute/stator housings for the Mark 9 pump (other than the original design) and for the Mark 15-F, 25, and 26 pumps were builtup welded steel structures.

2.4.3.2 HYDRODYNAMIC DESIGN

A complete discussion of volute and diffusion system hydrodynamic design is given in reference 1. The volute housings on axial-flow pumps have been designed such that the flow from the last axial stage enters an exit passage and is gradually turned toward a plane normal to the axis of pump rotation prior to its being collected in the volute proper. Vanes have been utilized in the exit passage to guide and diffuse the flow and to tie the volute walls together structurally. In the M-1, additional diffusion was accomplished between the 10-in. discharge section and the 12-in. discharge pipe attachment; in the other axial pumps, the

mean velocity in the volute was the same as that in the discharge pipe (i.e., there was no conical diffusion section). The diffuser vanes have been designed for zero incidence at the design flowrate, the vane angle and area distributions being chosen to minimize friction losses while maintaining a specified vane loading (maximum diffusion factor). The volutes proper have been designed on a one-dimensional basis with approximately constant velocity (ref. 56).

2.4.3.3 MECHANICAL DESIGN

The assembled volute, stator housing, and bearing housings form the structural foundation of the turbopump. From a stress standpoint, the volute/stator housing assembly must be designed to withstand internal pressure, stator assembly axial and circumferential loads, flange and mount reaction loads, and inertial loads. Sufficient rigidity must be provided so that housing deflections do not adversely affect bearing alignment, balance-piston orifice clearance, or blade and vane tip clearances.

Internal pressure and the pump stator axial and circumferential loads are determined from the hydrodynamic analysis. In order to account for increased internal pressure loading due to vehicle acceleration, engine excursions, and pressure oscillations and surges, a volute design pressure greater than that determined from the hydrodynamic analysis is used (an increase of 20% is typical). Flanges for propellant line connections must be sized to react both symmetric and asymmetric loads from possible line installation misalignment, line pressures, differential thermal growths, and line inertia forces. Turbopump mounts may be located on the volute/stator housing; in this case, rotor thrust loads and turbine stator assembly loads are additionally imposed on the housing assembly. Mount loads generally are of considerable magnitude, and the structure at the mount points must be designed to minimize deflections that could cause rubbing between stationary and rotating components.

The volute usually is the more critical from a structural standpoint. Stresses in volutes have been determined analytically by two approaches. In the first, the most critical cross section of the volute is represented by a simplified model consisting of rings, plates, and beams on elastic foundations. The deflections and rotations at the junctions are matched, and the equations are solved for moments and stresses. In the second approach, the volute shell is treated as an axisymmetric thin shell of revolution, and computer programs for either finite-difference or finite-element analysis are used to determine the volute stresses (refs. 57 and 58, resp.). The second approach has demonstrated reasonable accuracy when solutions were compared with test results.

Proof-pressure testing has been specified as a normal part of the manufacturing process on state-of-the-art volutes and stator housings. Because of volute complexity, new volute designs generally have been subjected to complete structural testing to verify the stress and deflection analyses.

2.4.4 Bearing Housings

2.4.4.1 TYPES

The primary function of the bearing housings is to provide and maintain radial and axial positioning and support to the turbopump rotating assembly. All state-of-the-art axial turbopumps have been supported at two bearing locations such that the axial pump is cradled between the bearings, with the inducer outboard of the front (pump end) bearing and the turbine outboard of the rear (turbine end) bearing. All of the front bearing housing designs have incorporated the vanes for the stator row of the inducer stage. Additionally, housing assemblies have included bearing spring packages, seal packages, axial bearing stops, and turbopump mounts.

Bearing housing types can be classified in terms of the degree of radial stiffness at the bearing mount (i.e., rigid or flexible). The bearing housing itself will in general be the same for either type, with the desired design stiffness being attained locally in the bearing carrier. Reference 6 presents a discussion of bearing mounts and their influence on critical speed.

Welded structures of 300-series CRES castings or forgings have been utilized in all state-of-the-art housings with the exception of the M-1 rear bearing housing, which was machined from a single casting. As with the M-1 volute and stator housing, flightweight design was not an immediate requirement for the M-1 bearing housings.

2.4.4.2 MECHANICAL DESIGN

As indicated in section 2.4.3, the assembled stationary components form the structural foundation of the turbopump. As a part of this assembly, the bearing housings are subjected to the axial and radial loads of the turbopump rotor, internal pressure, thermal gradients (which can be severe in the turbine end housing), and the external loads reacted at the flanges or turbopump mounts. In the design, particular attention is given to radial and axial alignment and deflection of the housings. Radial deflections must be minimized so that the desired blade and vane tip clearances are achieved. Axial rigidity is necessary to maintain desired clearances for the thrust balance piston and, in those designs with axially preloaded bearings, to maintain the proper bearing load.

The rotor radial loads that must be reacted by the bearing housings are discussed in reference 6; the reference also includes discussion of bearing housing radial spring rate and its effect on turbopump rotating-assembly critical speed. Rotor axial thrust loads that must be reacted by the housings are determined during the thrust-balance-system analysis (sec. 2.3.4) and include flight inertia loads of the turbopump rotor assembly. The design of the Mark 9, 15-F, 25, and 26 pumps was such that axial thrust toward pump suction was

transmitted to the turbopump housing assembly by the front bearing housing and thrust toward the turbine was transmitted by the rear bearing housing. Axial thrust in the M-1 pump was reacted only at the front bearing housing through a triple set of ball bearings and spring system, as shown in figure 25.

In general, the complexity of the bearing housing structure has made a precise analytical stress analysis of the total structure difficult. Stress analyses have consisted primarily in calculating local stresses that, in the opinion of the designer, could be of significance (e.g., inducer-vane stresses in the front bearing housing, stress due to mount reaction, and local flange stresses).

2.4.5 Housing Interfaces and Static Sealing

2.4.5.1 INTERFACE AND SEAL TYPES

The components making up the pump housing assembly are bolted at the interfaces. Structural continuity must be maintained across each of the interfaces during pump assembly and operation. Particular attention must be given to (1) diametral tolerances and concentricities that provide proper alignment of rotor to stationary components and (2) sealing that must reliably prevent propellant leakage.

Radial positioning in general has been accomplished by using an interference fit on the diameters of the mating flanges with the parts assembled at different temperatures to ease the buildup problems. The M-1 had three housing interfaces between the front and rear bearings. In this case, the machining that affected the rotor and stator clearance and concentricity was accomplished on subassemblies (i.e., the front bearing support and mainstage stator housing were machined as a unit, and the volute and rear bearing housing were machined as a unit). Axial positioning of the rotor relative to the stator in general has been accomplished by using shims during the final pump assembly.

Reference 59 presents a detailed discussion of static seals for liquid rocket engines. The types of seals that have been used in axial pumps are illustrated in figure 30. The interface design at the seal is dictated by the seal type and in general is specified by the seal manufacturer. Note that the M-1 axial pump utilized redundant seals (i.e., double conical seals with a monitoring port between the primary and secondary seals). During testing of the M-1, leaks developed in some of the joints, and in those cases where both the primary and secondary seal leaked, a helium purge was introduced through the monitoring port to prevent hydrogen leakage to the atmosphere. Reference 60 indicates that the leakage problems were associated with the difficult tolerance stackup of the double-sealed joints and with possible creep of the material, which was subjected to high loading for a long period of time.

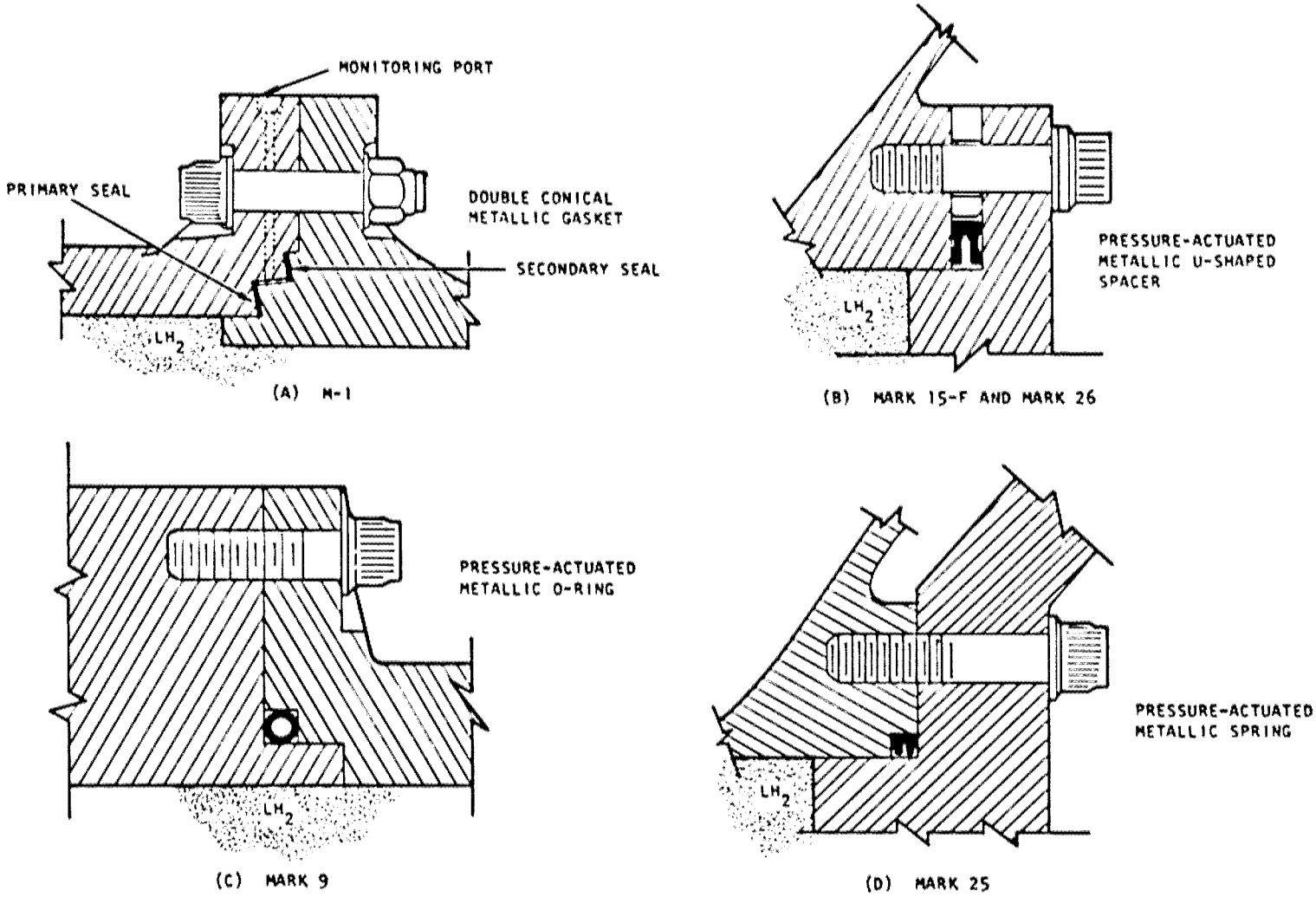

Figure 30. – Types of static seals used in axial pumps.

2.4.5.2 MECHANICAL DESIGN

A tight interface joint must be maintained for all load conditions. The bolt preload at assembly therefore must be great enough to ensure an adequate joint preload under all probable combinations of separating loads and thermal effects without exceeding allowable stresses in the bolt or flange at any of the probable combinations. Interface loads typically have been examined for the assembly conditions, for the pump steady-state operating conditions, and for transient temperature conditions. Each interface must be examined carefully to ensure that all potential loading is included in the analysis (e.g., pressure separating load, propellant line misalignment, and inertia loads that must be transmitted through the interface to the turbopump mount).

The interface joint is analyzed as a spring system. The elastic stiffness of the parts making up the joint are calculated for the environmental temperature condition being investigated and a spring model is used in determining the loads and stresses in each of the interface parts. Stresses and expansion or contractions resulting from thermal effects are included in the analysis.

Measurement of applied torque (torque wrench) is the most common method of achieving a required bolt preload at assembly. However, the uncertainties in friction coefficients normally result in a preload that can vary by a factor of 3 or 4. This condition means that each part in the joint assembly must be capable of withstanding a load 3 or 4 times the required preload.

Preload range can be minimized by measuring deflection of the tension or compression parts. This method is time consuming but may be warranted in critical assemblies. It has not been necessary to use this method in the stationary components of axial pumps.

2.5 MATERIALS

The materials utilized in the major components of axial pumps are noted in table IV. As stated previously, all of these pumps were designed for liquid-hydrogen applications. Thus the selection of materials was based on material properties at liquid-hydrogen temperature.

Relative merit of candidate materials has, in general, been evaluated on the basis of strength-to-weight ratio, ductility, fatigue strength, thermal expansion characteristics, and susceptibility to hydrogen-embrittlement failure. In flightweight designs, alloys with high strength-to-weight ratios are desirable in order to keep the pump weight low. Candidate alloys additionally must have adequate ductility in order to avoid fracture-type failure under steady stress conditions. In components such as blades that are exposed to significant steady-state and vibratory-stress conditions, fatigue strength is a consideration. Material

thermal-expansion rates must be considered in those components having a critical interface (e.g., bearings in a bearing housing), since a prescribed fit at both assembly and operating conditions is required. Consideration additionally is given to fabrication processes and operating environment in which hydrogen could be absorbed into or otherwise contaminate the material and result in hydrogen embrittlement and subsequent failure.

Considerable material property data have been obtained during rocket engine development programs. Much of the work done in support of cryogenic pump and other component development is reported in references 61 through 66. Thus, the discussion herein is limited to some of the more significant material problems that have occurred with axial pumps.

As noted previously, the M-1 rotor structure consisted of four forgings that were TIG welded to form a one-piece rotor. Extensive development work was conducted to establish welding and inspection procedures for the weldments (ref. 64). One pump rotor was fabricated and utilized in liquid-hydrogen turbopump testing. This rotor had known weld defects prior to the test program. Post-test examination of one of the rotor weldments indicated that nearly all of the defects propagated during testing (ref. 60). The effect that these defects would have on long-time operation of the rotor was not established, however, because pump testing was discontinued when the M-1 engine program was terminated.

As indicated in table IV, titanium alloy A110-AT-ELI was utilized for the M-1 transition rotor. Mechanical-property tests conducted on the forgings indicated the elongation to be an unacceptably low 1 percent at liquid-hydrogen temperature. It was determined that excessive hydrogen content in the forgings was responsible for the low ductility. Elongation of 10 percent at liquid-hydrogen temperature was achieved by degassing the forgings in a hard vacuum to lower the hydrogen content (ref. 67).

Carbon was used initially as the orifice insert material on the Mark 15-F thrust-balance system. This choice was made in order to avoid galling during contact of the balance piston and orifice insert. As noted previously, contact during pump operation was sufficient in some instances to break the carbon. The carbon particles contaminated the bearing coolant flow and at times resulted in bearing failures. To prevent these impact-type failures, the material was changed to leaded bronze, as noted in table IV.

2.6 SAFETY FACTORS

The various organizations responsible for the structural design of a turbopump or other propulsion system component employ individual manuals that contain comprehensive design instructions and policies on safety factors. Values for safety factors are specified by either the design organization or the responsible contracting agency. Terms used in structural design of pumps in general have been consistent with aeronautical engineering practice, but occasionally the definitions have differed from organization to organization. It is appropriate therefore to define the terms as used in this document and to indicate typical values for safety factors that have been utilized in the design of axial pumps.

Table IV. – Materials Used for Major Components on Axial-Flow Pumps

Component	Pump Configuration				
	Mark 9	Mark 15-F	Mark 25	Mark 26	M-1
	Material				
Rotor	310	K-Monel	K-Monel	Same as Mark 15-F	Inconel 718
Blades	310	K-Monel	K-Monel		Mainstage: Inconel 718; transition: Ti A110-AT-ELI
Volute	310	310	310		304 ELC
Stator housing	310	(Integral with volute)	310		304
Vanes	310	310	310		Inconel 718
Front bearing housing	310	310	310		347
Rear bearing housing	310	310	310		304
Balance piston	A1 2024	K-Monel	Inconel 718		Al 7075-T73
Balance piston orifice	Flame-plated tungsten carbide on 310	Leaded bronze	Silver-plated 310		304

Limit load. – The limit load is the maximum specified or calculated value of a service load or service pressure (excluding hydrostatic-proof-test pressure) that can be expected to occur under (1) the maximum 3-standard-deviation (3-sigma) operating limits of the engine or vehicle including all environmental and physical variables that influence loads, (2) the specified maximum operating limits of the engine or vehicle, or (3) the maximum engine or vehicle operating limits defined by a combination of 3-sigma limits and specified operating limits.

When there is uncertainty in the specified load or lack of 3-sigma data on conditions, a limit-load factor (a multiplying factor > 1) is applied to the specified or calculated maximum load. The following factors have been used in axial-pump design:

Type of load	Limit-load factor
Centrifugal load due to rotation (limit load factor is applied to rotational speed; result is sometimes called mechanical design speed)	1.1
Load on blades due to fluid forces	1.1
Structural load due to internal pressure	1.2
Load induced by thermal expansion and contraction	1.0
Inertial load due to engine thrust and gimballing	1.05

Design safety factor. – The design safety factor is an arbitrary multiplier (or divider) greater than 1 applied in design to account for design uncertainties, e.g., variations in material properties fabrication quality, and load distributions within the structure.

Design load (or pressure). – The design load (or pressure) is the product of the limit load (or pressure) and the design safety factor.

Design stress. – The design stress is the stress, in any structural element, resulting from the application of the design load or combination of design loads, whichever condition results in the highest stress.

Allowable load (or stress). – The allowable load (or stress) is the load that, if exceeded in the slightest, produces failure of the pump structural element under consideration. Failure may be defined as buckling, yielding, ultimate, or fatigue failure, whichever condition prevents the component from performing its intended function. Allowable load is sometimes referred to as criterion load or stress; allowable stress is equivalent to material strength.

Margin of safety. – The margin of safety (MS) is the fraction by which the allowable load or stress exceeds the design load or stress. The margin of safety is defined as

$$MS = \frac{1}{R} - 1$$

where R is the ratio of the design load or stress to the allowable load or stress.

Material endurance limits. – The material endurance limit (also called fatigue limit) is the maximum alternating stress that the material can sustain for an infinite number of cycles.

Proof pressure. – Proof pressure is the test pressure applied to a component to partially prove the adequacy of design and quality. The proof pressure is the product of the limit pressure and the proof-pressure factor. When proof testing at the design operating temperature is not feasible, the proof-test pressure is adjusted to compensate for the difference in material strength at operating temperature and the temperature at which the proof testing is conducted. Components that are to be subjected to proof-pressure tests are designed such that detrimental deformations do not occur during the proof test. Care is exercised in the design of the proof-pressure fixture to ensure that loading is properly simulated.

Proof-pressure factor. – Proof-pressure factor is a multiplying factor applied to the design pressure to obtain the proof pressure. A value of 1.2 typically has been used in testing the state-of-the-art axial pump components.

In practice in the design of axial pumps, a typical value for design safety factor for yield (based on 0.2% offset) has been 1.1; the typical factor for ultimate has been 1.5. The safety factor for fatigue, expressed as a ratio of material endurance limit to allowable alternating stress, typically has had a value of 1.33; the fatigue factor based on cycles to failure has had values of 4X predicted cycles for low-cycle fatigue, and 10X predicted cycles for high-cycle fatigue; i.e., the number of cycles to failure should be 4 or 10 times the number of predicted operating cycles.

3. DESIGN CRITERIA and Recommended Practices

3.1 OVERALL TURBOPUMP DESIGN

3.1.1 Turbopump Speed

Design criteria and recommended practices involved in selecting turbopump speed are presented in reference 7.

3.1.2 Turbopump Rotor Dynamics

Analytical predictions of turbopump rotor dynamics shall verify that unacceptable critical speeds or speeds at which self-excited nonsynchronous whirl occur do not exist in the operating-speed range.

An analytical model of the complete turbopump rotating assembly and support system should be formulated and utilized to predict critical speeds and the threshold speed of non-synchronous whirl (for rotors designed to operate above the first critical). References 6, 12, and 13 provide recommended analytical modeling techniques. Recommended margins between operating speeds and critical speeds are given in reference 6.

3.2 STAGE DESIGN

3.2.1 Realm of Operation

The selection of a pump type to satisfy given design and off-design head and flow requirements shall be based on examination of stage and total pump specific speed versus configuration and efficiency relationships, operating range capabilities, uprating potential, probable weights, and probable costs.

Reference 7 presents a complete discussion of the design considerations, design criteria, and recommended practices associated with the selection of the various types of pumps for rocket engine application.

It is recommended that an axial configuration be considered when stage specific speeds are above approximately 3000 and when throttleability and wide fixed-speed flow range are not

required. Additionally, it is recommended that a detailed examination of the axial-pump capabilities be made whenever pump uprating is a design requirement and the specific speed is appropriate to both the axial pump and the centrifugal pump. The axial pump, in which the addition of stages is relatively straightforward, is recommended when the competing centrifugal pump requires an additional stage to satisfy the uprating requirement.

3.2.2 Stage Hydrodynamic Design

The stage design shall reflect an acceptable compromise among hydrodynamic requirements, mechanical requirements, and overall pump configuration requirements.

The flow model used in the hydrodynamic design of axial-flow stages should approximate the three-dimensional real flow condition. It is recommended that design practices for axial-flow compressors be followed; in this approach, average flow conditions in the blade-to-blade planes are used to represent the flow in the hub-to-tip plane (ref. 18).

Prior to final selection of the detail stage hydrodynamic design, a parametric study involving flow coefficient, hub/tip ratio, and blade tip speed should be made so that an acceptable pump mechanical configuration is achieved. It is recommended that the following be used as guides in the parametric study:

- The stage design flow coefficient should not be less than 0.25.
- The stage hub/tip ratio should not be greater than 0.9.
- For stages with high hub/tip ratios ($\geqslant 0.8$), the blade design tip speed should be less than 1700 ft/sec for high-strength titanium alloys and less than 1500 ft/sec for high-strength nickel-base alloys.

3.2.2.1 BLADE LOADING, STALL MARGIN, AND EFFICIENCY

3.2.2.1.1 Blade Loading and Stall Margin

Design-point blade loading shall reflect an acceptable compromise of stall margin and efficiency.

It is recommended that the diffusion factor (eqs. (5) and (6)) be used as a measure of blade loading. For a given application, the stall-margin requirement of the pump will greatly influence the selection of the design-point diffusion factor. Stages designed for optimum

efficiency should have a maximum design-point diffusion factor between 0.45 and 0.55 (at any radius on either the rotor or stator). For pumps in which a minimum number of stages is desired, a design-point diffusion factor between 0.55 and 0.60 may be selected if stall-margin requirements permit.

3.2.2.1.2 Stage Efficiency

Predicted stage efficiency shall take into account losses due to profile, end-wall friction, and secondary flow.

It is recommended that cascade, compressor, and pump experimental data be used in predicting profile losses, as illustrated in figure 8. Data for axial-flow-pumps with highly staggered blades (ref. 22) do not compare favorably with results shown on figure 8, particularly in the tip region, and therefore care should be exercised in applying figure-8 data to highly staggered blading. Data for double-circular-arc and multiple-circular-arc blades with high stagger angles are reported in references 23 through 26.

Predictions of end-wall-friction (annulus) loss and secondary-flow loss, including tip clearance loss, should be added to the profile loss to obtain the overall stage efficiency. The magnitude of these losses can be estimated by methods presented in references 68 and 69.

3.2.2.2 VELOCITY DIAGRAMS

The radial pattern of flow and the type of velocity diagram shall be based on a suitable compromise of stage headrise, stage efficiency, and stall-margin requirements.

A free-vortex flow pattern with a symmetrical velocity diagram at the mean radius is recommended for designs having hub/tip ratios greater than 0.8. If it becomes necessary or desirable to use hub/tip ratios less than 0.8, the design should be examined to determine if alternate flow patterns might offer a more suitable compromise.

In the preparation of the velocity diagrams, the compressibility of the pump fluid, recirculation of bearing coolant and thrust-balance-system flow, and channel area reduction due to end-wall and blade-surface boundary layers should be considered. It is recommended that, for liquid-hydrogen pumps, density increases in excess of 6 percent be accounted for, preferably by linear taper in the flow path; the magnitude of the density change can be estimated by the method presented in reference 7 (pp. 99-102). As indicated previously, area reduction due to boundary layers normally is accounted for by using a blockage factor whose magnitude depends on the particular design as well as the design method being used. The factor should be selected by the designer on the basis of experience with similar designs.

Caution should be exercised because, as pointed out in reference 18, indiscriminate use of correction factors can lead to a design that is as poor or worse than one in which boundary-layer corrections are ignored completely.

3.2.2.3 BLADE ANGLES

Fluid turning, as a function of radius and as defined by fluid incidence, blade camber, and deviation angles, shall properly reflect the design velocity diagrams.

The selection of incidence angle is dependent on the specific application; e.g., optimum incidence from a cavitation standpoint will not necessarily be the same as that for minimum loss. Thus, a recommended magnitude for incidence angle is inappropriate. Acceptable procedures and guides for selecting incidence angles are given in references 18, 27, 68, and 70. References 23 through 26 provide data and correlations that extend the range of minimum-loss incidence rules given in reference 18.

Methods for calculating deviation angles are given in references 18, 27, 31, 68, and 70. Accurate prediction of the deviation angle is extremely important in achieving an acceptable design. In view of its successful use in the design of the Mark 9, 15-F, 25, and 26 pumps, it is recommended that the deviation-angle rule given in section 2.2.2.3 be used for nonstandard profiles having design parameters similar to those in table III. The deduced deviation-angle rules of reference 18 are recommended for NACA-series profiles and may also be used for standard double-circular-arc and C-series profiles. References 23 through 26 provide data and correlations that extend the range of deduced deviation-angle rules for double-circular-arc profiles; these references also provide performance and turning-angle correlations for multiple-circular-arc and slotted double-circular-arc profiles.

3.2.2.4 SOLIDITY

Solidity shall be within the range of values for which experimental data are available or which have been successfully demonstrated in axial-pump applications.

No exact rule for selecting a value for solidity can be specified. On the basis of magnitudes that have been demonstrated in axial-pump applications (table III), it is recommended that solidity selected be within a range of approximately 0.75 to 1.9. High-solidity stages, which are desirable for achieving high ideal headrise, should be analyzed to ensure that the efficiency degradation associated with increasing solidity is at a tolerable level (fig. 9).

3.2.2.5 CAVITATION

The pump mainstage shall not be subject to cavitation.

It is recommended that the inducer be designed to provide sufficient head to avoid cavitation in the initial mainstage for all anticipated pump operating conditions. Adequacy of the initial mainstage as free from cavitation should be determined from cavitation-test data for similar designs or from analysis of fluid velocities on the blade surface.

3.2.2.6 OFF-DESIGN PERFORMANCE

The pump stall point at any operating speed shall be at a flowrate less than that anticipated during either transient or steady-state pump operation

For designs with hub/tip ratios greater than 0.8, it is recommended that a diffusion factor of 0.75 or a retardation factor of 0.50 at any radius on either the rotor or stator be assumed as the condition at which stall will occur. It is further recommended that a diffusion factor of 0.70 or a retardation factor of 0.55 be used as a permissible operating condition corresponding to the minimum-flow-coefficient requirement of the pump.

3.2.2.7 CLEARANCES

3.2.2.7.1 Radial

Radial tip clearances on the blades and vanes shall minimize head losses

It is recommended that a radial tip clearance of not more than 2 percent of the blade or vane height be used as an operating clearance. The clearance analysis should include effects of deflection due to rotor imbalance (and hydrodynamic pressure imbalance if applicable), rotor and blade centrifugal growth, frame and housing deflections, component differential thermal contractions, and rotor dynamics effects.

3.2.2.7.2 Axial

Axial clearances shall minimize wake effects on adjacent blade or vane rows

It is recommended that an operating axial clearance between a blade (or vane) row and the succeeding vane (or blade) row be at least 10 percent of the chord length of the upstream row. The clearance analysis should include effects of assembly dimensional tolerance stackup, blade tilt in axial direction (if used), tip deflection due to steady-state and vibratory loads, rotor thrust-bearing deflection, frame deflections, rotor Poisson effect, and component differential thermal contractions.

The axial clearance recommended above is consistent with and is a necessary condition in the blade design practice outlined in section 3.3.1.2.3. Deviation from this clearance value may be desirable if, for example, the initial mainstage blade row is preceded by a long-chord inducer stator. A smaller axial clearance (i.e., less than 10% upstream chord) would increase the amplitude of the load fluctuation and would require that appropriate methods referenced in section 3.3.1.2.3 be utilized in designing the blade from the vibration standpoint.

3.3 PUMP ROTOR ASSEMBLY

3.3.1 Blades

3.3.1.1 PROFILE TYPES

The blade profile shall (1) produce the desired fluid turning with required blade-surface velocities and (2) provide the blade with adequate structural strength.

The selection of a profile type will depend on the particular application. To reduce cavitation to a minimum, improve stall margin, and reduce profile losses, avoid excessively high blade-surface velocities; a maximum suction-surface velocity no greater than 1.25 times the relative inlet velocity is recommended. Double-circular-arc profiles or nonstandard profiles designed to achieve the prescribed velocity distribution are recommended for mainstages where avoidance of cavitation is the predominant consideration. Of the common standard profiles (the NACA 65, British C-4, and double-circular-arc), the British C-4 offers the maximum section modulus for profiles having the same camber, chord, and maximum thickness-to-chord ratio. Thus, if standard profiles are utilized and maximum blade strength is required, the British C-4 profile is recommended. If the NACA-65-series profile is utilized, the trailing edge should be thickened over that defined by the standard thickness distribution.

As a general aerodynamic maxim, the best profile is the thinnest (ref. 43). It is recommended that a maximum thickness-to-chord ratio of 0.13 be used as an upper limit, with ratios of 0.10 or 0.11 preferred. If excessive bending stresses exist, structural adequacy should be achieved by increasing the chord length with maximum thickness-to-chord ratio held constant (within solidity limits).

Leading- and trailing-edge radii should be kept as small as possible within the limitations imposed by structural and manufacturing considerations. At subsonic speeds, a total trailing-edge thickness up to about one-quarter of the blade maximum thickness (i.e.,

trailing-edge radius equal to one-eighth of maximum thickness) should have little effect on aerodynamic performance (ref. 43). It is cautioned that a specified fluid outlet angle is demanded, and excessive tolerance within the above limit may not fulfill the outlet-angle requirement.

3.3.1.2 MECHANICAL DESIGN

3.3.1.2.1 Structural Strength

The mechanical design of axial-flow-pump blades shall be based on the combined effects of centrifugal, steady-state hydrodynamic, and vibratory loads.

It is recommended that the steady-state stress due to centrifugal loads be determined at a mechanical design speed that is at least 10 percent above the nominal design speed. This stress should be combined with the maximum steady-state stress due to hydrodynamic (fluid force) load (as determined from an examination of the nominal and off-design requirements of the pump) to establish the maximum steady-state stress magnitude. Vibratory stress should be determined and combined with this maximum steady-state stress magnitude in accordance with the criteria and practices in section 3.3.1.2.3.

3.3.1.2.2 Stress Distribution

The stress analysis shall identify the maximum stress condition and the stress distribution in the blade.

Stresses should be determined at a number of longitudinal (along the stacking axis) sections, and this determination should include an examination of the stress at the blade leading edge, trailing edge, and at the outermost point on the convex surface (see fig. 14); for cantilevered blades, the greatest steady-state stress usually is at the section where the blade is tangent to the root fillet radius. The stresses listed below should be considered, although some may be negligible for a particular design because the magnitudes vary with blade geometry:

- Normal stress due to centrifugal load
- Normal stress due to hydrodynamic bending moment
- Shear stress due to direct hydrodynamic load
- Normal and shear stresses due to untwist forces resulting from centrifugal load (on twisted airfoils) and hydrodynamic moment about the airfoil stacking line.

- Normal stress due to bending moments resulting from blade stacking-line tilt or offset.

If the direct and torsional shear stresses for the particular design are appreciable, it is recommended that the principal stresses be determined and that the Mises-Hencky theory of failure (distortion-energy theory) (ref. 71) be used to calculate an "effective" stress for comparision with uniaxial material property data.

3.3.1.2.2.1 Blade Tolerances

The stress analysis shall consider the effects of blade tolerances on stress magnitudes and natural frequencies.

The blade stress analysis should be conducted for that tolerance condition that gives maximum stress. This condition usually occurs when the hub section is at the minimum tolerance and the tip section is at the maximum. In the vibration analysis, it is recommended that the frequency range that could result from maximum and minimum tolerance conditions be used in lieu of the natural frequencies for a nominal blade.

3.3.1.2.3 Vibratory Stresses

The predicted stress state of the blade shall be less than the allowable alternating stress.

Predicted steady-state and vibratory stress on the blade should be within the limits of material property data as defined by modified Goodman diagrams. Modified Goodman diagrams should be based on adequate safety factors applied to yield strength, ultimate strength, and endurance limit. It is recommended that the allowable alternating stress line of the diagram be constructed as shown in figure 31, with safety factors of 1.33 on fatigue, 1.5 on ultimate, and 1.1 on yield. Note the additional conditions set forth in sections 3.3.1.2.3.1 through 3.3.1.2.3.5.

In view of the uncertainties involved in predicting vibratory stresses, proceed as follows:

(1) Assume a vibratory-stress magnitude equal to the steady-state stress due to hydrodynamic load. This magnitude should then be multiplied by a stress-concentration factor appropriate to the fillet at the root section of the blade. Section 3.3.1.3.2 provides criteria and recommended practices for the design of fillets.

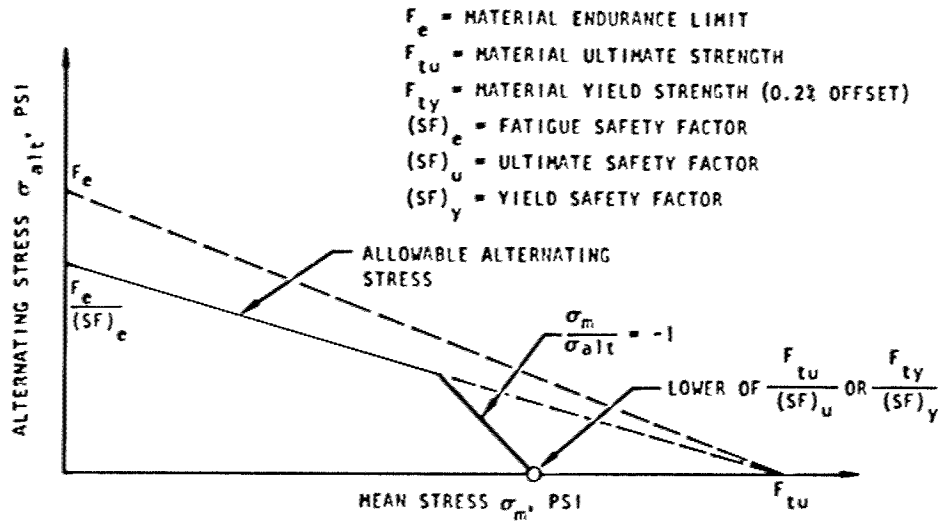

Figure 31. – Modified Goodman diagram illustrating safety factors.

(2) The stress state defined by the predicted steady-state (centrifugal plus fluid forces) stress and the vibratory stress determined in (1) above should be plotted on the modified Goodman diagram as shown in figure 16.

(3) Designs in which the stress state falls below the allowable alternating stress line are considered acceptable. If the point falls above the line, the blade geometry should be changed to reduce the predicted steady-state stress until an acceptable design is achieved.

The preceding practice neglects damping and is based on the premise that the nonresonant vibratory stress can be determined by the product of the steady-state stress due to hydrodynamic load, the amplitude of load fluctuation due to wakes from the upstream blade row, and the vibration magnification factor at the given wake-to-blade natural frequency ratio. Specifically, for the practice outlined, the following conditions must be met:

(1) The axial spacing between the blade row being analyzed and the upstream blade row should be equal to or greater than 10 percent of the upstream blade chord.

(2) The first natural frequency of the blade should be such that resonance due to wakes from the upstream blade row will not occur below a pump speed which is at least 15 percent above the mechanical design speed. Additionally, a 15-percent margin on speed should be maintained between the second harmonic of the wake forcing frequency and any of the blade natural frequencies (fig. 17).

It is recognized that it will not always be possible to apply the above practice – for example, in an axial pump with a wide operating range. In such cases, it is recommended that vibration amplitudes (and stresses) be estimated by the methods outlined in reference 41 or 42. Additionally, it is recommended that the designer consult references 72 and 73 to assist in the solution of design problems that might arise in a specific application. These references contain extensive bibliographies on the subject of blade stress and vibration.

3.3.1.2.3.1 Fabrication Effects

The stress analysis shall include the effects of manufacturing processes on material properties.

The material ultimate strength, yield strength, and endurance limit used in the design of the blades should be obtained from specimens that reflect the effects of manufacturing processes and surface finishes used for the manufactured blade.

3.3.1.2.3.2 Geometric and Environmental Effects

Calculations of blade natural frequencies shall include the effects of blade geometry and environment.

Analytical models that include geometric effects (i.e., taper, pre-twist, and camber) as well as the effect of centrifugal force should be employed (e.g., ref. 72). Additionally, the following should be considered:

Base fixity: The degree of base fixity depends on the type of attachment, and the judgment of the designer should be used for the specific design being analyzed. Experimental data for the M-1 dovetailed rotor blades are shown in figure 32. Note that at base loads equivalent to nominal design speed, the blade could be assumed to be "builtin" at the base.

Virtual mass of the fluid: Fluid virtual-mass effects depend on the blade geometry and the mode of vibration. Methods for determining the magnitude of this effect are given in references 74 and 75. In figure 33, experimental data (from ref. 74) for a 10-times-size Mark 15-F stator vane vibrating in air, oil, and water are compared with the results of the analytical-prediction method of reference 75. Note that in liquid hydrogen the effect will be small, but with denser fluids the frequency reduction is significant.

3.3.1.2.3.3 Verification of Natural Frequencies

Vibration testing of prototype or actual blades shall verify the calculated blade natural frequencies.

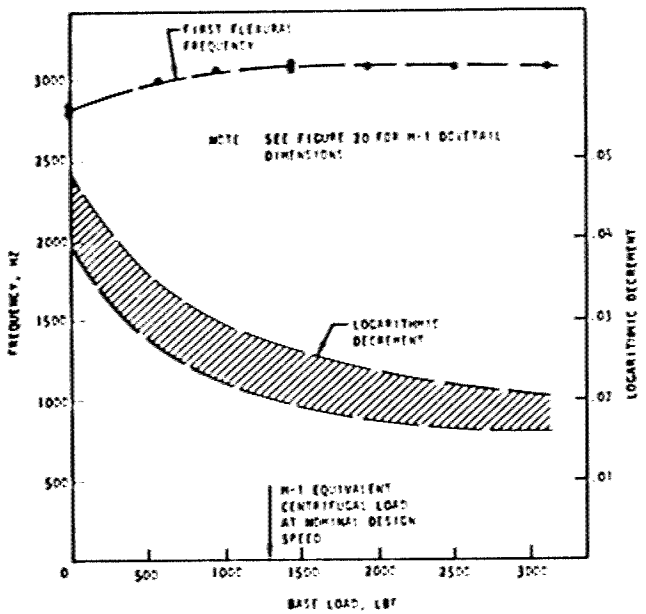

Figure 32. – Effect of base load on blade natural frequency and damping (M-1 dovetail).

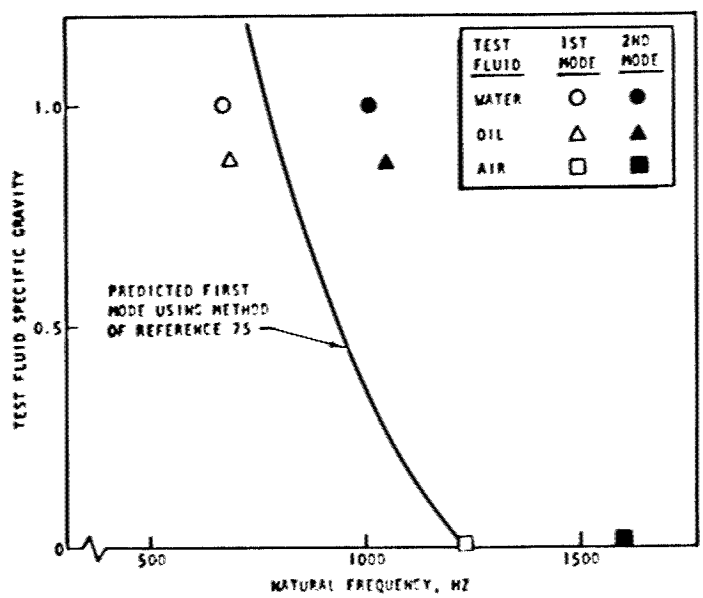

Figure 33. – Effects of fluid virtual mass on Mark 15-F vane natural frequency (data from ref. 74).

In view of the uncertainties involved in predicting the natural frequencies of low-aspect-ratio blading, it is recommended that bench testing be conducted on prototype or actual blades through a frequency range sufficient to encompass the known potential forcing frequencies within the pump. In the use of these frequencies in the vibration analysis, experimental magnitudes should be modified to account for operational and environmental effects (i.e., centrifugal effect, change in modulus of elasticity, and fluid virtual-mass effects).

3.3.1.2.3.4 Resonance Margin

Blade natural frequencies shall be separated from potential forcing frequencies by adequate margin under all conditions.

Campbell diagrams should be used to determine the proximity to resonance of blade natural frequencies with potential forcing frequencies. Figure 17 shows the recommended proximity-to-resonance margins applicable.

In addition to forcing frequencies due to wakes from adjacent blade rows, the pump should be examined for other sources of excitation (e.g., thrust-balance system or bearing-coolant return-flow ports).

3.3.1.2.3.5 Self-Excited Vibration

Blade size shall preclude self-excited vibration.

It is recommended that the empirical frequency-parameter rule noted below (adptd. from ref. 39) be used to avoid self-excited vibration:

$$\xi_t = \frac{2\pi f_t C}{w_1} \geqslant 1.6 \qquad (16)$$

$$\xi_b = \frac{2\pi f_b C}{w_1} \geqslant 0.33 \qquad (17)$$

where

ξ_t = torsional frequency parameter

f_t = first torsional frequency, Hz

f_b = first flexural frequency, Hz

C = blade chord length, ft

w_1 = fluid relative velocity at stall mid-radius, ft/sec

ξ_b = flexural frequency parameter

3.3.1.3 PROFILE TOLERANCES, SURFACE FINISH, AND FILLET RADII

3.3.1.3.1 Tolerances and Surface Finish

Profile tolerances and surface finish shall not adversely affect blade hydrodynamic performance or structural adequacy.

It is recommended that a maximum tolerance of ± 0.002 in. be specified on the basic profile with the restriction of a smooth and continuous fairing in both the transverse and longitudinal direction. Blade angles should be held within ¼°.

The specification of surface finish should consider the manufacturing technique that will be used in producing the blades. Surface finishes of 63 μin. rms or better are recommended. Transverse polish marks should not be permitted.

"Out-of-spec" parts. — There is evidence from the J-2 engine program (Mark 15-F pump) that local conditions that do not meet specifications ("out of spec") usually are of small consequence hydrodynamically. On the other hand, small deviations that prevail in all the rotor or stator blades, especially in the trailing-edge region, can seriously affect the hydrodynamic performance. In no case should an out-of-spec condition that would affect structural integrity be accepted.

3.3.1.3.2 Fillet Radii

Fillet radii shall be as small as possible within the limits imposed by structural considerations

A fillet radius equal to the maximum thickness of the blade is recommended. Available information (ref. 48) indicates a stress-concentration factor of approximately 1.1 would be applicable for the recommended fillet-to-blade thickness ratio for use in the blade design practice outlined in section 3.3.1.2.3. The reference noted above or other suitable data should be used in assessing stress-concentration factors for other fillet-to-blade thickness ratios.

3.3.2 Blade Attachment

3.3.2.1 METHODS

The blade attachment method shall reflect an acceptable compromise of weight, manufacturing, and assembly considerations.

An appropriate method for attaching the blades depends on the particular pump being designed. A single practice therefore cannot properly be recommended. A configuration study in which assembly, weight, and manufacturing (cost) considerations are evaluated should be made during the conceptual or preliminary design phase of the turbopump. The use of mechanically attached blades should receive consideration in applications requiring large production lots (potential lower cost at the expense of weight). If mechanically attached blades are selected, provision should be made to prevent incorrect assembly.

3.3.2.2 MECHANICAL DESIGN

3.3.2.2.1 Structural Strength

For mechanically attached blades, the attachment shall withstand loading equivalent to that which would cause airfoil failure.

Single-tang dovetails similar to those used on the M-1 pump are recommended if mechanically attached blades are utilized. A steady-state and vibratory-load condition at the dovetail corresponding to a stress state in the airfoil that would cause airfoil failure should be used in sizing the dovetail. This stress condition is shown on figure 16 and is the same as that determined by the practice defined in section 3.3.1.2.3.

The method used to retain the blade axially in the dovetail slot should provide positive retention of the blade under all probable load conditions. If shear pins are used, considerable safety margin must be applied, because it is difficult to ensure that the load will be reacted in pure shear.

3.3.2.2.2 Vibratory Stress

The predicted stress state in the attachment shall be less than the allowable alternating stress.

The predicted steady-state and vibratory stresses should be compared with material property data as defined by modified Goodman diagrams. Modified Goodman diagrams should be

constructed with adequate safety factors applied to yield strength, ultimate strength, and endurance limit. It is recommended that the diagram be constructed in accordance with the practice defined in section 3.3.1.2.3.

It is recommended that the maximum stress in the neck section of the dovetail be determined by methods based on the photoelastic test results (ref. 76). The vibratory stress magnitude should include an appropriate stress-concentration factor (ref. 48). Generous fillets should be used.

3.3.3 Rotor

3.3.3.1 CONFIGURATION

The basic rotor configuration (one-piece or builtup) shall reflect an acceptable compromise of weight, size, critical speed, cost, and assembly considerations.

A recommendation for a basic configuration that would be optimum for all applications cannot properly be made. Both builtup and one-piece configurations should be examined during the turbopump conceptual or preliminary design phase and a suitable choice made after evaluation of assembly methods, weight, and cost. Size permitting, a one-piece rotor machined from a single forging is preferred, because this construction precludes (1) disk interface, tie bolt, and bearing journal misalignment problems that may be associated with a builtup concpet, and (2) weldment-quality problems that may be associated with a one-piece welded configuration.

3.3.3.2 MECHANICAL DESIGN

Design criteria and recommended practices for mechanical design of the rotor are presented in reference 6.

3.3.4 Axial Thrust Balance System

3.3.4.1 TYPES OF SYSTEMS

The thrust-balance system shall preclude excessive thrust loads on the bearing.

It is recommended that a self-compensating thrust-balance system be used. The choice of system type (e.g., so-called series-flow or double-acting) depends on the particular

turbopump design. Each type should be examined during the conceptual or preliminary design phase of the turbopump to determine compromises in terms of recirculating-flow requirements (pump performance penalty), net thrust load magnitude and direction over the pump operating range, and potential instability.

3.3.4.2 MECHANICAL DESIGN

3.3.4.2.1 Design Basis

The design of the thrust-balance system shall be based on the net axial thrust of the pump and turbine over the total steady-state and transient operating range of the turbopump.

In view of the uncertainties involved in accurately predicting pump and turbine axial thrust both at design point and over the turbopump operating range, it is recommended that balance pistons be designed with excess load capability and with provision in the system to permit trimming during the turbopump development program. During the initial phase of the start transient, where it is normally not possible to counteract thrust with a thrust balance system, the axial load should be reacted by thrust bearings.

3.3.4.2.2 Structural Strength

The mechanical design of the thrust-balance piston shall be based on the combined effects of centrifugal, differential pressure, and differential thermal loads.

It is recommended that the stress due to centrifugal load be determined at a mechanical design speed that is at least 10 percent above the nominal design speed of the turbopump. This stress should be combined with the stress due to maximum differential pressure across the piston and the stress caused by differential thermal contraction at the piston/shaft interface.

3.3.4.2.2.1 Balance Piston Deflection

Axial deflection at the outer diameter of the balance piston due to pressure differential shall not adversely affect the flow system.

It is recommended that the piston be sized so that outer diameter axial deflection is less than 10 percent of the total axial piston travel.

3.3.4.2.3 Balance Piston/Pump Shaft Contact

Contact at the balance piston and pump shaft interface shall be positive under all operating conditions.

Recommended practices are presented in reference 6.

3.3.4.2.4 Balance Piston/Stationary Orifice Contact

The balance piston and stationary orifice shall not make contact at any operating condition.

It is recommended that stops be incorporated in the bearing package to avoid balance piston rubbing during the turbopump start transient. Reference 3 presents recommended practices. As a precaution, the stationary orifices should be fabricated from a material that will not shatter on impact or gall with the mating rotating surfaces (sec. 3.5).

3.3.4.3 SYSTEM STABILITY

3.3.4.3.1 Range of Stable Operation

The thrust-balance system shall be stable over the turbopump operating range.

Dynamic analysis should be conducted to establish a thrust-balance-system configuration that will be stable for all turbopump operating conditions. Methods of dynamic analysis are given in references 52, 54, and 55. From these references, it can generally be concluded that for liquid-hydrogen systems increased stability is achieved by

- Operating at high pressures (increased bulk modulus)
- Increasing cavity area
- Decreasing cavity volume
- Increasing total pressure drop.

3.3.4.3.2 Two-Phase Flow

The thrust-balance system shall not be subject to two-phase flow.

It is recommended that the thrust-balance-system return flow be introduced into the pumping system at a point where the pressure level is greater than the vapor pressure of the recirculating fluid. Conditions within the thrust balance system should be examined and the local static pressure of the fluid kept above fluid vapor pressure at all points within the flow circuit.

3.4 PUMP STATOR ASSEMBLY

3.4.1 Vanes

3.4.1.1 PROFILE TYPES

Design criteria and recommended practices for vane profile types are the same as for blade profile types (section 3.3.1.1).

3.4.1.2 MECHANICAL DESIGN

With the exception of centrifugal-load effects, the design criteria and recommended practices for vane mechanical design are the same as for blades (section 3.3.1.2).

3.4.1.3 PROFILE TOLERANCES, SURFACE FINISH, AND FILLET RADII

Design criteria and recommended practices for vane profile tolerances, surface finish, and fillet radii are the same as for blades (section 3.3.1.3).

3.4.2 Vane Attachment

3.4.2.1 METHODS

The vane attachment method shall reflect an acceptable compromise of weight, manufacturing, and assembly considerations.

As is the case with the blades, an appropriate method for attaching the vanes depends on the particular pump being designed, and a single practice cannot be recommended. The configuration study made in selecting a suitable method should include evaluation of weight, assembly difficulty, and cost. The use of individual vanes will in general require a

stator housing with a greater envelope diameter than that required for vanes machined integrally on segmented rings or cylinders. Thus, from a weight standpoint, the latter method is preferable. Individual vanes should be considered when large production lots are required.

3.4.2.2 MECHANICAL DESIGN

3.4.2.2.1 Structural Strength

The vane attachment shall withstand loading equivalent to that which would cause airfoil failure

A steady-state and vibratory load condition at the attachment corresponding to a stress state in the airfoil that would cause airfoil failure should be used in sizing the attachment. With the exception of centrifugal load considerations, this condition is the same as that shown on figure 16.

3.4.2.2.2 Vibratory Stresses

The predicted stress state in the vane attachment shall be below the allowable alternating stress.

The predicted attachment steady-state and vibratory stress should be compared with material property data as defined by modified Goodman diagrams. Modified Goodman diagrams should be constructed with adequate safety factors applied to yield strength, ultimate strength, and endurance limit. It is recommended that the diagram be constructed in accordance with the practice defined in section 3.3.1.2.3.

Vane attachments with lug-type projections should be examined to determine if a stress concentration should be applied to the projection fillet steady-state stress similar to that used in a blade dovetail design process (sec. 3.3.2.2.2). The vibratory stress magnitude should include an appropriate stress-concentration factor (ref. 48). A generous fillet from the projection to the vane platform should be used.

3.4.2.2.3 Load Transmittal

The method used to transmit stator assembly circumferential and axial loads to the housing shall provide positive load transmittal under all probable load conditions

Keys acting in shear have been successfully utilized to transmit stator torque loads on all state-of-the-art configurations and are therefore recommended. With regard to axial load, the stator assembly should be designed to be captive in the pump housing assembly. Differential thermal contraction of the housing and stator assembly in the axial direction should be matched to the extent that excessive looseness (or conversely excessive stress) is avoided.

3.4.3 Stator and Volute Housings

3.4.3.1 HOUSING TYPES

The stator/volute housing design shall reflect an acceptable compromise of hydrodynamic, stress and deflection, weight, and fabrication considerations.

Reference 1 should be consulted for a detailed state-of-the-art discussion along with design criteria and recommended practice for the volute portion of stator/volute housings. For axial pumps, a recommended basic housing configuration that would be optimum for all applications cannot properly be made. During the conceptual or preliminary design phase, hydrodynamic load, stress and deflection, weight, and fabrication (cost) considerations should be examined in arriving at a suitable configuration.

A "folded" volute (fig. 29) is preferred from both a weight and hydrodynamic standpoint. To avoid excessive losses, the flow from the last axial stage radially into the volute proper should be gradual. Diffuser vanes in the flow passage are recommended; these vanes guide and diffuse the flow and tie the volute walls together structurally. Welded structures should be selected if weight is a predominant consideration, and cast structures if fabrication lead time and cost are predominant. As noted, however, the lead time and cost advantages of castings have not always been achieved in practice. Thus, the fabrication methods should be carefully considered. With either welded or cast structures, if the total pump assembly concept permits, it is recommended that the stator/volute housing be an integral unit.

3.4.3.2 HYDRODYNAMIC DESIGN

Design criteria and recommended practices are presented in reference 1.

3.4.3.3 MECHANICAL DESIGN

Design criteria and recommended practices are presented in reference 1.

3.4.4 Bearing Housings

3.4.4.1 TYPES

The bearing housing shall satisfy radial stiffness requirements imposed by turbopump rotor system critical speed considerations and axial stiffness requirements imposed by the thrust balance system.

Radial and axial stiffness requirements of the bearing housings will be established during the conceptual or preliminary design phase of the turbopump assembly. The bearing housings themselves should be rigid structures with high spring constants. Low values for radial stiffness, if required from a critical-speed standpoint, should be achieved locally in a specially designed bearing carrier with stops provided to limit radial movement (ref. 10). The same principal should be used if a specified axial spring rate is desired. If, for example, preloaded ball bearings are used, the preload should be achieved by spring loading with axial stops provided in the housing. Rotor axial movement beyond the stop position should be reacted by a housing with high axial spring constant to preclude contact with the balance piston orifice (ref. 3).

3.4.4.2 MECHANICAL DESIGN

3.4.4.2.1 Structural Strength

The mechanical design of the bearing housing shall be based on the combined effects of pressure loading, internal loading, external loading, and thermal gradients.

Internal and external loads to which the bearing housing will be subjected will be partially dependent on the specific turbopump design. It is recommended that internal pressure (common to all designs) be assumed to be equal to 1.2 times the maximum pressure as determined from the hydrodynamic analysis. Rotor loads (common to all designs) should be determined in accordance with the criteria and practices defined in reference 6. External loads at the flanges can be caused by line installation misalignment, line pressure, differential thermal contractions, and inertia forces of attached components (sec. 3.4.5). It may also be necessary to consider turbopump mount reaction loads (dependent on turbopump assembly mount points). Turbine-end bearing housings that separate cryogenic propellant from a hot-gas turbine must be designed to withstand the stresses and deflections due to thermal gradients.

3.4.4.2.2 Clearances and Tolerances

The bearing housing design shall preclude rubbing of rotating and stationary turbopump components.

The pump housing assembly (i.e., the front and rear bearing housings, volute, and stator housing) must be examined as a unit in establishing the probable rotor and stator axial and radial clearance. As a part of this assembly, the bearing housings contribute strongly to rotor and stator alignment. Interference joints with mating housings should be dimensioned with diametral tolerances and concentricities suitable to achieve the desired "built-up" rotor and stator clearances. Absolute magnitudes will be dependent on the particular design. Axial dimensional tolerances should be controlled to the extent that the desired axial clearance can conveniently be achieved during pump assembly by shimming.

The radial deflection analysis should consider the rotor movement due to radial load on the rotor (high bearing-housing spring rate is desired to limit radial deflection). The bearing-housing structure at turbopump mount points should be sufficiently rigid to limit local deflection to magnitudes below those that would cause rubbing.

3.4.4.2.3 Safety Factors

Adequate safety factors shall protect the bearing housing against ultimate and yield failure.

It is recommended that safety factors of 1.5 on ultimate strength and 1.1 on 0.2 percent yield be utilized. The complexity of the specific design will dictate the method to be used in the stress and deflection analysis. Finite-element methods are recommended for analysis of complex-shape, thick-shell structures. If webs are used in the structure, web thickness-to-fillet radius ratios of 1.0 or greater are recommended.

Verify the stress and deflection analysis by structural testing of bearing housings as a component or as part of the total turbopump housing assembly.

3.4.5 Housing Interfaces and Static Sealing

3.4.5.1 INTERFACE AND SEAL TYPES

3.4.5.1.1 Alignment

The housing-to-housing interfaces and seals shall provide for and maintain radial and axial alignment of the rotor relative to the turbopump housing assembly.

It is recommended that interference-fit pilot diameters be used on housing-to-housing joints and that some degree of interface fit be maintained under all interface environmental conditions. Note that the recommended practice here does not apply to those interfaces where an extreme temperature differential may exist (e.g., between the pump housing and turbine manifold).

3.4.5.1.2 Leakage

The housing-to-housing interface and seal shall reliably prevent propellant leakage throughout the turbopump operating range.

Available seal types should be examined during the conceptual or preliminary design phase of the turbopump and a suitable seal type selected. A seal type that has demonstrated reliable sealing in previous applications with the same fluid should be utilized wherever possible. Reference 59 provides design guidance on seals.

3.4.5.2 MECHANICAL DESIGN

3.4.5.2.1 Structural Strength

Structural continuity shall exist in all housing-to-housing interface joints throughout the turbopump operating range.

The interface joint should be preloaded such that the joint remains tight under all operating conditions. The interface should be examined for symmetric and asymmetric loads at the assembly conditions, the pump steady-state operating conditions, and transient-temperature conditions. In determining the required bolt preload, the elastic stiffness of the parts making up the joint assembly should be calculated for each of the environmental conditions and a spring model used in determining loads and stresses.

3.4.5.2.2 Bolt Preload

The method for preloading the bolt at assembly shall reliably induce the preload without exceeding allowable stresses.

In critical joints, it is recommended that bolt elongation or other positive preload indicators be used. In those joints where torque measurement is specified, the maximum permissible assembly torque and the minimum probable coefficient of friction should be employed in determining maximum stress. The minimum permissible assembly torque and the maximum probable coefficient of friction should be used in determining minimum joint preload.

3.4.5.2.3 Safety Factors

Design safety factors shall ensure that the joint will not fail in either ultimate or yield.

Since the joint design is based on the elastic stiffness of the components making up the assembly, it is important to stay within the linear range of the stress-strain diagram. Safety factors of 1.5 on ultimate strength and 1.1 on 0.2 percent yield generally are recommended. However, these safety factors should be examined for each design to ensure that the allowable stresses are within the linear range. The "effective" stress of the bolt should be used in comparing bolt design stress to material property data. The Mises-Hencky theory of failure (ref. 71) is recommended.

3.5 MATERIALS

Criteria and recommended practices given here are applicable to axial-flow pumps for use with liquid-hydrogen propellant.

3.5.1 Property Data

Selection of materials for components in liquid-hydrogen axial-flow pumps shall be based on guaranteed minimum properties or typical property data adjusted to reflect probable minumum property values.

Typical property data at liquid-hydrogen temperature for various materials are given in references such as 61 through 66. Recommended materials that have been utilized successfully in liquid-hydrogen axial pumps are noted in Table IV. Data for these materials are given principally in references 62, 63, 64, and 66 and include the appropriate heat treatment for the heat-treatable alloys.

3.5.2 Ductility

Materials shall possess adequate ductility at liquid-hydrogen temperatures.

It is recommended that materials with an elongation of at least 4 percent in four diameters at liquid-hydrogen temperature be utilized for components that may be subject to local yielding under steady load conditions.

3.5.3 Impact Strength

Materials for components that may be subject to impact loading shall possess adequate impact strength at liquid-hydrogen temperature.

If impact loading is anticipated, it is recommended that the materials possess an impact strength (Charpy V-notch) of at least 12 ft-lbf (or equivalent) at liquid-hydrogen temperature.

In particular, materials for thrust-balance-system components that may be subject to rubbing should not shatter on impact or gall with mating surfaces. The following material combinations have demonstrated non-shattering and anti-galling characteristics in liquid-hydrogen thrust-balance-systems and hydrostatic bearings and are therefore recommended:

Rotating Component	Stationary Component
K-Monel	Leaded bronze
Inconel 718 (tungsten-carbide plated)	Leaded bronze (ref. 77)
Titanium (Ti-A110-AT-ELI)	Leaded bronze

3.5.4 Endurance Limit

Materials for components subject to combined steady-state and appreciable vibratory stress shall possess adequate endurance limit.

Experimental data defining the endurance limit at liquid-hydrogen temperature have been obtained only on a few selected alloys. If endurance-limit data are not available for the alloy selected, it may be necessary to assume an endurance ratio in the preliminary design phase of the turbopump. However, the significance of the endurance-limit magnitude in the design of blades or vanes, for example, clearly indicates that final designs should be based on experimental data with specimens that reflect manufacturing processes and surface finishes comparable to those of the production component.

APPENDIX A

Conversion of U.S. Customary Units to SI Units

Physical quantity	U.S. customary unit	SI unit	Conversion factor[a]
Angle	deg	rad	1.745×10^{-2}
Flowrate	gpm	m^3/sec	6.309×10^{-5}
Force	lbf	N	4.448
Headrise	ft	m	3.048×10^{-1}
	ft-lbf/lbm	J/kg	2.989
Impact energy	ft-lbf	J	1.356
Length	ft	m	3.048×10^{-1}
	in.	cm	2.54
Load	lbf	N	4.448
Mass	lbm	kg	4.536×10^{-1}
NPSH	ft	m	3.048×10^{-1}
	ft-lbf/lbm	J/kg	2.989
Pressure	psi ($lbf/in.^2$)	N/cm^2	6.895×10^{-1}
	psf(lbf/ft^2)	N/m^2	4.788×10^{1}
Rotational speed	rpm	rad/sec	1.047×10^{-1}
Stress	psi ($lbf/in.^2$)	N/cm^2	6.895×10^{-1}
Surface finish	μin.	μm	2.54×10^{-2}
Temperature	°F	K	$K = \frac{5}{9}(°F + 459.67)$
Volume	ft^3	m^3	2.832×10^{-2}
	gal	m^3	3.785×10^{-3}

[a]Except for temperature, where the conversion is made as shown, multiply value given in U.S. customary unit by conversion factor to obtain equivalent value in SI unit. For a complete listing of conversion factors for basic physical quantities, see Mechtly, E. A.: The International System of Units. Physical Constants and Conversion Factors. Second Revision, NASA SP-7012, 1973.

APPENDIX B
GLOSSARY

Term	Definition
allowable load (or stress)	the load that, if exceeded in the slightest, produces failure of the pump structural element under consideration. Failure may be defined as buckling, yielding, ultimate, or fatigue failure, whichever condition prevents the component from performing its intended function. Allowable load is sometimes referred to as criterion load or stress; allowable stress is equivalent to material strength.
aspect ratio	ratio of blade height (or length) to chord length
balance drum (balancing drum)	special balancing device used to balance axial thrust in multi-stage pumps; it can be used in combination with an automatic balancing disk or alone (seldom)
base fixity	index of the relative tightness in the mounting of the blade in the rotor or the vane in the vane support
blockage	decrease in effective flow area due to the boundary layer on the blades and end wall
blockage factor	the fraction or percentage by which design flow area is increased to account for blockage; conversely, the ratio of flow area corrected for blockage to design flow area
cavitation	formation of vapor bubbles in a flowing liquid whenever the static pressure becomes less than the fluid vapor pressure
chord length	linear distance between the end points of the blade-profile leading and trailing edges as measured on the chord line (a line joining the points of intersection of the blade profile leading edge and trailing edge with the mean camber line)
creep	permanent deformation of material caused by a tensile load that is less than the load necessary to yield the material; some time is required to obtain creep
critical speed	shaft rotational speed at which a natural frequency of a rotor/stator system coincides with a possible forcing frequency
cryogenic	fluids or conditions at low temperatures, usually at or below –238°F

Term	Definition
curvic coupling	trade name of the Gleason Works for a face-gear type of coupling generated in a manner similar to that used for bevel gears
design load (or pressure)	product of the limit load (or pressure) and the design safety factor
design stress	the stress, in any structural element, that results from the application of the design load or combination of design loads, whichever condition results in the highest stress
deviation angle	angle between fluid outlet direction and the tangent to the blade mean camber line at the trailing edge
D-factor (diffusion factor)	an index of local diffusion on the blade suction surface: $(DF)_R = 1 - \frac{w_2}{w_1} + \frac{\Delta w_u}{2\sigma w_1}$ $(DF)_S = 1 - \frac{V_3}{V_2} + \frac{\Delta V_u}{2\sigma V_2}$
end wall	surface of the housing and rotor hub between adjacent blades
endurance limit (fatigue limit)	maximum alternating stress at which a material presumably can endure an infinite number of cycles
forced-vortex flow	flow in which the fluid tangential velocity is forced to vary in a manner other than inversely with radius
free-vortex flow	flow in which the fluid axial velocity is constant from hub to tip while the fluid tangential velocity varies inversely with radius
hub/tip ratio	ratio of rotor radius at blade hub to rotor radius at blade tip
hydrogen embrittlement	loss of ductility in a metal as a result of the exposure of the metal to newly formed gaseous hydrogen
impulse stage	stage in which there is no change in static headrise across the rotor
incidence angle	angle between fluid-inlet direction and tangent to blade mean camber line at leading edge
limit load (or pressure)	maximum expected load (or pressure) that will occur in a structure under the specified conditions of operation, with allowance for statistical variation

Term	Definition
Mach number	ratio of the speed of fluid flow to the speed of sound in the fluid
magnification factor	ratio of the deflection produced by an alternating load to the deflection produced by a steady load of the same magnitude
margin of safety (MS)	the fraction by which the allowable load or stress exceeds the design load or stress $$MS = \frac{1}{R} - 1$$
net positive suction head (NPSH)	$$NPSH = \left[\frac{\text{total fluid pressure} - \text{fluid vapor pressure}}{\text{fluid density}} \right] \text{ at inlet}$$
proof pressure	design pressure multiplied by the proof-test safety factor (proof pressure is the reference from which the pressure levels for acceptance testing are established)
radial equilibrium	flow condition in an annular passage in which there is no radial velocity component; i.e., the fluid pressure forces in the radial direction are in equilibrium with the centrifugal forces
reaction	the ratio of static headrise in the rotor to static headrise in the stage
recovery moment	bending caused by centrifugal force in a blade that is tilted from a radial line
retardation factor	an index of blade-passage diffusion: $$(RF)_R = \frac{w_2}{w_1} ; \; (RF)_S = \frac{V_3}{V_2}$$
root	juncture of blade and rotor hub
safety factor	an arbitrary multiplier (or divider) greater than 1 applied in design to account for uncertainties in design, e.g., variations in material properties, fabrication quality, and load distributions within the structure
solidity (blade)	ratio of blade chord length to blade spacing
stacking axis (or line)	imaginary line on which the centers of gravity of the profile sections are stacked to form the blade or vane shape from hub to tip

Term	Definition
stagger angle	the angle between the chord line and a reference direction that usually is the axis normal to the plane of the blade row
stall	loss of pumping capability as a result of flow separation on the suction surface of the blades
stall margin	margin between pump operation at the design-point flow coefficient and operation at the flow coefficient at which the pump will stall
thrust-balance flow	flow through the thrust balance system that provides the (pressure X area) force necessary to balance axial thrust
untwist forces	forces acting on a twisted blade that produce a torque tending to reduce the blade twist
virtual mass	mass of fluid near a vibrating blade that vibrates with the blade
volute	spiral-shaped portion of the housing that collects the fluid from the last stage of a pump

Symbol	Definition
C	chord length
C-4	designation for a family of airfoil shapes
D	diameter
D_s	specific diameter, $D_s = DH^{1/4}/Q^{1/2}$
DF	diffusion factor
DN	index to bearing speed capability, the product of bearing bore size (D) in mm and rotational speed (N) in rpm
ELC	extra low carbon (content)
F	material strength
f	frequency
g	acceleration due to gravity
g_c	gravitational constant, 32.17 $\frac{\text{lbm-ft}}{\text{lbf-sec}^2}$

Symbol	Definition
H	headrise, $H = H_2 - H_1$ (stage)
i	fluid incidence angle
k	stress-concentration factor
MS	margin of safety
N	pump rotational speed
N_s	specific speed, $N_s = NQ^{1/2}/H^{3/4}$
NPSH	net positive suction head
O/F	ratio of mass flowrate of oxidizer to mass flowrate of fuel
Q	volume flowrate
P	pressure
R	(1) reaction (2) ratio of design load or stress to allowable load or stress
RF	retardation factor
r	radius
S	blade tangential spacing
S_s	suction specific speed, $S_s = NQ^{1/2}/(NPSH)^{3/4}$
SF	safety factor
TIG	tungsten-inert-gas (welding method)
T73	designation for a heat-treating and tempering process for aluminum alloys
u	blade tangential velocity
V	fluid absolute velocity
w	fluid velocity relative to blade

Symbol	Definition
Z	cavitation-breakdown correlation parameter, $Z = \phi \tan(\beta_T/2)$
65 series	NACA designation for a family of airfoil shapes
α	stagger angle
β	fluid angle
δ	deviation angle
η	efficiency
θ	blade camber angle
ν	hub-to-tip radius ratio, $\nu = r_H/r_T$
ξ	frequency parameter
σ	(1) stress; (2) solidity, $\sigma = C/S$
τ_R	cavitation parameter, $\tau_R = NPSH/(u^2/2g_c)$
ϕ	flow coefficient, $\phi = V_m/u$
ψ	head coefficient, $\psi = g_c H/u^2$
$\bar{\omega}$	total-pressure-loss coefficient: $\bar{\omega}_R = \dfrac{H_{loss}}{w_1^2/2g_c}$; $\bar{\omega}_S = \dfrac{H_{loss}}{V_2^2/2g_c}$

Subscripts

a	axial
alt	alternating
b	flexural
cf	centrifugal forces
e	endurance
eq	equivalent
exit	outlet

Subscripts

f	fluid
ff	fluid forces
H	hub; hydraulic
i	ideal
l	liquid (fluid)
m	meridional; mean
R	rotor
S	stator
ss	steady state
T	tip
t	torsional
tu	tensile ultimate
ty	tensile yield
u	tangential
v	vapor
1	rotor inlet
2	rotor outlet or stator inlet
3	stator outlet or second rotor inlet

Material	Identification
CRES	corrosion-resistant steel
helium	pressurant helium (He) per MIL-P-27407
Inconel 718	trade name of International Nickel Co. for nickel-base alloys (AMS 5597A)

Material	Identification
K-Monel	trade name of International Nickel Co. for a wrought, age-hardenable alloy containing Ni, Cu, and Al
leaded bronze	copper alloy containing zinc and lead
LH_2	liquid hydrogen (H_2), propellant grade per MIL-P-27201
LOX	liquid oxygen, propellant grade per MIL-P-25508
polyurethane	any of various thermoplastic polymers that contain -NHCOO- linkages; produced as fibers, coatings, flexible and rigid foams, elastomers, and resins
Ti-A110-AT-ELI	an extra-low-interstitial (ELI) grade of Ti-5Al-2.5Sn in which the interstitial elements O, N, and H and the substitutional element Fe are controlled at lower-than-normal contents; strength-to-density ratio, notch toughness, and ductility remain at acceptable levels down to $-423^{\circ}F$ (LH_2 temperature)
300 Series (e.g., 304, 310, 347)	series of austenitic stainless steels
304L (304 ELC)	extra-low-carbon variety of 304 austenitic steel; used in weldments for corrosive conditions where intergranular carbide precipitation must be avoided
2024	wrought aluminum alloy with Cu as principal alloying element
7075	wrought aluminum alloy with Zn as principal alloying element

ABBREVIATIONS

Organization	Identification
AF	Air Force
AIAA	American Institute for Aeronautics & Astronautics
ASME	American Society of Mechanical Engineers
NAA	North American Aviation, Inc.
NACA	National Advisory Committee for Aeronautics (now NASA)

Organization	Identification
NREC	Northern Research and Engineering Corporation
PWA	Pratt & Whitney Aircraft
WADC	Wright Air Development Center

REFERENCES

1. Anon.: Liquid Rocket Engine Centrifugal Flow Turbopumps. NASA Space Vehicle Design Criteria Monograph, NASA SP-8109, December 1973.

2. Anon.: Liquid Rocket Engine Turbopump Inducers. NASA Space Vehicle Design Criteria Monograph, NASA SP-8052, May 1971.

3. Anon.: Liquid Rocket Engine Turbopump Bearings. NASA Space Vehicle Design Criteria Monograph, NASA SP-8048, March 1971.

4. Anon.: Liquid Rocket Engine Turbopump Rotating-Shaft Seals. NASA Space Vehicle Design Criteria Monograph, NASA SP-8121, February 1978.

5. Anon.: Liquid Rocket Engine Turbines. NASA Space Vehicle Design Criteria Monograph, NASA SP-8110, January 1974.

6. Anon.: Liquid Rocket Engine Turbopump Shafts and Couplings. NASA Space Vehicle Design Criteria Monograph, NASA SP-8101, September 1972.

7. Anon.: Turbopump Systems for Liquid Rocket Engines. NASA Space Vehicle Design Criteria Monograph, NASA SP-8107, August 1974.

8. Severud, L. K.; and Reeser, H. G.: Analysis of the M-1 Liquid Hydrogen Turbopump Shaft Critical Whirling Speed and Bearing Loads. NASA CR-54825, Aerojet-General Corp., Dec. 20, 1965.

9. Gunn, S. V.; and Dunn, C.: Dual Turbopump Liquid Hydrogen Feed System Experience. Paper presented at the Ninth Liquid Propulsion Symposium (St. Louis, MO), Oct. 25-27, 1967.

10. Graham, R. D.; Rowan, B. F.; and Shen, F. A.: Axial Pump Rotordynamic Study, Final Report. NASA CR-72302, R-6982, Rocketdyne Div., N. Am. Aviation, Inc., Oct. 1, 1967.

11. Gunter, E. J., Jr.: Analysis of Rocketdyne Nuclear Feed System Turbopump Failure. W-12-229, Res. Lab. for Engineering Sciences, Univ. of Virginia, June 1966.

12. Childs, D. W.: The Space Shuttle Main Engine High Pressure Fuel Turbopump Rotordynamic Instability Problem. Paper 77-GT-49, Gas Turbine Conference (Philadelphia, PA), March 27-31, 1977.

13. Choy, K. C.; Gunter, E. J.; and Allaire, P. E.: Rotor Transient Analysis by the Modal Method. Vol. 1 – Theory; Vol. 2 – Computer Program. Rep. 528144 (MAE 77/105), Univ. of Virginia, Sept. 8, 1977.

14. Balje, O. E.: A Study on Design Criteria and Matching of Turbomachines. J. Eng. Power, Trans. ASME, Series A, vol. 84, 1962, pp. 83-114.

15. Crouse, J. E.; Montgomery, J. C.; and Soltis, R. F.: Investigation of the Performance of an Axial Flow Pump Stage Designed by the Blade Element Theory – Design and Overall Performance. NASA TN D-591, February 1961.

16. Crouse, J. E.; and Sandercock, D. M.: Blade-Element Performance of 0.7 Hub-Tip Radius Ratio Axial-Flow-Pump Rotor with Tip Diffusion Factor of 0.43. NASA TN D-2481, September 1964.

17. Miller, M. J.; and Crouse, J. E.: Design and Over-All Performance of an Axial-Flow-Pump Rotor with a Blade-Tip Diffusion Factor of 0.66. NASA TN D-3024, September 1965.

18. Johnsen, I. A.; and Bullock, R. O., eds.: Aerodynamic Design of Axial-Flow Compressors. NASA SP-36, 1965.

19. Farquhar, J.; and Lindley, B. K.: Hydraulic Design of the M-1 Liquid Hydrogen Turbopump. NASA CR-54822, Aerojet-General Corp., July 15, 1966.

20. Lieblein, S.; Schwenk, F. C.; and Broderick, R. L.: Diffusion Factor for Estimating Losses and Limiting Blade Loading in Axial Compressor Blade Elements. NACA RME53D01, 1953.

21. Lieblein, S.: Analysis of Experimental Low Speed Loss and Stall Characteristics of Two-Dimensional Compressor Blade Cascades. NACA RME57A28, 1957.

22. Miller, M. J.; Crouse, J. E.; and Sandercock, D. M.: Summary of Experimental Investigation of Three Axial-Flow Pump Rotors Tested in Water. J. Eng. Power, Trans. ASME, Series A, October 1967, pp. 589-599.

23. Taylor, W. E.; Murrin, T. A.; and Colombo, R. M.: Systematic Two-Dimensional Cascade Tests, Vol. 1 – Double-Circular-Arc Hydrofoils. NASA CR-72498, UARL-H910254-50, United Aircraft Corp., December 1969.

24. Taylor, W. E.; Murrin, T. A.; and Colombo, R. M.: Systematic Two-Dimensional Cascade Tests. Vol. 2 – Multiple Circular-Arc Hydrofoils. NASA CR-72499, UARL-J910254-56, United Aircraft Corp., April 6, 1970.

25. Colombo, R. M.; and Murrin, T. A.: Systematic Two-Dimensional Cascade Tests. Vol. 3 – Slotted Double-Circular-Arc Hydrofoils. NASA CR-72870, United Aircraft Corp., May 1, 1972.

26. Murrin, T. A.; and Taylor, W. E.: Systematic Two-Dimensional Cascase Tests. Vol. 4 – Cascade Test Data. NASA CR-121101, United Aircraft Corp., March 15, 1973.

27. Shepard, D. G.: Principles of Turbomachinery. The Macmillan Co. (New York), 1956.

*28. Anon.: Parametric Studies. Part V of Pump Hydrodynamic Design. Rocketdyne Div., N. Am. Aviation, Inc., unpublished, pp. 33-40.

* Dossier for the design criteria monograph "Liquid Rocket Engine Axial-Flow Turbopumps" Unpublished Collected source material available for inspection at NASA Lewis Research Center, Cleveland, Ohio

*29. Campbell, W. E.; Robertson, C. F.; and Yoshikawa, D. K.: The Design and Evaluation of an Axial-Flow Impulse Pump. Aerojet-General Corp., December 1962.

30. Bissell, W. R.; King, J. A.; Umemoto, G. A.; and Wong, G. S.: Investigation of Liquid Hydrogen Axial Flow Impulse Pump (U). Bull. 7th Liquid Propulsion Symp., vol. 2, Johns Hopkins Univ., November 1967, pp. 233-258. (CONFIDENTIAL)

31. Howell, A. R.: Fluid Dynamics of Axial Compressors. Proc. Inst. Mech. Engrs. (London), vol. 153, 1945, p. 445.

32. Crouse, J. E.; Soltis, R. F.; and Montgomery, J. C.: Investigation of the Performance of an Axial-Flow-Pump Stage Designed by the Blade-Element Theory – Blade Element Data. NASA TN D-1109, December 1961.

33. Crouse, J. E.; and Sandercock, D. M.: Design and Over-All Performance of an Axial-Flow-Pump Rotor with a Blade-Tip Diffusion Factor of 0.43. NASA TN D-2295, May 1964.

34. Miller, M. J.; and Sandercock, D. M.: Blade Element Performance of Axial-Flow-Pump Rotor with Blade-Tip Diffusion Factor of 0.66. NASA TN D-3602, September 1966.

35. Stripling, L. D.; and Acosta, A. J.: Cavitation in Turbopumps. Parts 1 and 2, J. Basic Eng., Trans. ASME, Series D, vol. 84, 1962, pp. 326-350.

36. Serovy, G. K.; and Tysen, J. C.: Prediction of Axial Flow Turbomachine Performance by Blade Element Methods. Paper 61-WA-135, ASME Winter Ann. Mtg., Nov. 26-Dec. 1, 1961.

37. King. J. A.: Testing Pumps in Air. Paper 67-WA/FE- 4, ASME Winter Ann. Mtg., Nov. 12-17, 1967.

38. Lieblein, S.; and Roudebush, W. H.: Low Speed Wake Characteristics in Two-Dimensional Cascades and Isolated Airfoil Sections. NACA TN-3771, 1956.

39. Armstrong, E. K.; and Stevenson, R. E.: Some Practical Aspects of Compressor Blade Vibration. J. Royal Aeron. Soc., vol. 64, no. 591, March 1960, pp. 117-130.

40. Kemp, N. H.; and Sears, W. R.: Aerodynamic Interference Between Moving Blade Rows. J. Aeron. Sci., vol. 20, no. 9, September 1953, pp. 585-597, 612.

41. Smith, J. E.: Vibration of Blades in Axial Turbomachinery. Paper 66-WA/GT-12, ASME Winter Ann. Mtg., New York, NY, Nov. 27-Dec. 1, 1966.

42. Traupel, Walter: Thermische Turbomaschinen. Erster Band, Springer Verlag (Berlin; Gottingen; Heidelberg), 1958.

43. Carter, A. D. S.: Blade Profiles for Axial-Flow Fans, Pumps, Compressors, etc. Proc. Inst. Mech. Engineers (London), vol. 175, no. 15, 1961, pp. 775-806.

* Dossier for the design criteria monograph "Liquid Rocket Engine Axial-Flow Turbopumps." Unpublished. Collected source material available for inspection at NASA Lewis Research Center, Cleveland, Ohio.

44. Anon.: J-2 Program, Quarterly Progress Report, Period ending August 31, 1963. NAA-R R-2600-12, Rocketdyne Div., N. Am. Aviation, Inc.

45. Sawyer, J. W., ed.: Gas Turbine Engineering Handbook. Gas Turbine Publications, Inc. (Stamford, CT), 1966.

46. Severud, L. K.; and Chinn, T.: Analytical and Experimental Vibration Analysis of the Turbine Buckets for the M-1 Liquid Oxygen Turbopump. NASA CR-54830, Aerojet-General Corp., 1965.

47. Regan, P. J.: Mechanical Design of the M-1 Axial Flow Liquid Hydrogen Fuel Pump. NASA CR-54823, Aerojet-General Corp., Feb. 15, 1966.

48. Peterson, R. E.: Stress Concentration Factors. John Wiley & Sons, Inc. (New York), 1953.

49. Anon.: J-2 Program, Quarterly Progress Report, Period Ending October, 1960. NAA-R R-2600-1, Rocketdyne Div., N. Am. Aviation, Inc., November, 1960.

50. Anon.: Development of a 1,500,000-lb-Thrust (Nominal Vacuum) Liquid Hydrogen/Liquid Oxygen Engine. Quarterly Tech. Prog. Rep. 4014-02Q-2, Aerojet-General Corp., July 25, 1963.

51. Lynn, E. K.: Experimental Stress Analysis in the Design of a Liquid Hydrogen Pump Rotor. Experimental Mechanics, vol. 2, no. 12, December 1962, pp. 19A-23A.

52. Watters, W. E.; and Luehr, L.: Development of Steady-State and Dynamic Performance Prediction Methods for Turbopump Self-Compensating Thrust Balance Systems. NASA CR-72630, AGC-9400-19, Rev. 1, Aerojet-General Corp., March 30, 1970.

53. Young, W. E.; and Due, H. F.: Investigation of Pressure Prediction Methods for Radial Flow Impellers, Phase II, Final Report. PWA FR-1276, Pratt & Whitney Aircraft Div. of United Aircraft, March 8, 1965.

54. Connelly, R. E.: Design Study of the Mark 9 Pump. WADC-TN-59-122, Rep. R-1354, Rocketdyne Div., N. Am. Aviation, Inc., March 1959.

*55. Anon.: Dynamic Stability Study of a Series-Flow Thrust Balance System. Appendix B, R6809P-1, Rocketdyne Div., N. Am. Aviation, Inc., 1968, unpublished.

56. Stepanoff, A. J.: Centrifugal and Axial Flow Pumps. Second ed. John Wiley & Sons, Inc. (New York), 1957.

57. Radkowski, P. P.; Davis, R. M.; and Bodul, M. R.: A Numerical Analysis of the Equation of Thin Shells of Revolution. ARS J., vol. 32, no. 1, January 1962, pp. 36-41.

58. Becker, E. B.; and Brisbane, J. J.: Application of the Finite-Element Method to Stress Analysis of Solid Propellant Rocket Grains. Rep. S-76, vol. I (AD 474031), November 1965; vol. II, part 1 (AD 476515) and vol. II, part 2 (AD 476735), Rohm & Haas Co., January 1966.

* Dossier for the design criteria monograph "Liquid Rocket Engine Axial-Flow Turbopumps" Unpublished Collected source material available for inspection at NASA Lewis Research Center, Cleveland, Ohio.

59. Anon.: Liquid Rocket Disconnects, Couplings, Fittings, Fixed Joints, and Seals. NASA Space Vehicle Design Criteria Monograph, NASA SP-8119, September 1976.

60. Blakis, R.; Lindley, B. K.; Ritter, J. A.; and Watters, W. E.: Initial Test Evaluation of the M-1 Liquid Hydrogen Turbopump Including Installation, Test Procedures, and Test Results. NASA CR-54827, Aerojet-General Corp., July 20, 1966.

61. Sessler, J. G.; and Weiss, V.: Aerospace Structural Metals Handbook. 2 vols. ASD-TDR-63-741, (Syracuse University), Air Force Materials Lab., March 1967.

62. Williams, L. R.; Young, J. D.; and Schmidt, E. H.: Design and Development Engineering Handbook of Thermal Expansion Properties of Aerospace Materials at Cryogenic and Elevated Temperatures. R-6981, Rocketdyne Div., N. Am. Aviation, Inc., March 30, 1967.

63. Janser, G. R.: Summary of Materials Technology of M-1 Engine. NASA CR-54961, Aerojet-General Corp., July 22, 1966.

64. Inouye, F. T.; Hunt, V.; Janser, G. R.; and Frick, V.: Application of Alloy 718 in M-1 Engine Components. NASA CR-788, Aerojet-General Corp., June 1967.

65. Inouye, F. T.: Properties of Large 7079 Aluminum Alloy Forgings in a Cryogenic Environment. NASA CR-513, Aerojet-General Corp., July 1966.

*66. Malin, Craig: Typical Low-Temperature Mechanical Properties of Several Materials. Memo MPR-3-251-369, Rocketdyne Div., N. Am. Aviation, Inc., 1963, unpublished.

67. Anon.: Development of a 1,500,000-lb-Thrust (Nominal Vacuum) Liquid Hydrogen/Liquid Oxygen Engine. Quarterly Tech. Prog. Rep. 2555-04Q-1, January – March 1965, Aerojet-General Corp., April 20, 1965.

68. Carter, A. D. S.: The Axial Compressor. Sec. 5 of Gas Turbine Principles and Practice, Sir H. R. Cox, ed., D. Van Nostrand Co., Inc. (New York), 1955.

69. Vavra, M. H.: Aero-Thermodynamics and Flow in Turbomachines. John Wiley & Sons, Inc. (NY) 1960.

70. Horlock, J. H.: Axial Flow Compressors. Butterworth Scientific Publications (London), 1958.

71. Roark, R. J.: Formulas for Stress and Strain. Fourth ed., McGraw-Hill Book Co. (New York), 1965.

72. Anon.: The Vibration of Blades in Axial Turbomachinery, Part 1: Theory and Practice of Design and Development. Rep. 1088-1 (AD 645156), Northern Research and Engineering Corp. (Cambridge, MA), April 29, 1965.

73. Anon.: The Vibration of Blades in Axial Turbomachinery, Part 2: Design and Development Handbook. Rep. 1088-2, Northern Research and Engineering Corp. (Cambridge, MA), April 29, 1965.

* Dossier for the design criteria monograph "Liquid Rocket Engine Axial-Flow Turbopumps." Unpublished. Collected source material available for inspection at NASA Lewis Research Center, Cleveland, Ohio.

*74. Turner, J. D.: The Effect of Fluid Density On Stator Blade Resonant Frequency. SM 3111-8073A, Rocketdyne Div., N. Am. Aviation, Inc., 1963, unpublished.

75. Bisplinghoff, R. L.; and Ashley, H.: Principles of Aeroelasticity. John Wiley & Sons, Inc. (New York), 1962.

76. Heywood, R. B.: Designing by Photoelasticity. Chapman and Hall, Ltd. (London), 1952.

77. Young, W. E.; and Reddecliff, J. M.: Investigation of Hydrostatic Bearings for use in High Pressure Cryogenic Turbopumps, Final Report, March 1, 1966 – March 31, 1967 (U). AFRPL-TR-67-130, Pratt & Whitney Aircraft Div., United Aircraft, May 15, 1967. (CONFIDENTIAL)

* Dossier for the design criteria monograph "Liquid Rocket Engine Axial-Flow Turbopumps." Unpublished Collected source material available for inspection at NASA Lewis Research Center, Cleveland, Ohio.

NASA SPACE VEHICLE DESIGN CRITERIA MONOGRAPHS ISSUED TO DATE

ENVIRONMENT

SP-8005	Solar Electromagnetic Radiation, Revised May 1971
SP-8010	Models of Mars Atmosphere (1974), Revised December 1974
SP-8011	Models of Venus Atmosphere (1972), Revised September 1972
SP-8013	Meteoroid Environment Model–1969 (Near Earth to Lunar Surface), March 1969
SP-8017	Magnetic Fields–Earth and Extraterrestrial, March 1969
SP-8020	Surface Models of Mars (1975), Revised September 1975
SP-8021	Models of Earth's Atmosphere (90 to 2500 km), Revised March 1973
SP-8023	Lunar Surface Models, May 1969
SP-8037	Assessment and Control of Spacecraft Magnetic Fields, September 1970
SP-8038	Meteoroid Environment Model–1970 (Interplanetary and Planetary), October 1970
SP-8049	The Earth's Ionosphere, March 1971
SP-8067	Earth Albedo and Emitted Radiation, July 1971
SP-8069	The Planet Jupiter (1970), December 1971
SP-8084	Surface Atmospheric Extremes (Launch and Transportation Areas), Revised June 1974
SP-8085	The Planet Mercury (1971), March 1972
SP-8091	The Planet Saturn (1970), June 1972
SP-8092	Assessment and Control of Spacecraft Electromagnetic Interference, June 1972

SP-8103	The Planets Uranus, Neptune, and Pluto (1971), November 1972
SP-8105	Spacecraft Thermal Control, May 1973
SP-8111	Assessment and Control of Electrostatic Charges, May 1974
SP-8116	The Earth's Trapped Radiation Belts, March 1975
SP-8117	Gravity Fields of the Solar System, April 1975
SP-8118	Interplanetary Charged Particle Models (1974), March 1975
SP-8122	The Environment of Titan (1975), July 1976

STRUCTURES

SP-8001	Buffeting During Atmospheric Ascent, Revised November 1970
SP-8002	Flight-Loads Measurements During Launch and Exit, December 1964
SP-8003	Flutter, Buzz, and Divergence, July 1964
SP-8004	Panel Flutter, Revised June 1972
SP-8006	Local Steady Aerodynamic Loads During Launch and Exit, May 1965
SP-8007	Buckling of Thin-Walled Circular Cylinders, Revised August 1968
SP-8008	Prelaunch Ground Wind Loads, November 1965
SP-8009	Propellant Slosh Loads, August 1968
SP-8012	Natural Vibration Modal Analysis, September 1968
SP-8014	Entry Thermal Protection, August 1968
SP-8019	Buckling of Thin-Walled Truncated Cones, September 1968
SP-8022	Staging Loads, February 1969
SP-8029	Aerodynamic and Rocket-Exhaust Heating During Launch and Ascent, May 1969
SP-8030	Transient Loads From Thrust Excitation, February 1969
SP-8031	Slosh Suppression, May 1969

SP-8032	Buckling of Thin-Walled Doubly Curved Shells, August 1969
SP-8035	Wind Loads During Ascent, June 1970
SP-8040	Fracture Control of Metallic Pressure Vessels, May 1970
SP-8042	Meteoroid Damage Assessment, May 1970
SP-8043	Design-Development Testing, May 1970
SP-8044	Qualification Testing, May 1970
SP-8045	Acceptance Testing, April 1970
SP-8046	Landing Impact Attenuation for Non-Surface-Planing Landers, April 1970
SP-8050	Structural Vibration Prediction, June 1970
SP-8053	Nuclear and Space Radiation Effects on Materials, June 1970
SP-8054	Space Radiation Protection, June 1970
SP-8055	Prevention of Coupled Structure-Propulsion Instability (Pogo), October 1970
SP-8056	Flight Separation Mechanisms, October 1970
SP-8057	Structural Design Criteria Applicable to a Space Shuttle, Revised March 1972
SP-8060	Compartment Venting, November 1970
SP-8061	Interaction with Umbilicals and Launch Stand, August 1970
SP-8062	Entry Gasdynamic Heating, January 1971
SP-8063	Lubrication, Friction, and Wear, June 1971
SP-8066	Deployable Aerodynamic Deceleration Systems, June 1971
SP-8068	Buckling Strength of Structural Plates, June 1971
SP-8072	Acoustic Loads Generated by the Propulsion System, June 1971
SP-8077	Transportation and Handling Loads, September 1971

SP-8079	Structural Interaction with Control Systems, November 1971
SP-8082	Stress-Corrosion Cracking in Metals, August 1971
SP-8083	Discontinuity Stresses in Metallic Pressure Vessels, November 1971
SP-8095	Preliminary Criteria for the Fracture Control of Space Shuttle Structures, June 1971
SP-8099	Combining Ascent Loads, May 1972
SP-8104	Structural Interaction With Transportation and Handling Systems, January 1973
SP-8108	Advanced Composite Structures, December 1974

GUIDANCE AND CONTROL

SP-8015	Guidance and Navigation for Entry Vehicles, November 1968
SP-8016	Effects of Structural Flexibility on Spacecraft Control Systems, April 1969
SP-8018	Spacecraft Magnetic Torques, March 1969
SP-8024	Spacecraft Gravitational Torques, May 1969
SP-8026	Spacecraft Star Trackers, July 1970
SP-8027	Spacecraft Radiation Torques, October 1969
SP-8028	Entry Vehicle Control, November 1969
SP-8033	Spacecraft Earth Horizon Sensors, December 1969
SP-8034	Spacecraft Mass Expulsion Torques, December 1969
SP-8036	Effects of Structural Flexibility on Launch Vehicle Control Systems, February 1970
SP-8047	Spacecraft Sun Sensors, June 1970
SP-8058	Spacecraft Aerodynamic Torques, January 1971
SP-8059	Spacecraft Attitude Control During Thrusting Maneuvers, February 1971

SP-8065	Tubular Spacecraft Booms (Extendible, Reel Stored), February 1971
SP-8070	Spaceborne Digital Computer Systems, March 1971
SP-8071	Passive Gravity-Gradient Libration Dampers, February 1971
SP-8074	Spacecraft Solar Cell Arrays, May 1971
SP-8078	Spaceborne Electronic Imaging Systems, June 1971
SP-8086	Space Vehicle Displays Design Criteria, March 1972
SP-8096	Space Vehicle Gyroscope Sensor Applications, October 1972
SP-8098	Effects of Structural Flexibility on Entry Vehicle Control Systems, June 1972
SP-8102	Space Vehicle Accelerometer Applications, December 1972

CHEMICAL PROPULSION

SP-8089	Liquid Rocket Engine Injectors, March 1976
SP-8087	Liquid Rocket Engine Fluid-Cooled Combustion Chambers, April 1972
SP-8124	Liquid Rocket Engine Self-Cooled Combustion Chambers, September 1977
SP-8113	Liquid Rocket Engine Combustion Stabilization Devices, November 1974
SP-8120	Liquid Rocket Engine Nozzles, July 1976
SP-8107	Turbopump Systems for Liquid Rocket Engines, August 1974
SP-8109	Liquid Rocket Engine Centrifugal Flow Turbopumps, December 1973
SP-8052	Liquid Rocket Engine Turbopump Inducers, May 1971
SP-8110	Liquid Rocket Engine Turbines, January 1974
SP-8081	Liquid Propellant Gas Generators, March 1972
SP-8048	Liquid Rocket Engine Turbopump Bearings, March 1971
SP-8121	Liquid Rocket Engine Turbopump Rotating-Shaft Seals, February 1978

SP-8101	Liquid Rocket Engine Turbopump Shafts and Couplings, September 1972
SP-8100	Liquid Rocket Engine Turbopump Gears, March 1974
SP-8088	Liquid Rocket Metal Tanks and Tank Components, May 1974
SP-8094	Liquid Rocket Valve Components, August 1973
SP-8097	Liquid Rocket Valve Assemblies, November 1973
SP-8090	Liquid Rocket Actuators and Operators, May 1973
SP-8119	Liquid Rocket Disconnects, Couplings, Fittings, Fixed Joints, and Seals, September 1976
SP-8123	Liquid Rocket Lines, Bellows, Flexible Hoses, and Filters, April 1977
SP-8112	Pressurization Systems for Liquid Rockets, October 1975
SP-8080	Liquid Rocket Pressure Regulators, Relief Valves, Check Valves, Burst Disks, and Explosive Valves, March 1973
SP-8064	Solid Propellant Selection and Characterization, June 1971
SP-8075	Solid Propellant Processing Factors in Rocket Motor Design, October 1971
SP-8076	Solid Propellant Grain Design and Internal Ballistics, March 1972
SP-8073	Solid Propellant Grain Structural Integrity Analysis, June 1973
SP-8039	Solid Rocket Motor Performance Analysis and Prediction, May 1971
SP-8051	Solid Rocket Motor Igniters, March 1971
SP-8025	Solid Rocket Motor Metal Cases, April 1970
SP-8093	Solid Rocket Motor Internal Insulation, December 1976
SP-8115	Solid Rocket Motor Nozzles, June 1975
SP-8114	Solid Rocket Thrust Vector Control, December 1974
SP-8041	Captive-Fired Testing of Solid Rocket Motors, March 1971